



AFRL-AFOSR-JP-TR-2019-0058

Investigation of Flight Dynamics and Controls for a Solar-Tracker-Mounted UAV

Sarot Srang
INSTITUTE OF TECHNOLOGY OF CAMBODIA
Russian Federation Boulevard
Phnom Penh, 120404
KH

09/16/2019
Final Report

DISTRIBUTION A: Distribution approved for public release.

Air Force Research Laboratory
Air Force Office of Scientific Research
Asian Office of Aerospace Research and Development
Unit 45002, APO AP 96338-5002

REPORT DOCUMENTATION PAGE				<i>Form Approved</i> <i>OMB No. 0704-0188</i>	
<p>The public reporting burden for this collection of information is estimated to average 1 hour per response, including the time for reviewing instructions, searching existing data sources, gathering and maintaining the data needed, and completing and reviewing the collection of information. Send comments regarding this burden estimate or any other aspect of this collection of information, including suggestions for reducing the burden, to Department of Defense, Executive Services, Directorate (0704-0188). Respondents should be aware that notwithstanding any other provision of law, no person shall be subject to any penalty for failing to comply with a collection of information if it does not display a currently valid OMB control number.</p> <p>PLEASE DO NOT RETURN YOUR FORM TO THE ABOVE ORGANIZATION.</p>					
1. REPORT DATE (DD-MM-YYYY) 16-09-2019		2. REPORT TYPE Final		3. DATES COVERED (From - To) 31 May 2017 to 30 Nov 2018	
4. TITLE AND SUBTITLE Investigation of Flight Dynamics and Controls for a Solar-Tracker-Mounted UAV				5a. CONTRACT NUMBER	
				5b. GRANT NUMBER FA2386-17-1-0148	
				5c. PROGRAM ELEMENT NUMBER 61102F	
6. AUTHOR(S) Sarot Srang				5d. PROJECT NUMBER	
				5e. TASK NUMBER	
				5f. WORK UNIT NUMBER	
7. PERFORMING ORGANIZATION NAME(S) AND ADDRESS(ES) INSTITUTE OF TECHNOLOGY OF CAMBODIA Russian Federation Boulevard Phnom Penh, 120404 KH				8. PERFORMING ORGANIZATION REPORT NUMBER	
9. SPONSORING/MONITORING AGENCY NAME(S) AND ADDRESS(ES) AOARD UNIT 45002 APO AP 96338-5002				10. SPONSOR/MONITOR'S ACRONYM(S) AFRL/AFOSR IOA	
				11. SPONSOR/MONITOR'S REPORT NUMBER(S) AFRL-AFOSR-JP-TR-2019-0058	
12. DISTRIBUTION/AVAILABILITY STATEMENT A DISTRIBUTION UNLIMITED: PB Public Release					
13. SUPPLEMENTARY NOTES					
14. ABSTRACT This report presents kinematic, inverse kinematic, dynamic modeling and simulation for a Solar-Tracker-Mounted UAV system. Kinematic and inverse kinematic for the tracker is briefly described using classical methods. Dynamic modeling for the system is one of the most challenging engineering problems. To deal with it, kinematic constraints of all joints are determined. Undetermined close form reaction forces at joints are obtained from the kinematic constraints. Using Newtons method, a dynamic equation for each body exerted by external forces and reaction forces is formulated. A fully determined equation, which is a system of algebraic-differential equations, is obtained by appending kinematic and dynamic equations. Simulation for a parallel-mechanism-mounted UAV can describe the position of all bodies in the whole system. From the result, there are three cases to discuss. Three case studies are illustrated.					
15. SUBJECT TERMS solar tracking, tracking simulation, UAV tracking					
16. SECURITY CLASSIFICATION OF:			17. LIMITATION OF ABSTRACT SAR	18. NUMBER OF PAGES	19a. NAME OF RESPONSIBLE PERSON KNOPP, JEREMY
a. REPORT Unclassified	b. ABSTRACT Unclassified	c. THIS PAGE Unclassified			19b. TELEPHONE NUMBER (Include area code) 315-227-7006

Final Report for AOARD Grant FA2386-17-1-0148

“Investigation of Flight Dynamics and Controls for Solar-Tracker-Mounted UAV”

Date: January 27, 2019

Name of Principal Investigator (PI and Co-PIs): Sarot SRANG, and Masaki YAMAKITA

- Email address: srangsarot@itc.edu.kh
- Institution: Institute of Technology of Cambodia
- Mailing address: Russian Federation Boulevard, P.O.Box 86, Phnom Penh, Cambodia
- Phone: +855 85 68 98 58

Period of Performance: May 31, 2017 – November 30, 2018

REPORT PART I

**DYNAMIC MODELING AND SIMULATION FOR 2DOF
PARALLEL MECHANISM**

ABSTRACT

My thesis aims to model the dynamic behavior of a 2 DOF parallel mechanism which can be used as dual axis solar tracker. Specifically, the change in orientation of the solar tracker is studied under different conditions of externally applied loads. The task of the parallel mechanism is to orientate the solar panel such that its surface is perpendicular to the sunlight. Kinematic constraints are determined to account for the dynamic interaction of the parallel mechanism at joints. Then undetermined close form reaction forces at joints are obtained from the kinematic constraints. Finally, a fully determined equation of motion, which is a system of algebraic-differential equations, is obtained by appending kinematic and dynamic equations. For both kinematic and dynamic equations, Cartesian coordinate and Euler parameter are used to describe translation and rotation motions respectively. As a verification, the equation of motion for the mechanism is applied to the case of one body attached to the ground by a spherical joint of which the close form solution is known. The application results of Euler parameters differ by only 10^{-9} in comparison to those given by the close form solution. This is practically zero error and suggests that the equation of motion for the parallel mechanism is reliable. Having verified the solution with the case mentioned above, three cases of externally applied loads were selected to examine their effects on the orientations of the solar panel. Results showed that the solar panel changed its orientation as expected for each case study.

ABBREVIATION AND SYMBOLS

DOF	Degree of Freedom
γ	Vector of right-hand side of acceleration equations
$\xi_i \eta_i \zeta_i$	Local (body-fixed) Cartesian coordinate system
ω_i	Angular velocity vector with respect to Global frame for body i
ω'_i	Angular velocity vector with respect to Body-fixed frame for body i
Φ	Vector of constraint
Φ_q	Jacobian matrix of constraints
b	Number of bodies
d	Vector with its end on two different bodies(Variable magnitude)
e_0, e_1, e_2, e_3	Euler parameter
e_i	Vector of three Euler parameters e_1, e_2, e_3 for body i
f_i	Vector of force acting on body i with respect to Global frame for body i
f'_i	Vector of force acting on body i with respect to Body-fixed frame for body i
g	Vector of forces for a system
g^c	Vector of constraint reaction forces
m	Mass of a particle
n_i	Vector of moment acting on body i with respect to Global frame
n'_i	Vector of moment acting on body i with respect to Body-fixed frame
p_i	Vector of four Euler parameters e_0, e_1, e_2, e_3 for body i
q_i	Vector of coordinates for body i
q	Vector of coordinates for a system
r_i	Translational position vector with respect to Global frame for body i
s_i	Vector with both ends on body i (constant magnitude) with respect to Global frame
s'_i	Vector with both ends on body i (constant magnitude) with respect to Body-fixed frame
t	time
u	unit vector
xyz	Global Cartesian coordinate system
A_i	Rotational transformation matrix for body i
G_i	3×4 transformation matrix for body i
I	Identity matrix
J_i	Global inertia tensor for body i

J'_i	Local (constant) inertia tensor for body i
L_i	3×4 transformation matrix for body i
M_i	6×6 mass matrix for body i containing N_i and J'_i
M	Mass matrix for a system
N_i	3×3 diagonal mass matrix for body i
\mathbf{r}	Vector of link OO_3
r^h	Length of link OO_3
\mathbf{a}_i	The position vector of point A_i with respect to $O - xyz$
\mathbf{b}_i	The position vector of point B_i with respect to $O - x_3y_3z_3$
q_i^h	The height of slider
r_i^h	The length of link B_iC_i
z_i	The position vector of link B_iC_i

TABLE OF CONTENTS

ABSTRACT	i
ABBREVIATIONS AND SYMBOLS.....	ii
TABLE OF CONTENTS.....	iv
LIST OF FIGURES.....	v
LIST OF TABLES	vi
1 INTRODUCTION	1
1.1 Background.....	1
1.2 Problem Statement.....	1
1.3 Goal and Objectives.....	1
1.4 Scope.....	2
2 LITERATURE REVIEW	3
3 KINEMATICS	4
3.1 Relative constraints between two vectors.....	4
3.2 Two perpendicular vectors.....	5
3.3 Two parallel vectors	5
3.4 Parallel mechanism joint.....	7
3.5 Position, velocity and acceleration analysis.....	10
4 DYNAMICS.....	12
4.1 Equations of motions for an unconstraint body	12
4.2 Equations of motion for constraint body.....	13
4.3 Example of system with one body.....	18
5 RESULTS AND DISCUSSION.....	22
6 CONCLUSIONS AND RECOMMENDATION	26
6.1 Conclusions.....	26
6.2 Recommendation for Future Works	26
REFERENCES.....	27
APPENDICES	29

LIST OF FIGURES

Figure 3.1: Vector with constant and varying magnitude	4
Figure 3.2: Spherical Joint	7
Figure 3.3: Universal Joint	8
Figure 3.4: Revolute Joint	9
Figure 3.5: Translational Joint	10
Figure 4.1: Parallel Mechanism	17
Figure 4.2: Two bodies connected by spherical joint	18
Figure 4.3: Error of Euler parameters between close form solution and Matlab ode	21
Figure 5.1: The orientation of solar panel with respect to time $t(s)$ for case 1, $f_2 = [0, 0, 4 \sin 4\pi t]^T N$ & $f_3 = [0, 0, 4 \sin 4\pi t]^T N$	23
Figure 5.2: The orientation of solar panel with respect to time $t(s)$ for case 2, $f_7 = [0, 0, -3]^T N$	24
Figure 5.3: The orientation of solar panel with respect to time $t(s)$ for case 3, $n'_7 = [0, 0.1, 0]^T N$	25
Figure 6.1: Global and Local coordinates	29

LIST OF TABLES

Table 3.1: Components in the Expansion of the Most Common Constraints	11
Table 4.1: Components in the Expansion of the Most Common Constraints	18
Table 6.1: Mass (m), Vector from origin to center of mass (r) Initial Euler parameter of each body (p) from SolidWorks Model	30
Table 6.2: Inertia Matrix for each body from SolidWorks Model	31

1. INTRODUCTION

1.1. Background

Solar trackers are defined as devices which have a role of improving the efficiency by keeping the solar panel perpendicular to the sun rays. The first automated solar tracking system was proposed by Mcfee [1]. There are two types of solar tracker: single-axis trackers and dual-axis tacker [2]. Solar trackers with one axis have much better performance than fixed systems, but two-axis systems allow to obtain an optimal tracking of the sun's path, since they keep the orientation of the collectors perpendicular to the solar radiation at any time in any season. The main challenge of these kinds of devices is that they have to consume certain energy in order to move the collectors following the sun trajectory [3].

1.2. Problem Statement

Dual axis solar tracker has been of interest research topic for many researchers, and a number of techniques have been developed to obtain the better efficiency with the desired optimal power consumption of the system . For this reason, parallel mechanism is introduced. J. Wu et al [4] developed and tested a two-axis decoupled solar tracking system based on parallel mechanism and showed that the tracker requires less driving torque, thus less power consumption than the conventional serial tracker does. Appealingly, complexity and weight of the system are also reduced. When parallel mechanism is attached to the fixed platform, the dynamic effect would not have much impact to the system. Nevertheless, dynamic effect should be considered when parallel mechanism is attached to a moving platform. The moving platform can be a boat, an aerial vehicle, a land vehicle etc. In our study, we use this tracking system on board and account for dynamic modeling.

1.3. Goal and Objectives

The purpose of this work is to develop a dynamic model that can describe and simulate the change in orientation of solar panel subjected to external forces applied. The solar panel is attached to a 2DOF parallel mechanism upon which loads are externally applied to change the panel orientation. The parallel mechanism was chosen because it has been proven to be energy efficient. The equation of motion of the system will be derived by determining the constraint reaction force exerted by each kinematic link so that the behavior of the configuration can be investigated. Due to the effect of external forces acting on the linear actuator, we would observe the movement of the solar panel. The result from this works lays the groundwork for controlling

orientation of solar tracker to obtain optimal solar energy.

1.4. Scope

Dynamic modeling is taken into account by deriving the kinematics constraints of all joints of the system. The solution of these equations is solved by using Matlab-built in function (ode45). In addition, the m vector Lagrange multipliers associate with constraint equations are not considered. Instead, coordinate vector describing the system will be determined. While the prototype of the system was not built, the data of center of mass and moment of inertia are obtained from the model drawing in SolidWorks program. They are assumed to be constant during the operation.

2. LITERATURE REVIEW

There has been intense research for decades to develop solar technologies since it is free and nonpolluting [5]. As stated in [6], there are three types of sun tracker such as passive tracker, chronological tracker and active tracker. The passive tracker which uses no motors, no gears and no controls that can fail. This type of sun tracker produce bad quality of orientation precision. The chronological tracker which is very simple and accurate solar tracker. The process control is ensured by a motor that rotates at a very slow rate (about $15^\circ = h$). The active tracker makes use of two motors and a gear trains to drive the tracker by a controller matched to the solar radiation.

Many researches on energy gain from solar tracking systems compared to tilted fixed panel had been done both theoretically and experimentally [7]. It is also been reported that the tracking device would consume 2-3% of the increased energy [7]. Helwa et al [8] have determined the maximum collectable solar energy by many kinds of solar tracking system. They are fixed system facing south and tilted 40° , a vertical-axis tracker, a 6° tilted-axis tracker, and a two-axis tracker. Their result showed that the higher energy gain is from two axis solar tracker. Energy gain from a single axis solar tracker was reported to be 20% [9] while energy gain from a dual axis solar tracker was 30-40% [10]. There are many researchers working on parallel mechanism because of its outperformance over single axis solar tracker [11]. It is been stated that a parallel kinematic solar tracker provides an orientation error lower than 0.4° during the sun tracking [12]. Where the orientation error is the relative alignment between the sun and the system.

3. KINEMATICS

3.1. Relative constraints between two vectors

A constraint stands for any condition that reduce the number of degree of freedom in a system. Prior to deriving the constraint equation formulation, the algebraic relations between two vectors must be derived. To construct the kinematic constraints equation, there exists the relation that the two vectors remain parallel or perpendicular. Two cases are considered such that a vector may have fixed length or variable length.

Vector \vec{s}_i which is fixed in body i has constant magnitude as shown in **Figure 3.1**. Its orientation relative to the $\xi_i \eta_i \zeta_i$ axes does not change.

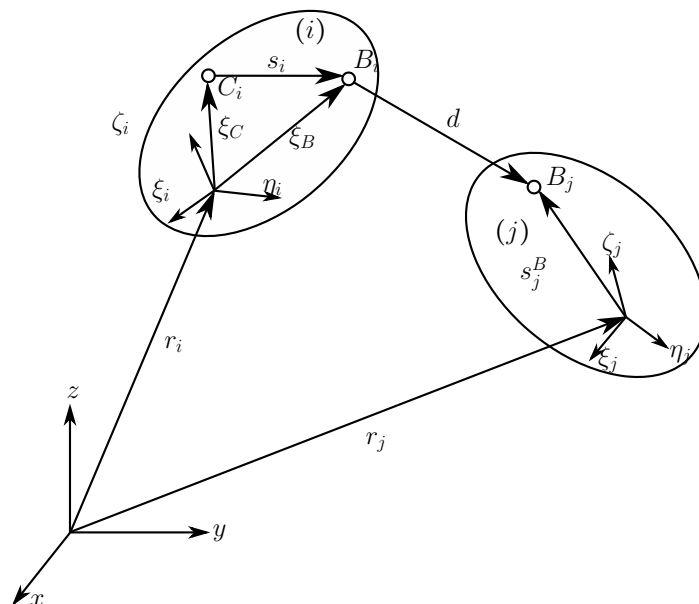


Figure 3.1. Vector with constant and varying magnitude

Therefore, the global component of \vec{s}_i is:

$$\begin{aligned}
 s_i &= s_i^B - s_i^C \\
 &= A_i s_i'^B - A_i s_i'^C \\
 &= A_i (s_i'^B - s_i'^C)
 \end{aligned} \tag{3.1}$$

Where $\mathbf{s}_i'^B = [\xi^B, \eta^B, \zeta^B]_i^T$ and $\mathbf{s}_i'^C = [\xi^C, \eta^C, \zeta^C]_i^T$ are known constant quantities.

Vector \vec{d} has variable length and connects two points on bodies i and j as illustrated in **Fig-**

ure 3.1. The global component of \vec{d} is written as:

$$\begin{aligned} d &= (r_j + s_j^B) - (r_i + s_i^B) \\ &= r_j + A_j s_j'^B - r_i - A_i s_i'^B \end{aligned} \quad (3.2)$$

Where $s_j'^B = [\xi^B, \eta^B, \zeta^B]_j^T$ is constant.

In the following subsection, constraint equations are assigned a superscript with two indices:

The first index denotes the type of constraint.

The second index denotes the number of independent equations.

Two types of constraints are introduced:

Type 1: Constraint between two vectors having constant magnitude.

Type 2: Constraint between two vectors, one having fixed magnitude and the other being variable.

For example: $\Phi^{(n1,1)}$ stands for the constraint equation which is considered in the constraint type one, and there is one independent equation.

3.2. Two perpendicular vectors

One constraint relation is placed to provide the perpendicularity between two vectors. Vectors \vec{s}_i and \vec{s}_j remain perpendicular if their scalar product is zero.

$$\begin{aligned} \Phi^{(n1,1)} &\equiv s_i^T s_j \\ &= s_i'^T A_i^T A_j s_j' = 0 \end{aligned} \quad (3.3)$$

Similarly, if the vector \vec{d} in remain perpendicular to \vec{s}_i :

$$\begin{aligned} \Phi^{(n2,1)} &\equiv s_i^T d \\ &= s_i'^T A_i^T (r_j + A_j s_j'^B - r_i - A_i s_i'^B) = 0 \end{aligned} \quad (3.4)$$

3.3. Two parallel vectors

Two vectors are set to be parallel by letting the vector product to zero. Consequently, two algebraic constraint equations are obtained:

In the case of parallel type one: $\Phi^{(p1,2)}$

$$\begin{aligned}\Phi^{(p1,2)} &\equiv \tilde{s}_i s_j \\ &= A_i \tilde{s}'_i A_i^T A_j s'_j = 0\end{aligned}\tag{3.5}$$

In the case of parallel type one: $\Phi^{(p2,2)}$

$$\begin{aligned}\Phi^{(p2,2)} &\equiv \tilde{s}_i d \\ &= A_i \tilde{s}'_i A_i^T (r_j + A_j s_j^{IB} - r_i - A_i s_i^{IB}) = 0\end{aligned}\tag{3.6}$$

In the case of parallel type one: $\Phi^{(p1,2)}$

$$\begin{aligned}\Phi^{(p1,2)} &\equiv \tilde{s}_i s_j \\ &= A_i \tilde{s}'_i A_i^T A_j s'_j = 0\end{aligned}\tag{3.7}$$

In the case of parallel type one: $\Phi^{(p2,2)}$

$$\begin{aligned}\Phi^{(p2,2)} &\equiv \tilde{s}_i d \\ &= A_i \tilde{s}'_i A_i^T (r_j + A_j s_j^{IB} - r_i - A_i s_i^{IB}) = 0\end{aligned}\tag{3.8}$$

Note that $\Phi^{(p1,2)} = 0$ and $\Phi^{(p2,2)} = 0$ provide three equations each. However, two equations are needed for deriving the constraint equations for the parallel vectors. Therefore, the following way is used to define these two equations.

$$\tilde{s}_i s_j = 0\tag{3.9}$$

$$\begin{bmatrix} 0 & -s_z & s_y \\ s_z & 0 & -s_x \\ -s_y & s_x & 0 \end{bmatrix}_i \begin{bmatrix} s_x \\ s_y \\ s_z \end{bmatrix}_j = \begin{bmatrix} 0 \\ 0 \\ 0 \end{bmatrix}\tag{3.10}$$

$$-s_{zi}s_{yj} + s_{zj}s_{yi} = 0$$

$$s_{zi}s_{xj} - s_{xi}s_{zj} = 0$$

$$-s_{yi}s_{xj} + s_{xi}s_{yj} = 0$$

Accordingly, a technique for the selection of a proper set of equations can be stated as follows. **Compare the absolute values of s_{xi}, s_{yi}, s_{zi} and select the two equations(out of three) having the largest term.** Therefore, six conditions can be stated as follows:

- If $|s_x|_i < |s_y|_i < |s_z|_i$ OR $|s_y|_i < |s_x|_i < |s_z|_i$

Eliminate the third equation.

- If $|s_x|_i < |s_z|_i < |s_y|_i$ OR $|s_z|_i < |s_x|_i < |s_y|_i$

Eliminate the second equation.

- If $|s_y|_i < |s_z|_i < |s_x|_i$ OR $|s_z|_i < |s_y|_i < |s_x|_i$

Eliminate the first equation.

3.4. Parallel mechanism joint

Two bodies(i, j) that are connected by spherical joint as shown in **Figure 3.2.**, consist of one center point which is called the center of spherical joint P . The coordinate of point P with respect to the $\xi_i\eta_i\zeta_i$ and $\xi_j\eta_j\zeta_j$ coordinate system is constant. Therefore, the constraint equation for this joint can be found from the vector equation $\vec{r}_i + \vec{s}_i^p - \vec{s}_j^p - \vec{r}_j = \vec{0}$ as follow:

$$\Phi^{(s,3)} \equiv r_i + A_i s_i^p - r_j - A_j s_j^p = 0 \quad (3.11)$$

Since there are three algebraic equations for this joint, there are three relative degrees of freedom.

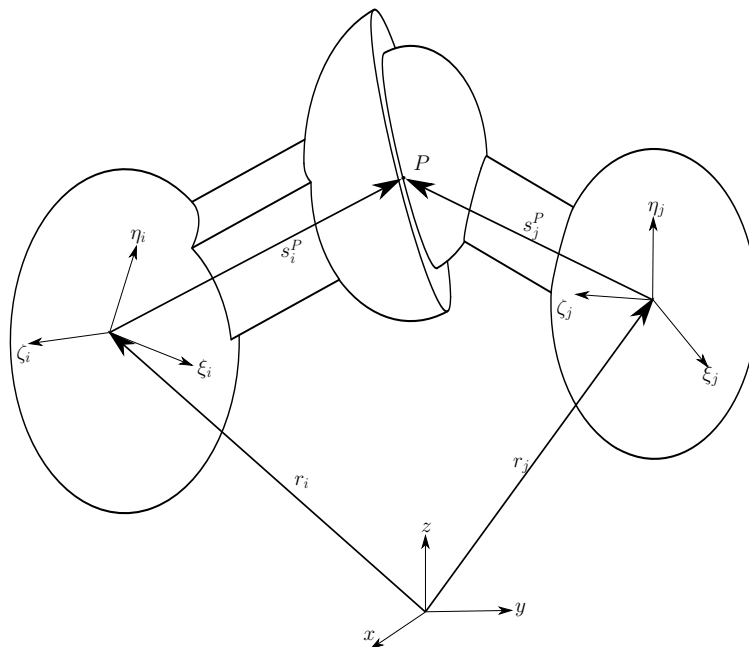


Figure 3.2. Spherical Joint

Two bodies(i, j) that are connected by a Universal or Hook Joint as shown in **Figure 3.3.**, consist of two relationship. The first relationship is that point P , the intersection of

the axes of the bar, has constant coordinates with respect to both body-fixed coordinate system. Thus, the above equation can be used. The second relationship is that the two vectors \vec{s}_i and \vec{s}_j remain perpendicular. Therefore, there are four algebraic equations for universal joint and two relative degrees of freedom for this joint.

$$\begin{aligned} \Phi^{(s,3)} &= 0 \\ \Phi^{(n1,1)} &\equiv s_i^T s_j = 0 \end{aligned} \tag{3.12}$$

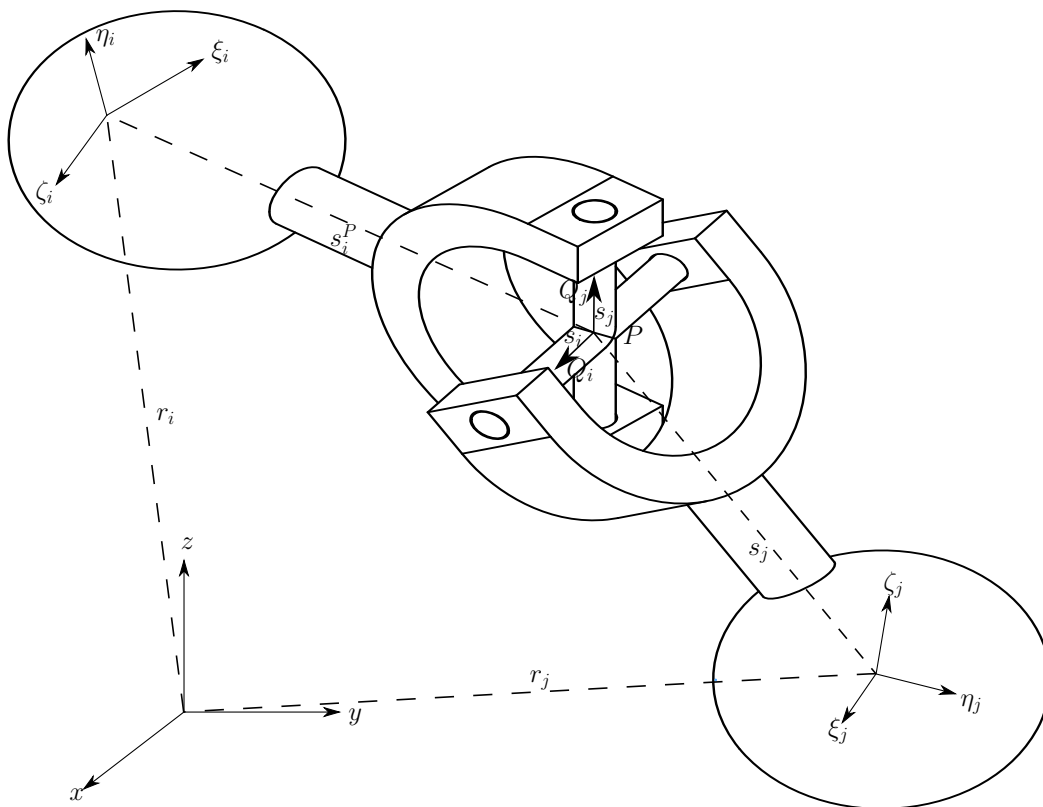


Figure 3.3. Universal Joint

There exists two condition for two bodies(i, j) that are connected by a revolute joint as shown in **Figure 3.4.** The first one is that the coordinate of any point on the revolute joint is constant. Accordingly the **Eq. 3.11.** can still be used. The second one is that vectors \vec{s}_i and \vec{s}_j must remain parallel. Therefore, the kinematic constraint equations for this joint are constructed in five algebraic equations as follow:

$$\begin{aligned} \Phi^{(s,3)} &= 0 \\ \Phi^{(p1,2)} &= \tilde{s}_i s_j = 0 \end{aligned} \tag{3.13}$$

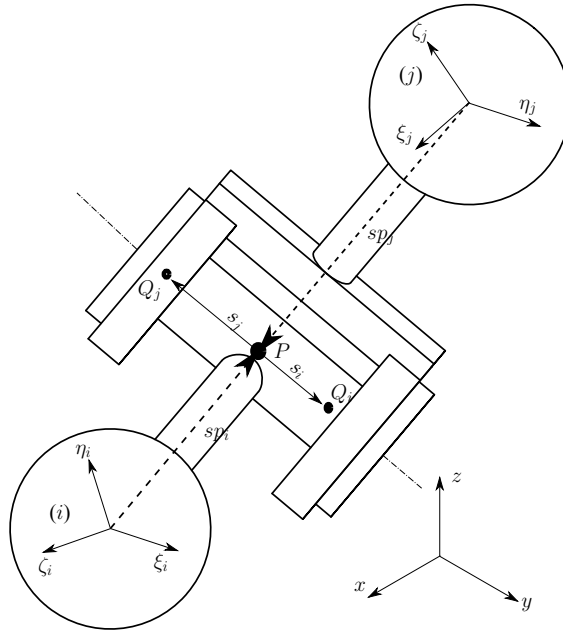


Figure 3.4. Revolute Joint

There are five algebraic constraint equations for two bodies (i, j) that are connected by translational joint. It is derived such that the bodies i and j are able to move along one common axis, the relative rotation about this axis is not allowed. As shown in **Figure 3.5**, point P_i, Q_i on body i and P_j, Q_j on body j are chosen arbitrarily on the joint axes. The relationship of translational joint can be made such that the vectors of constant magnitude, \vec{s}_i and \vec{s}_j , and variable magnitude, \vec{d} are remain collinear. Additionally, vector \vec{h}_i and \vec{h}_j , as shown in **Figure 3.5** must remain perpendicular. Therefore five algebraic equations of translational joint are obtained:

$$\begin{aligned}
 \Phi^{(p1,2)} &\equiv \tilde{s}_i s_j = 0 \\
 \Phi^{(p2,2)} &\equiv \tilde{s}_i d = 0 \\
 \Phi^{(n1,1)} &\equiv h_i^T h_j = 0
 \end{aligned}
 \tag{3.14}$$

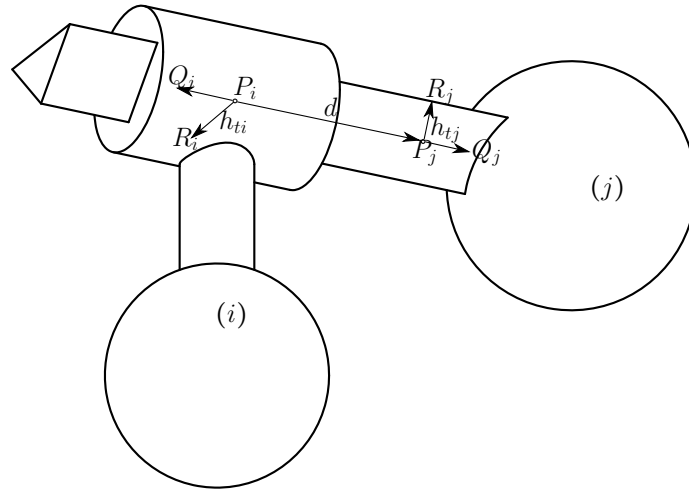


Figure 3.5. Translational Joint

3.5. Position, velocity and acceleration analysis

The kinematic constraint equations Φ derived in the preceding sections for spatial kinematic joints (Spherical, Universal, Rotational and Translational joints) are generally nonlinear in terms of the coordinates $q_i = [x, y, z, e_0, e_1, e_2, e_3]_i^T$ where $i = 1 \dots 7$ denote the body number ranging from 1 to 7. Generally, the constraint equations are consisted of m equations in the form.

$$\Phi \equiv \Phi(q) = 0 \quad (3.15)$$

For the parallel mechanism with 7 bodies, the number of constraints equations is defined in terms of each joint. Spherical joint creates 3 constraints equations, and two spherical joints create 6 constraint equations. Universal joint creates 4 constraints equations, and two universal joints create 8 constraint equations. Rotational joint creates 5 constraint equations, and two rotational joints create 10 constraint equations. Translational joint creates 5 constraint equations, and two translational joints create 10 constraint equations. Thus, the total number of constraint equations of the system is 34.

To describe the kinematic analysis, the first and second time derivatives of **Eq. 3.15.** are evaluated as follow: The first time derivative of constraint equation is given by:

$$\Phi_q \dot{q} = 0 \quad (3.16)$$

The second time derivative of constraint equation is given by:

$$\begin{aligned}\Phi_q \ddot{q} + (\Phi_q \dot{q})_q \dot{q} &= 0 \\ \Phi_q \ddot{q} &= \gamma\end{aligned}\tag{3.17}$$

Where $\gamma = -(\Phi_q \dot{q})_q \dot{q}$ is called the right side of the kinematic acceleration equation, and Φ_q is the Jacobian matrix. Both γ and Φ_q of each joint are given in the **Table 3.1**.

Table 3.1. Components in the Expansion of the Most Common Constraints

Φ	$\Phi_{r_i}^{(m)}$	$\Phi_{P_i}^{(m)}$	$\Phi_{r_j}^{(m)}$	$\Phi_{P_j}^{(m)}$	$\gamma^{(m)}$
$\Phi^{n1,1}$	0^T	$2s_j^T G_i \bar{s}'_i$	0^T	$2s_i^T G_j \bar{s}'_j$	$s_i^T h_j + s_j^T h_i - 2\dot{s}_i^T \dot{s}_j$
$\Phi^{n2,1}$	$-s_i^T$	$-2s_j^T G_i \bar{s}'_i{}^B + 2d^T G_i \bar{s}'_i$	s_i^T	$2s_i^T G_j \bar{s}'_j{}^B$	$-s_i^T (h_i^B - h_j^B) + d^T h_i - 2\dot{s}_i^T \dot{d}$
$\Phi^{(p1,2)}$	0	$-2\tilde{s}_j G_i \bar{s}'_i$	0	$2\tilde{s}_i G_j \bar{s}'_j$	$\tilde{s}_i h_j - \tilde{s}_j h_i - 2\tilde{\dot{s}}_i \dot{s}_j$
$\Phi^{(p2,2)}$	$-\tilde{s}_i$	$-2\tilde{s}_i G_i \bar{s}'_i{}^B - 2\tilde{d} G_i \bar{s}'_i$	\tilde{s}_i	$2\tilde{s}_i G_j \bar{s}'_j{}^B$	$\tilde{s}_i (h_j^B - h_i^B) - \tilde{d} h_i - 2\tilde{\dot{s}}_i \dot{d}$
$\Phi^{(s,3)}$	I	$2G_i \bar{s}'_i{}^p$	$-I$	$-2G_j \bar{s}'_j{}^p$	$h_i^p - h_j^p$
$\Phi^{(s-s,1)}$	$-2d^T$	$-4d^T G_i \bar{s}'_i{}^p$	$2d^T$	$4d^T G_j \bar{s}'_j{}^p$	$2d^T (h_i^p - h_j^p) - 2\dot{d}^T \dot{d}$

The components in **Table 3.1.** are modified jacobian matrix $\Phi_q^{(m)}$ and modified vector $\gamma^{(m)}$. It can be derived from the corresponding kinematic constraint equations by taking its second time derivative and using the equation in [13, p. 171].

$$\begin{aligned}\Phi_{p_i}^{(m)} \ddot{p}_i &= -(\Phi_{p_i}^{(m)} \dot{p}_i)_{p_i} \dot{p}_i \\ \ddot{A}a &= 2\dot{G}\dot{L}^T a + 2G\ddot{a}\ddot{p}\end{aligned}$$

4. DYNAMICS

Two Newton's Law equations will be used for deriving the equations of motion for Multi-Rigid bodies of Parallel Mechanism. There is one equation for describing the translational motion of the system, and another one is the equation of rotational motion. All equations are written in terms of Euler parameters.

4.1. Equations of motions for an unconstraint body

For an unconstrained body i with mass m_i and moment of inertia J'_i with respect to its center of mass exerted by external force f_i and moment n'_i measured in body-fixed frame, the equation of translational motion for body i is written as:

$$N_i \ddot{r}_i = f_i \quad (4.1)$$

The rotational equation of motion (Euler's equation of motion) for body i is given as:

$$J'_i \dot{\omega}'_i + \tilde{\omega}'_i J'_i \omega'_i = n'_i \quad (4.2)$$

Equation (4.1) and (4.2) can be expressed in matrix form as:

$$\begin{bmatrix} N & 0 \\ 0 & J' \end{bmatrix}_i \begin{bmatrix} \ddot{r} \\ \dot{\omega}' \end{bmatrix}_i + \begin{bmatrix} 0 \\ \tilde{\omega}' J' \omega' \end{bmatrix}_i = \begin{bmatrix} f \\ n' \end{bmatrix}_i \quad (4.3)$$

Where $N_i = \text{diag} \left(\begin{bmatrix} m & m & m \end{bmatrix} \right)_i$ and ω'_i is the angular velocity defined in body-fixed frame.

To use Euler parameters, the equation of rotational motion **Eq. 4.2.** is transformed by using the relationship of angular velocity and Euler parameter as follows:

$$\begin{aligned} \omega' &= 2L\dot{p} \\ \dot{\omega}' &= 2L\ddot{p} \end{aligned} \quad (4.4)$$

Substituting **Eq. 4.4.** into **Eq. 4.2.** results in:

$$\begin{aligned} 2J'_i L_i \ddot{p}_i + 4\widetilde{L_i \dot{p}_i} J'_i L_i \dot{p}_i &= n'_i \\ 2J'_i L_i \ddot{p}_i + 4L_i \dot{L}_i^T J'_i L_i \dot{p}_i &= n'_i \\ 2J'_i L_i \ddot{p}_i + L_i H_i \dot{p}_i &= n'_i \end{aligned} \quad (4.5)$$

Where $\widetilde{L}_i \dot{p}_i = L_i \dot{L}_i^T, H_i = 4\dot{L}_i^T J_i^T L_i, p = [e_0, e^T]^T = [e_0, e_1, e_2, e_3]^T$ stands for the Euler parameter

Since the four Euler parameters are not independent, there exists a relationship such that:

$$p^T p - 1 = 0 \quad (4.6)$$

The first time derivative of **Eq. 4.6.** results:

$$\begin{aligned} \dot{p}^T p + p^T \dot{p} &= 0 \\ 2p^T \dot{p} &= 0 \\ p^T \dot{p} &= 0 \end{aligned}$$

The second time derivative of **Eq. 4.6.** results:

$$p^T \ddot{p} + \dot{p}^T \dot{p} = 0$$

For body i the above equation can be written as:

$$p_i^T \ddot{p}_i + \dot{p}_i^T \dot{p}_i = 0 \quad (4.7)$$

The equation **Eq. 4.5.** and **Eq. 4.7.** can be written in matrix form as follow:

$$\begin{aligned} 2J_i^T L_i \ddot{p}_i + L_i H_i \dot{p}_i &= n'_i \\ p_i^T \ddot{p}_i + \dot{p}_i^T \dot{p}_i &= 0 \end{aligned}$$

$$\begin{bmatrix} 2J^T L \\ p^T \end{bmatrix}_i \ddot{p}_i + \begin{bmatrix} LH \\ \dot{p}^T \end{bmatrix}_i \dot{p}_i = \begin{bmatrix} n' \\ 0 \end{bmatrix}_i \quad (4.8)$$

4.2. Equations of motion for constraint body

For a constraint mechanical system, there are constraint reaction forces and moment created by each joint in the system. Consequently, the reaction forces would have taken into account with translation and rotational equations of motions.

Thus, the equation **Eq. 4.1.** and **Eq. 4.5.** become:

$$\begin{aligned} N_i \ddot{r}_i &= f_i + f_i^{(c)} \\ 2J'_i L_i \ddot{p}_i + L_i H_i \dot{p}_i &= n'_i + n_i'^{(c)} \end{aligned} \quad (4.9)$$

In [13], the constraint reaction force and moment are given as:

$$\begin{aligned} f_i'^{(c)} &= \Phi_{ri}^T \lambda \\ n_i'^{(c)} &= \Phi_{pi}^T \lambda \end{aligned} \quad (4.10)$$

Where $\lambda = [\lambda_1, \dots, \lambda_2]$ is known as Lagrange Multipliers, and $[\Phi_{ri}, \Phi_{pi}] = \Phi_{qi}$ is Jacobian Matrix of the kinematic constraint $\Phi \equiv \Phi(q)$ with respect to q_i .

The constraint reaction moment $n_i'^{(c)}$ is derived such that it can be used in the four rotational equation of motion associated with Euler parameter. $n_i'^{(c)}$ contains four components, and the transformation between n'_i and $n_i'^{(c)}$ is expressed in the following method.

$(n_i'^{(c)}, \omega_i')$ and $(n_i'^{(c)}, \dot{p}_i)$ are given in the same coordinate system respectively. Therefore, the scalar product of these two terms remains equal.

$$\dot{p}_i^T n_i'^{(c)} = \omega_i'^T n_i'^{(c)}$$

In [13, p. 175] the angular velocity measured in body-fixed frame is given to be:

$$\begin{aligned} \omega' &= 2L\dot{p} \\ L_i L_i^T &= I \end{aligned}$$

Thus, **Eq. 4.11.** becomes:

$$\begin{aligned} \dot{p}_i^T n_i'^{(c)} &= 2\dot{p}_i^T L_i^T n_i'^{(c)} \\ n_i'^{(c)} &= 2L_i^T n_i'^{(c)} \\ \frac{1}{2} n_i'^{(c)} &= L_i^T n_i'^{(c)} \\ \frac{1}{2} L_i n_i'^{(c)} &= L_i L_i^T n_i'^{(c)} \\ n_i'^{(c)} &= \frac{1}{2} L_i n_i'^{(c)} = \frac{1}{2} L_i \Phi_{pi}^T \lambda \end{aligned} \quad (4.11)$$

The equation **Eq. 4.9.** now becomes:

$$\begin{aligned} N_i \ddot{r}_i - \Phi_{r_i}^T \lambda &= f_i \\ 2J'_i L_i \ddot{p}_i + L_i H_i \dot{p}_i - \frac{1}{2} L_i \Phi_{p_i}^T \lambda &= n'_i \end{aligned} \quad (4.12)$$

For the system with i bodies for parallel mechanism, the dynamic equations can be constructed by using equations **Eq. 4.12.** and **Eq. 4.7.**, as follow:

$$\begin{aligned} N_i \ddot{r}_i - \Phi_{r_i}^T \lambda &= f_i \\ 2J'_i L_i \ddot{p}_i + L_i H_i \dot{p}_i - \frac{1}{2} L_i \Phi_{p_i}^T \lambda &= n'_i \\ p_i^T \ddot{p}_i + \dot{p}_i^T \dot{p}_i &= 0 \end{aligned} \quad (4.13)$$

In matrix form:

$$\begin{bmatrix} N_i & 0 & \Phi_{r_i}^T \\ 0 & 2J'_i L_i & \frac{1}{2} L_i \Phi_{p_i}^T \\ 0 & p_i^T & 0 \end{bmatrix} \begin{bmatrix} \ddot{r}_i \\ \ddot{p}_i \\ -\lambda \end{bmatrix} + \begin{bmatrix} 0 \\ L_i H_i \dot{p}_i \\ p_i^T \dot{p}_i \end{bmatrix} = \begin{bmatrix} f_i \\ n'_i \\ 0 \end{bmatrix} \quad (4.14)$$

For the system of 7 bodies, the dynamic equations can be obtained in compact form as:

$$\begin{bmatrix} M & B^T \\ P & 0 \end{bmatrix} \begin{bmatrix} \ddot{q} \\ -\lambda \end{bmatrix} + \begin{bmatrix} b \\ c \end{bmatrix} = \begin{bmatrix} g \\ 0 \end{bmatrix} \quad (4.15)$$

To solve this equation for q and λ , the constraint equation of Spherical Joint, Revolute Joint, Translational Joint and Universal Joint are used. Denote Φ_q is the kinematic constraint equation. Therefore, the constraint equation can be expressed as follows.

$$\Phi \equiv \Phi(q) = 0 \quad (4.16)$$

The first time derivative of constraint equation is given by:

$$\Phi_q \dot{q} = 0$$

The second time derivative of constraint equation is given by:

$$\begin{aligned} \Phi_q \ddot{q} + (\Phi_q \dot{q})_q \dot{q} &= 0 \\ \Phi_q \ddot{q} &= \gamma \end{aligned} \quad (4.17)$$

Where $\gamma = -(\Phi_q \dot{q})_q \dot{q}$ is called the right side of the kinematic acceleration equation.

This equation is then appended with equation (4.13) to yield a system of algebraic-differential equation as:

$$\begin{aligned}
 N_i \ddot{r}_i - \Phi_{r_i}^T \lambda &= f_i \\
 2J'_i L_i \ddot{P}_i + L_i H_i \dot{P}_i - \frac{1}{2} L_i \Phi_{P_i}^T \lambda &= n'_i \\
 P_i^T \ddot{P}_i + \dot{P}_i^T \dot{P}_i &= 0 \\
 \Phi_q \ddot{q} &= \gamma
 \end{aligned} \tag{4.18}$$

In matrix form:

$$\begin{bmatrix} M & B^T \\ P & 0 \\ \Phi_q & 0 \end{bmatrix} \begin{bmatrix} \ddot{q} \\ -\lambda \end{bmatrix} + \begin{bmatrix} b \\ c \\ 0 \end{bmatrix} = \begin{bmatrix} g \\ 0 \\ \gamma \end{bmatrix} \tag{4.19}$$

$$\text{Where } M = \begin{bmatrix} N_1 & 0 & \dots & 0 & 0 \\ 0 & 2J'_1 L_1 & \dots & 0 & 0 \\ \vdots & \vdots & \ddots & \vdots & \vdots \\ 0 & 0 & \dots & N_7 & 0 \\ 0 & 0 & \dots & 0 & 2J'_7 L_7 \end{bmatrix}, B = [\Phi_{r_1}, \frac{1}{2} \Phi_{p_1} L_1^T, \dots, \Phi_{r_7}, \frac{1}{2} \Phi_{p_7} L_7^T],$$

$$P = \begin{bmatrix} 0^T & p_1^T & \dots & 0^T & 0^T \\ \vdots & \vdots & \ddots & \vdots & \vdots \\ 0^T & 0^T & \dots & 0^T & p_7^T \end{bmatrix}, b = \begin{bmatrix} 0 \\ L_1 H_1 \dot{p}_1 \\ \vdots \\ 0 \\ L_7 H_7 \dot{p}_7 \end{bmatrix}, c = \begin{bmatrix} \dot{p}_1^T \dot{p}_1 \\ \vdots \\ \dot{p}_7^T \dot{p}_7 \end{bmatrix} \text{ and}$$

$$g = \begin{bmatrix} f_1 \\ n'_1 \\ \vdots \\ f_7 \\ n'_7 \end{bmatrix}, \ddot{q} = [\ddot{r}_1^T \quad \ddot{p}_1^T \quad \dots \quad \ddot{r}_7^T \quad \ddot{p}_7^T]^T = [\ddot{x}, \ddot{y}, \ddot{z}, \ddot{e}_0, \ddot{e}_1, \ddot{e}_2, \ddot{e}_3]_i^T \quad (i = 1, 2, \dots, 7)$$

To solve the system algebraic differential **Eq. 4.19.**, we need to write it in state equation.

Denote:

$$\begin{aligned}
 x_1 = q &= [x_1, y_1, z_1, [e_0, e_1, e_2, e_3]_1, \dots, x_7, y_7, z_7, [e_0, e_7, e_7, e_7]_7] \\
 x_2 = \dot{q} &= [\dot{x}_1, \dot{y}_1, \dot{z}_1, [\dot{e}_0, \dot{e}_1, \dot{e}_2, \dot{e}_3]_1, \dots, \dot{x}_7, \dot{y}_7, \dot{z}_7, [\dot{e}_0, \dot{e}_1, \dot{e}_2, \dot{e}_3]_7]
 \end{aligned} \tag{4.20}$$

$$\dot{x}_1 = x_2 = \dot{q}$$

$$\dot{x}_2 = \ddot{q} = \begin{bmatrix} [I]_{49 \times 49} & [0]_{49 \times 34} \end{bmatrix} \begin{bmatrix} M & B^T \\ P & 0 \\ \Phi_q & 0 \end{bmatrix}^{-1} \begin{bmatrix} g - b \\ -c \\ \gamma \end{bmatrix} \quad (4.21)$$

The initial condition and input for Mass, Initial matrix are shown in **Appendix C** and **Appendix D** respectively.

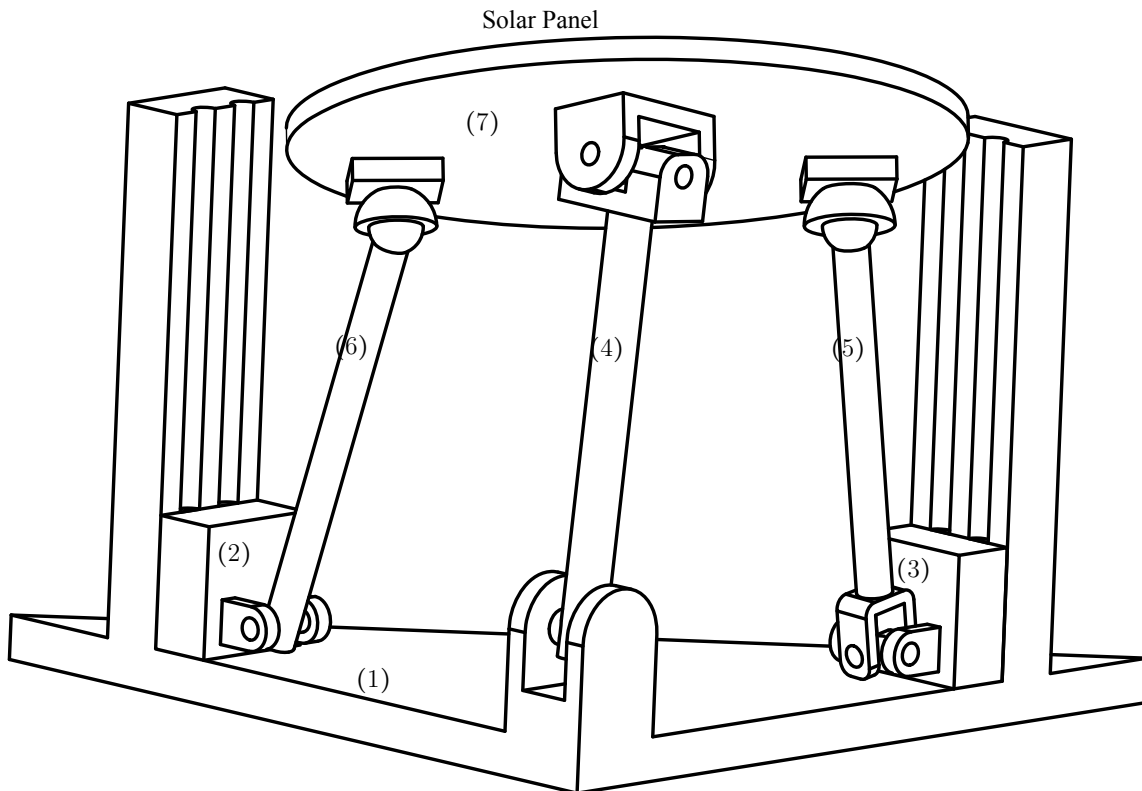


Figure 4.1. Parallel Mechanism

Table 4.1. Components in the Expansion of the Most Common Constraints

Φ	$\Phi_{r_i}^{(m)}$	$\frac{1}{2}\Phi_{P_i}^{(m)} L_i^T$	$\Phi_{r_j}^{(m)}$	$\frac{1}{2}\Phi_{P_j}^{(m)} L_j^T$	$\gamma^\#$
$\Phi^{n1,1}$	0^T	$-s_j^T \tilde{s}_i A_i$	0^T	$-s_i^T \tilde{s}_j A_j$	$-2\dot{s}_i^T \dot{s}_j + \dot{s}_i^T \tilde{\omega}_i s_j + \dot{s}_j^T \tilde{\omega}_j s_i$
$\Phi^{n2,1}$	$-s_i^T$	$-(d + s_i^B)^T \tilde{s}_i A_i$	s_i^T	$-s_i^T \tilde{s}_j^B A_j$	$-2\dot{d}^T \dot{s}_i - d^T \tilde{\omega}_i \dot{s}_i + s_i^T (\tilde{\omega}_i \dot{s}_i^B - \tilde{\omega}_j \dot{s}_j^B)$
$\Phi^{(p1,2)}$	0	$\tilde{s}_j \tilde{s}_i A_i$	0	$-\tilde{s}_i \tilde{s}_j A_j$	$-2\tilde{s}_i \dot{s}_j + \tilde{s}_j \tilde{\omega}_i \dot{s}_i - \tilde{s}_i \tilde{\omega}_j \dot{s}_j$
$\Phi^{(p2,2)}$	$-\tilde{s}_i$	$(\tilde{s}_i \tilde{s}_i^B + \tilde{d} \tilde{s}_i) A_i$	\tilde{s}_i	$-\tilde{s}_i \tilde{s}_j^B A_j$	$-2\tilde{s}_i \dot{d} + \tilde{s}_i (\tilde{\omega}_i \dot{s}_i^B - \tilde{\omega}_j \dot{s}_j^B) + \tilde{d} \tilde{\omega}_i \dot{s}_i$
$\Phi^{(s,3)}$	I	$-\tilde{s}_i^p A_i$	$-I$	$\tilde{s}_j^p A_j$	$-\tilde{\omega}_i \dot{s}_i^p + \tilde{\omega}_j \dot{s}_j^p$
$\Phi^{(s-s,1)}$	$-2d^T$	$2d^T \tilde{s}_i^p A_i$	$2d^T$	$-2d^T \tilde{s}_j^p A_j$	$-2d^T d + 2d^T (\tilde{\omega}_i \dot{s}_i^p - \tilde{\omega}_j \dot{s}_j^p)$

4.3. Example of system with one body

To validate the equation of motion for the simulation of the parallel mechanism solar tracker, the system of two body connected by spherical joint as shown in **Figure 4.2.** has been determined. The moment n'_ζ applied along the ζ axis.

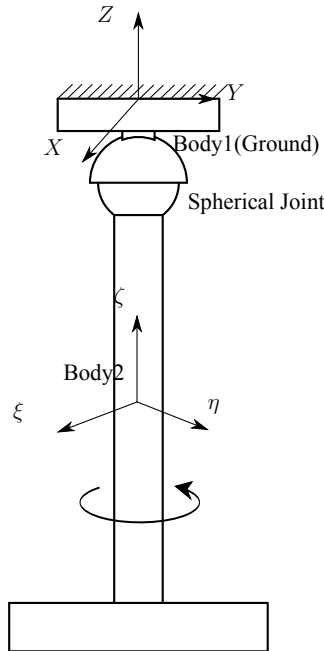


Figure 4.2. Two bodies connected by spherical joint

$$\begin{bmatrix} N_i & 0 & \Phi_{ri}^T \\ 0 & 2J'_1 L_i & \frac{1}{2} L_i \Phi_{Pi}^T \\ 0 & p_i^T & 0 \\ \Phi_{ri} & \Phi_{Pi} & 0 \end{bmatrix} \begin{bmatrix} \ddot{r}_i \\ \ddot{p}_i \\ -\lambda \end{bmatrix} + \begin{bmatrix} 0 \\ L_i H_i \dot{p}_i \\ \dot{p}_i^T \dot{p}_i \\ 0 \end{bmatrix} = \begin{bmatrix} f_i \\ n'_i \\ 0 \\ \gamma \end{bmatrix} \quad (4.22)$$

$$\begin{bmatrix} N_1 & 0 & 0 & 0 & \Phi_{r1}^T \\ 0 & 2J'_1 L_1 & 0 & 0 & \frac{1}{2} L_1 \Phi_{p1}^T \\ 0 & 0 & N_2 & 0 & \Phi_{r2}^T \\ 0 & 0 & 0 & 2J'_2 L_2 & \frac{1}{2} L_2 \Phi_{p2}^T \\ 0 & p_1^T & 0 & 0 & 0 \\ 0 & 0 & 0 & p_2^T & 0 \\ \Phi_{r1} & \Phi_{p1} & \Phi_{r2} & \Phi_{p2} & 0 \end{bmatrix} \begin{bmatrix} \ddot{r}_1 \\ \ddot{p}_1 \\ \ddot{r}_2 \\ \ddot{p}_2 \\ -\lambda \end{bmatrix} + \begin{bmatrix} 0 \\ L_1 H_1 \dot{p}_1 \\ 0 \\ L_2 H_2 \dot{p}_2 \\ \dot{p}_1^T \dot{p}_1 \\ \dot{p}_2^T \dot{p}_2 \\ 0 \end{bmatrix} = \begin{bmatrix} f_1 \\ n'_1 \\ f_2 \\ n'_2 \\ 0 \\ 0 \\ \gamma \end{bmatrix} \quad (4.23)$$

$$\begin{bmatrix} \ddot{r}_1 \\ \ddot{p}_1 \\ \ddot{r}_2 \\ \ddot{p}_2 \\ -\lambda \end{bmatrix} = \begin{bmatrix} N_1 & 0 & 0 & 0 & 0 \\ 0 & 2J'_1 L_1 & 0 & 0 & 0 \\ 0 & 0 & N_2 & 0 & \Phi_{r2}^T \\ 0 & 0 & 0 & 2J'_2 L_2 & \frac{1}{2} L_2 \Phi_{p2}^T \\ 0 & p_1^T & 0 & 0 & 0 \\ 0 & 0 & 0 & p_2^T & 0 \\ \Phi_{r1} & \Phi_{p1} & \Phi_{r2} & \Phi_{p2} & 0 \end{bmatrix}^{-1} \begin{bmatrix} f_1 \\ n'_1 - L_1 H_1 \dot{p}_1 \\ f_2 \\ n'_2 - L_2 H_2 \dot{p}_2 \\ \dot{p}_1^T \dot{p}_1 \\ \dot{p}_2^T \dot{p}_2 \\ \gamma \end{bmatrix} \quad (4.24)$$

Note: To assign a ground body, It is assumed that any kinematic constraint reaction forces to the ground body equal to zeros. It is because the constraint reaction force of the joint applies to the ground body has been eliminated by the ground itself. The example is shown in **Eq. 4.27.**

Denote:

$$\begin{aligned} x_1 = q &= [x_1, y_1, z_1, [e_0, e_1, e_2, e_3]_1, x_2, y_2, z_2, [e_0, e_1, e_2, e_3]_2] \\ x_2 = \dot{q} &= [\dot{x}_1, \dot{y}_1, \dot{z}_1, [\dot{e}_0, \dot{e}_1, \dot{e}_2, \dot{e}_3]_1, \dot{x}_2, \dot{y}_2, \dot{z}_2, [\dot{e}_0, \dot{e}_1, \dot{e}_2, \dot{e}_3]_2] \end{aligned} \quad (4.25)$$

$$\dot{x}_1 = x_2 = \dot{q}$$

$$\dot{x}_2 = \ddot{q} = \begin{bmatrix} [I]_{14 \times 14} & [0]_{14 \times 3} \end{bmatrix} \begin{bmatrix} N_1 & 0 & 0 & 0 & 0 \\ 0 & 2J'_1 L_1 & 0 & 0 & 0 \\ 0 & 0 & N_2 & 0 & \Phi_{r2}^T \\ 0 & 0 & 0 & 2J'_2 L_2 & \frac{1}{2} L_2 \Phi_{p2}^T \\ 0 & p_1^T & 0 & 0 & 0 \\ 0 & 0 & 0 & p_2^T & 0 \\ \Phi_{r1} & \Phi_{p1} & \Phi_{r2} & \Phi_{p2} & 0 \end{bmatrix}^{-1} \begin{bmatrix} f_1 \\ n'_1 - L_1 H_1 \dot{p}_1 \\ f_2 \\ n'_2 - L_2 H_2 \dot{p}_2 \\ \dot{p}_1^T \dot{p}_1 \\ \dot{p}_2^T \dot{p}_2 \\ \gamma \end{bmatrix} \quad (4.26)$$

Input for matrix B

$$\begin{aligned} B &= [\Phi_{r1}, \frac{1}{2} \Phi_{p1} L_1^T, \Phi_{r2}, \frac{1}{2} \Phi_{p2} L_2^T] = \begin{bmatrix} 0_{3 \times 3} & 0_{3 \times 3} & -I_{3 \times 3} & \tilde{s}_2^p A_2 \end{bmatrix} \\ -\tilde{s}_1^p A_1 &= -(A_1 \tilde{s}_1'^p A_1^T) A_1 = -A_1 \tilde{s}_1'^p \\ \tilde{s}_2^p A_2 &= (A_2 \tilde{s}_2'^p A_2^T) A_2 = A_2 \tilde{s}_2'^p \\ B^T &= \begin{bmatrix} \Phi_{r1}^T \\ \frac{1}{2} L_1 \Phi_{p1}^T \\ \Phi_{r2}^T \\ \frac{1}{2} L_2 \Phi_{p2}^T \end{bmatrix} = \begin{bmatrix} 0_{3 \times 3} \\ 0_{3 \times 3} \\ -I_{3 \times 3} \\ -\tilde{s}_2'^p A_2^T \end{bmatrix} \end{aligned} \quad (4.27)$$

Input for Jacobian Matrix Φ_q

$$\Phi_q = [\Phi_{r1}, \Phi_{p1}, \Phi_{r2}, \Phi_{p2}] = \begin{bmatrix} I_{3 \times 3} & 2G_1 \tilde{s}_1'^p & -I_{3 \times 3} & -2G_2 \tilde{s}_2'^p \end{bmatrix}$$

By applying moment about ζ -axis to the sample shown in **Figure 4.2.**, the value of euler parameter can be calculated in two different methods.

First, it can be calculated by using the close form solution. [13, page 166] $\zeta \parallel z$ result in Euler Parameter:

$$\begin{aligned} p_{cal} &= \left[\cos \frac{\phi}{2} \quad 0 \quad 0 \quad \sin \frac{\phi}{2} \right]_{calc}^T = \begin{bmatrix} e0 & e1 & e2 & e3 \end{bmatrix}_{calc}^T \\ J_{zz} \ddot{\phi} &= n'_\zeta \\ \ddot{\phi} &= \frac{n'_\eta}{J_{yy}} = \frac{0.0001}{20756.82 \times 10^{-9}} = 4.8176 \\ \phi &= \frac{1}{2} \times 4.8176 t^2 \end{aligned} \quad (4.28)$$

Where $t = 0 : 0.001 : 5$

Second, it can be calculated in Matlabs by using ode45 (**APPENDIX E** and (**APPENDIX F**)) to

obtain the result of euler parameter $p_{ode} = \begin{bmatrix} e_0 & e_1 & e_2 & e_3 \end{bmatrix}_{ode}^T$. The Figure illustrates the error of euler parameter from these two calculation methods by comparing the value of e_0 and e_3 .

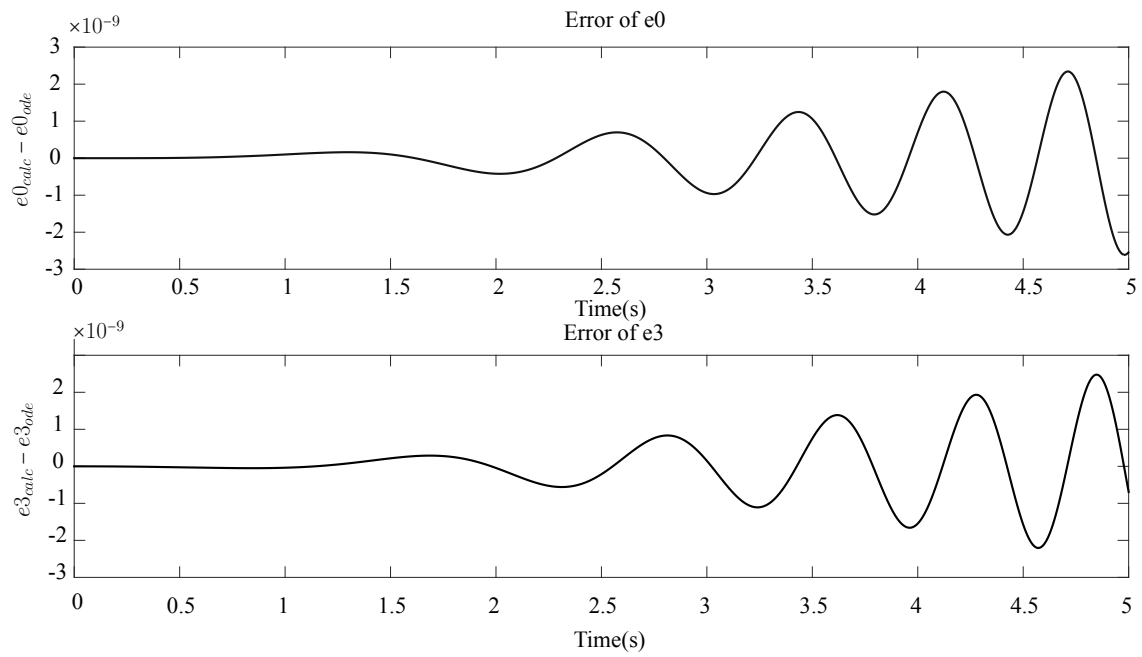


Figure 4.3. Error of Euler parameters between close form solution and Matlab ode

5. RESULTS AND DISCUSSION

The numerical results from the dynamic equations of motions **Eq. 4.19.** described the position and orientation of the system. Matlab program was used to solve this equation (See **Appendix G** and **Appendix H**) There are three cases of force to be considered. In the graph below, the orientation of body 7(Solar Panel) is represented by three different cases.

Case1: The force applied to the actuator(body 2 and 3) is:

$$f_2 = [0, 0, 4 \sin 4\pi t]^T \text{ N}$$

$$f_3 = [0, 0, 4 \sin 4\pi t]^T \text{ N}$$

Where f_2 and f_3 are the external force applied to body 2 and body 3 as illustrated in **Figure 4.1** respectively.

These two forces are expected to move the solar panel to rotate back and forth.

Case2: The external force is applied to body 7(Solar Panel).

$$f_7 = [0, 0, -3]^T \text{ N}$$

Where f_7 is the external force applied to body 7, see **Figure 4.1.**

This force is expected to move the solar panel to rotate and translate in the downward direction.

Case3: The external moment is applied to body 7 (Solar Panel) about η_7 axis.

$$n'_7 = [0, 0.1, 0]^T \text{ Nm}$$

Where n'_7 is the external moment applied to body 7, see **Figure 4.1.**

This moment is expected to move the solar panel to rotate about y-axis.

The simulation results to each cases are shown in **Figure 5.1.**, **Figure 5.2.**, and **Figure 5.3.** respectively.

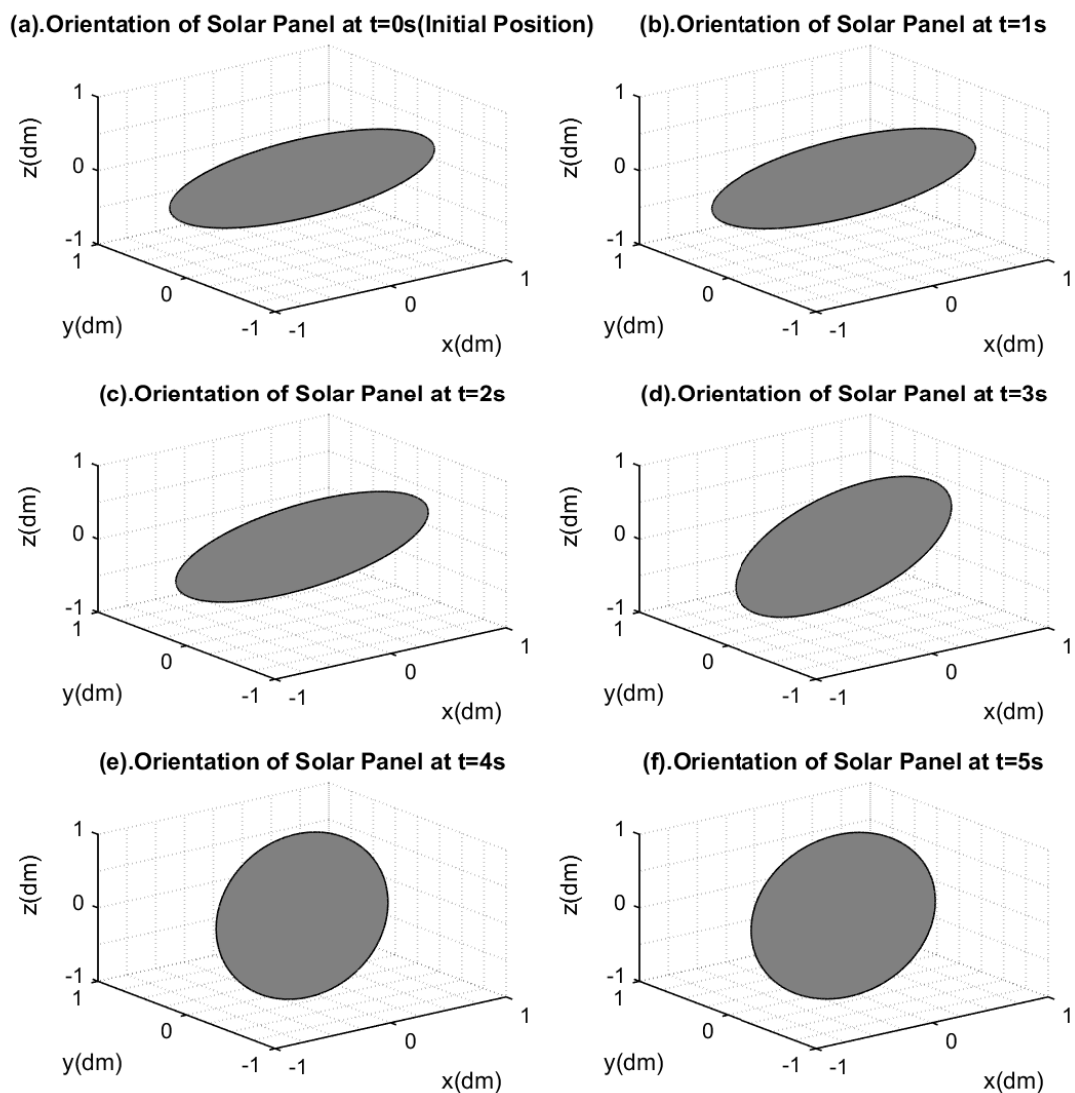


Figure 5.1. The orientation of solar panel with respect to time $t(s)$ for case 1, $f_2 = [0, 0, 4 \sin 4\pi t]^T N$ & $f_3 = [0, 0, 4 \sin 4\pi t]^T N$

See **Figure 4.1.** for body illustration.

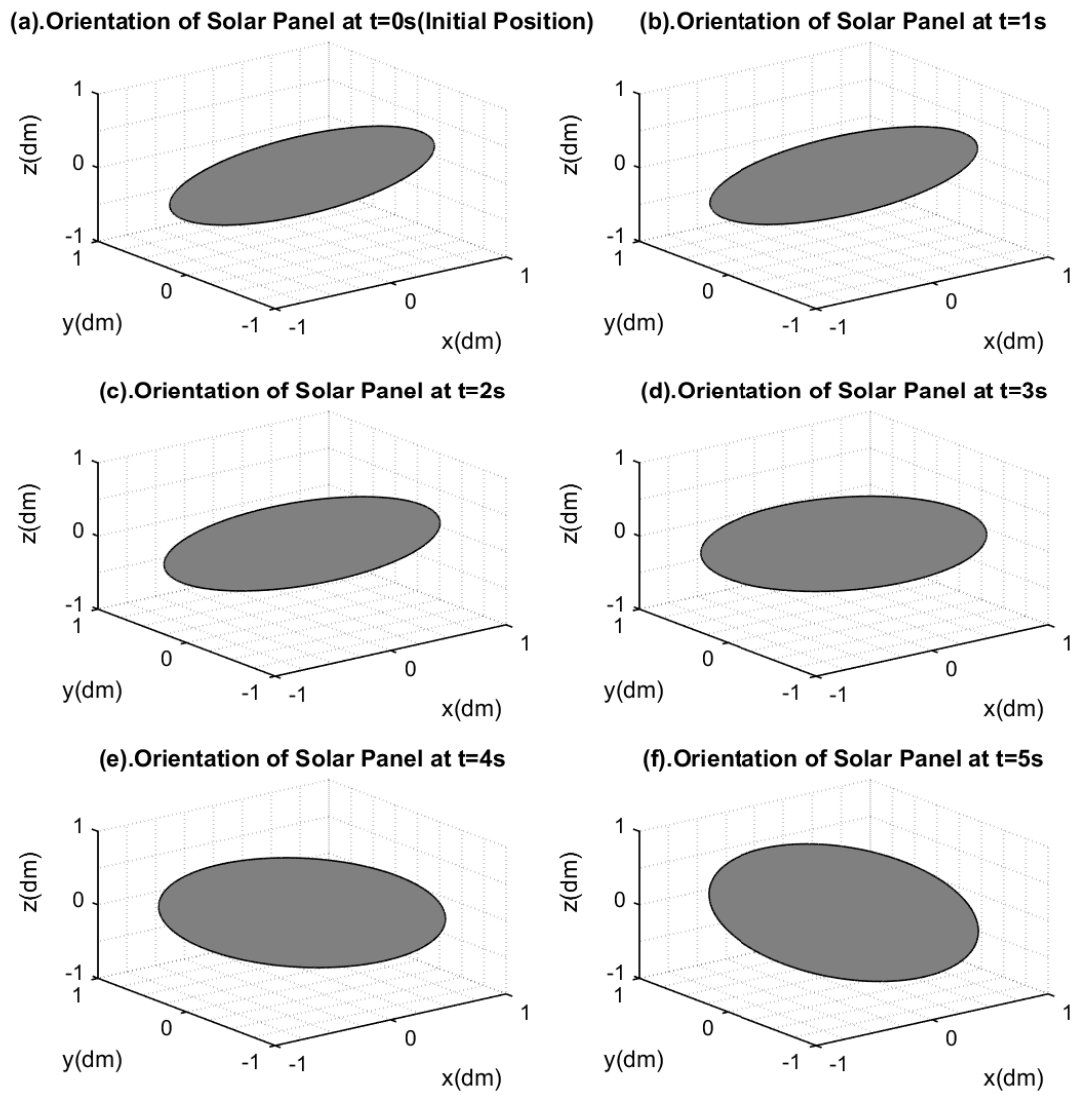


Figure 5.2. The orientation of solar panel with respect to time $t(s)$ for case 2, $f_7 = [0, 0, -3]^T N$

See **Figure 4.1.** for body illustration.

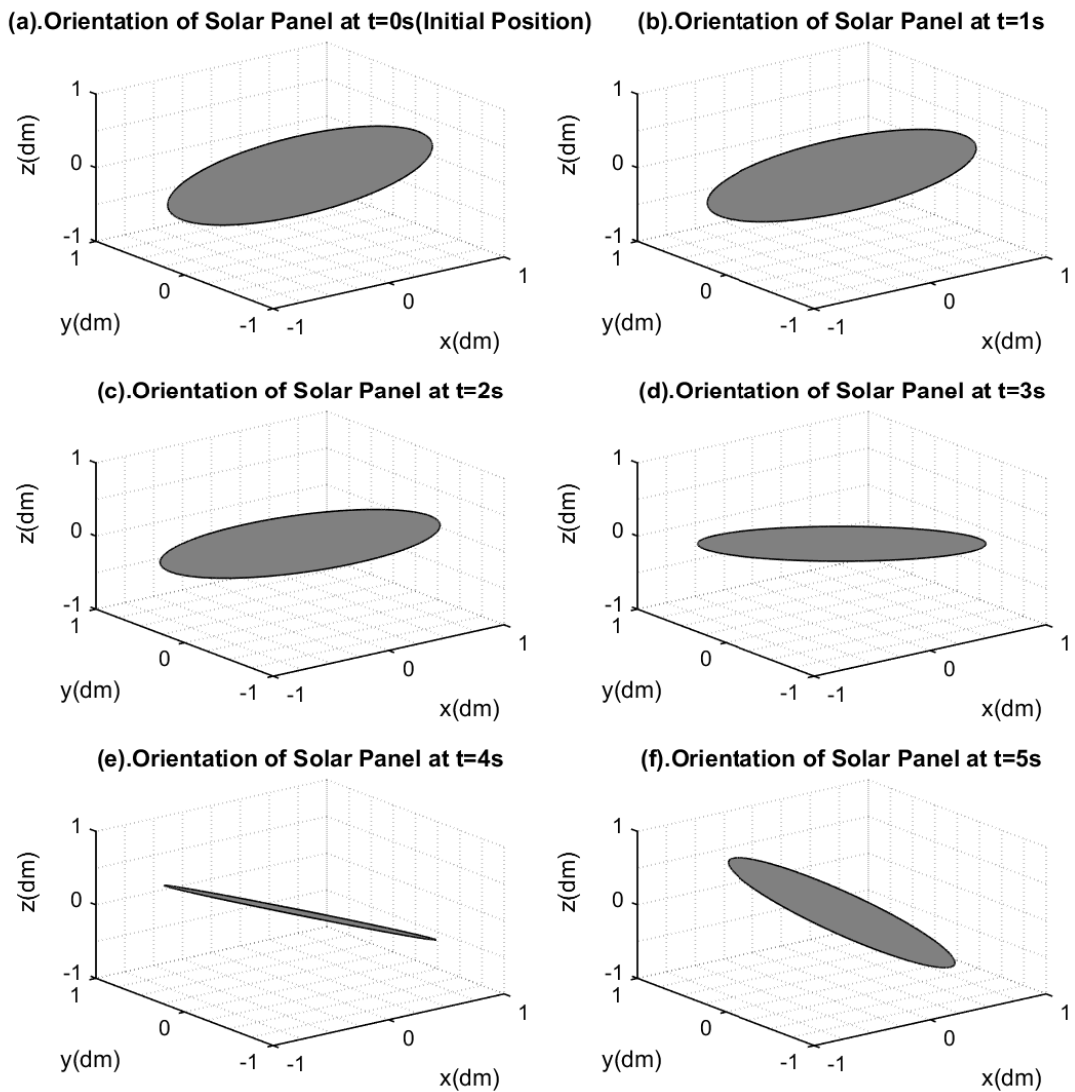


Figure 5.3. The orientation of solar panel with respect to time $t(s)$ for case 3, $n_7^l = [0, 0.1, 0]^T N$

See **Figure 4.1.** for body illustration.

Overall, the result of the study showed that the movement of solar panel can be illustrated corresponding to the dynamic equations. After applying the force in three cases as mentioned above, the orientation of solar panel is moved as described in each cases. Therefore, we are definitely able to handle with forces from any direction applied on the parallel mechanism system.

6. CONCLUSIONS AND RECOMMENDATION

6.1. Conclusions

In summary, the modeling of the behavior in terms of algebraic-differential equations for 2 DOF Parallel Mechanism is obtained in this thesis. The study result demonstrates that the equation of motion **Eq. 4.19.** derived above can fully describe the motion of each body . This is justified by the change of orientation of the solar panel with respect to the different conditions of the external forces. The result also implies that we can observe the response of the mechanism with respect to the external applied-forces from any directions.

6.2. Recommendation for Future Works

Generalized Coordinates System is introduced for my future research. There are more benefits such that the number of coordinates to describe the system could be reduced. Accordingly, the number of generalized coordinates is defined as the number of degree of freedom of the system. Simultaneously, there are less number of differential equations. Moreover, there is also less algebraic constraint equations obtained, which result in better computational efficiency.

After obtaining the dynamic modeling, control using existing controller will be carried out and discuss. Moreover, to validate the simulation result, the prototype will be built.

References

- [1] RH McFee. Power collection reduction by mirror surface nonflatness and tracking error for a central receiver solar power system. *Applied optics*, 14(7):1493–1502, 1975.
- [2] M Comsit and I Visa. Design of the linkages type tracking mechanisms of the solar energy conversion systems by using multi body systems method. 2007.
- [3] Oscar Altuzarra, Erik Macho, Jokin Aginaga, and Victor Petuya. Design of a solar tracking parallel mechanism with low energy consumption. *Proceedings of the Institution of Mechanical Engineers, Part C: Journal of Mechanical Engineering Science*, 229(3):566–579, 2015.
- [4] Jun Wu, Xiaolei Chen, and Liping Wang. Design and dynamics of a novel solar tracker with parallel mechanism. *IEEE/ASME Transactions on Mechatronics*, 21(1):88–97, 2016.
- [5] Michael Boles Yunus Cengel. *Thermodynamics: An Engineering Approach*. McGraw-Hill Science/Engineering/Math.
- [6] Ahmed Rhif and Sundarapandian Vaidyanathan. Sliding mode control design for a sensorless sun tracker. In *Applications of Sliding Mode Control in Science and Engineering*, pages 419–434. Springer, 2017.
- [7] Hossein Mousazadeh, Alireza Keyhani, Arzhang Javadi, Hossein Mobli, Karen Abrinia, and Ahmad Sharifi. A review of principle and sun-tracking methods for maximizing solar systems output. *Renewable and sustainable energy reviews*, 13(8):800–1818, 2009.
- [8] NH Helwa, ABG Bahgat, AMR El Shafee, and ET El Shenawy. Maximum collectable solar energy by different solar tracking systems. *Energy sources*, 22(1):23–34, 2000.
- [9] M Stern, G Duran, G Fourer, K Mackamul, W Whalen, M van Loo, and R West. Development of a low-cost integrated 20-kw-ac solar tracking subarray for grid-connected pv power system applications. final technical report. Technical report, National Renewable Energy Lab., Golden, CO (US); Utility Power Group, Chatsworth, CA (US), 1998.
- [10] P Yu Vorobiev, J González-Hernández, and Yuri V Vorobiev. Optimization of the solar energy collection in tracking and non-tracking photovoltaic solar system. In *Electrical and Electronics Engineering, 2004.(ICEEE). 1st International Conference on*, pages 310–314. IEEE, 2004.

- [11] Tung-Sheng Zhan, Whei-Min Lin, Ming-Huang Tsai, and Guo-Shiang Wang. Design and implementation of the dual-axis solar tracking system. In *Computer Software and Applications Conference (COMPSAC), 2013 IEEE 37th Annual*, pages 276–277. IEEE, 2013.

- [12] Stefano Mauro, Alessandro Battezzato, Gabriele Biondi, and Cristina Scarzella. Design and test of a parallel kinematic solar tracker. *Advances in Mechanical Engineering*, 7(12): 1687814015618627, 2015.

- [13] Parviz E Nikravesh. *Computer-aided analysis of mechanical systems*, volume 186. Prentice-hall Englewood Cliffs, NJ, 1988.

APPENDIX A

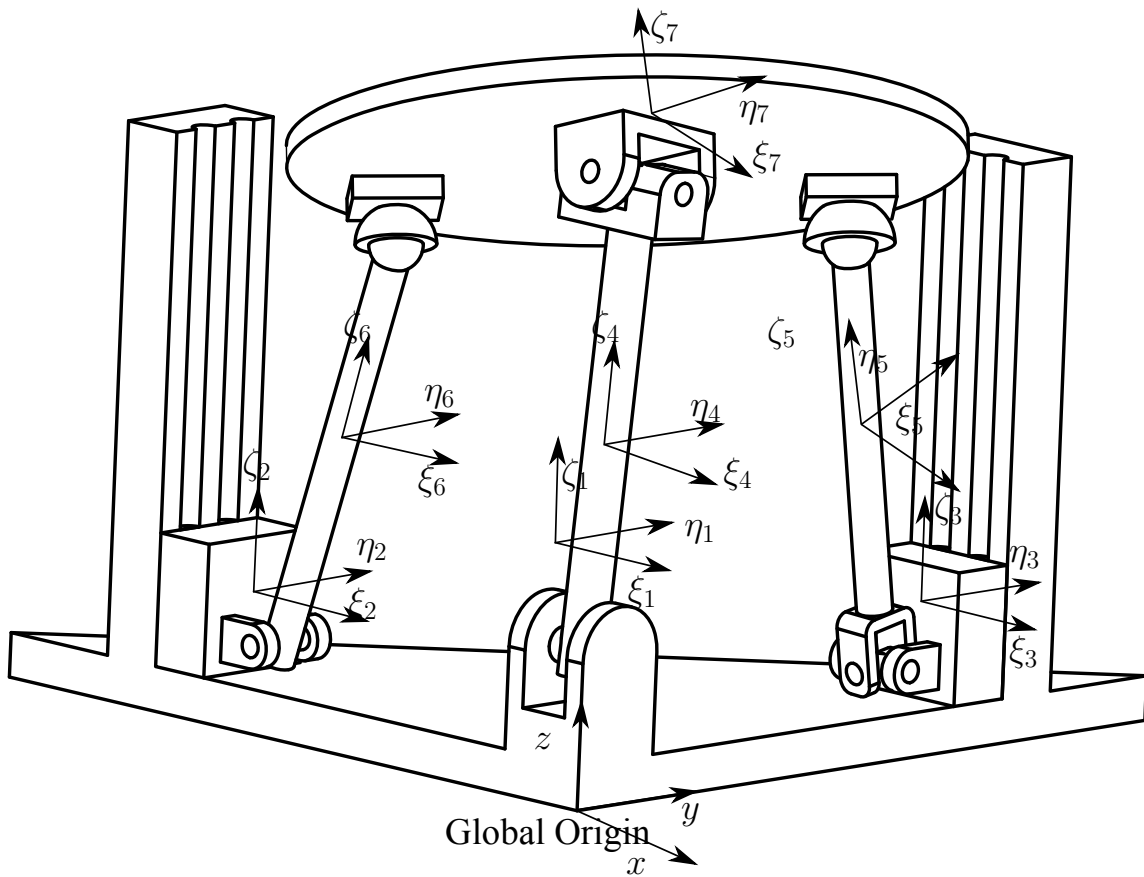


Figure 6.1. Global and Local coordinates

APPENDIX B

Table 6.1. Mass (m), Vector from origin to center of mass (r) Initial Euler parameter of each body (p) from SolidWorks Model

Symbols	Description	Value	Unit
$m1$	Mass of body number 1	475.09×10^{-3}	Kg
$m2$	Mass of body number 2	189.7×10^{-3}	Kg
$m3$	Mass of body number 3	189.7×10^{-3}	Kg
$m4$	Mass of body number 4	104.45×10^{-3}	Kg
$m5$	Mass of body number 5	53.25×10^{-3}	Kg
$m6$	Mass of body number 6	54.4×10^{-3}	Kg
$m7$	Mass of body number 7	890.5×10^{-3}	Kg
$r1$	Vector $r1$	$10^{-3}[-63.93 \ 63.93 \ 30.41]^T$	m
$r2$	Vector $r2$	$10^{-3}[-123.99 \ 15 \ 24.6]^T$	m
$r3$	Vector $r3$	$10^{-3}[-15 \ 123.99 \ 24.6]^T$	m
$r4$	Vector $r4$	$10^{-3}[-11.50 \ 18.37 \ 99.21]^T$	m
$r5$	Vector $r5$	$10^{-3}[-12.99 \ 98.33 \ 68.84]^T$	m
$r6$	Vector $r6$	$10^{-3}[-92.31 \ 15 \ 66.27]^T$	m
$r7$	Vector $r7$	$10^{-3}[-34.28 \ 42.89 \ 136.56]^T$	m
$p1$	Initial Euler parameter of body 1	$[1 \ 0 \ 0 \ 0]^T$	
$p2$	Initial Euler parameter of body 2	$[1 \ 0 \ 0 \ 0]^T$	
$p3$	Initial Euler parameter of body 3	$[1 \ 0 \ 0 \ 0]^T$	
$p4$	Initial Euler parameter of body 4	$[0.9987 \ 0.0517 \ 0 \ 0]^T$	
$p5$	Initial Euler parameter of body 5	$[0.9955 \ 0.0906 \ 0.020001 \ -0.00398]^T$	
$p6$	Initial Euler parameter of body 6	$[0.9880 \ 0 \ 0.1545 \ 0]^T$	
$p7$	Initial Euler parameter of body 7	$[0.9768 \ -0.1355 \ -0.1482 \ 0.0188]^T$	

APPENDIX C

Table 6.2. Inertia Matrix for each body from SolidWorks Model

Symbols	Description	Value	Unit
J'_1	Inertia matrix of body number 1	$\begin{bmatrix} 0.0020 & 0.0008 & -0.0001 \\ 0.0008 & 0.0020 & 0.0001 \\ -0.0001 & 0.0001 & 0.0026 \end{bmatrix}$	Kgm^2
J'_2	Inertia matrix of body number 2	$10^{-4} \begin{bmatrix} 0.2774 & 0 & -0.0102 \\ 0 & 0.2015 & 0 \\ -0.0102 & 0 & 0.1987 \end{bmatrix}$	Kgm^2
J'_3	Inertia matrix of body number 3	$10^{-4} \begin{bmatrix} 0.2015 & 0 & 0 \\ 0 & 0.2774 & 0.0102 \\ 0 & 0.0102 & 0.1987 \end{bmatrix}$	Kgm^2
J'_4	Inertia matrix of body number 4	$10^{-3} \begin{bmatrix} 0.1217 & 0.0000 & 0 \\ 0.0000 & 0.1248 & 0 \\ 0 & 0 & 0.0054 \end{bmatrix}$	Kgm^2
J'_5	Inertia matrix of body number 5	$10^{-4} \begin{bmatrix} 0.5827 & 0 & -0.0824 \\ 0 & 0.5940 & 0 \\ -0.0824 & 0 & 0.0172 \end{bmatrix}$	Kgm^2
J'_6	Inertia matrix of body number 6	$10^{-4} \begin{bmatrix} 0.6242 & 0 & 0 \\ 0 & 0.6231 & -0.0000 \\ 0 & -0.0000 & 0.0058 \end{bmatrix}$	Kgm^2
J'_7	Inertia matrix of body number 7	$\begin{bmatrix} 0.0012 & 0.0000 & 0.0001 \\ 0.0000 & 0.0012 & 0.0000 \\ 0.0001 & 0.0000 & 0.0024 \end{bmatrix}$	Kgm^2

REPORT PART II

**DYNAMIC MODELING AND SIMULATION FOR A
PARALLEL-MECHANISM-MOUNTED UAV**

ABSTRACT

Our work proposes a promising methodology to extend the flight duration of a Vertical Take-Off and Landing Unmanned Aerial Vehicle (VTOL UAV). This is done by mounting a 2 degree of freedom (DOF) parallel mechanism-based solar tracker on the UAV. The integration of the solar tracker was considered with the aim to maximize the energy collection from the sun. The parallel mechanism was chosen because it has been reported to consume lower energy to drive the mechanism during the sun tacking when compared to other mechanisms in the literature.

In this thesis, we present kinematic, inverse kinematic, dynamic modeling and simulation for the system. Kinematic and inverse kinematic for the tracker is briefly described using classical method. Dynamic modeling for the system is one of the most challenging engineering problems. To deal with it, kinematic constraints of all joints are determined. Undetermined close form reaction forces at joints are obtained from the kinematic constraints. Using Newton's method, dynamic equation for each body exerted by external forces and reaction forces is formulated. A fully determined equation, which is a system of algebraic-differential equations, is obtained by appending kinematic and dynamic equations. For both kinematic and dynamic equations, Cartesian coordinate and Euler parameter are used to describe translation and rotation motions respectively.

To verify the dynamic equation, we examine a simple system with two bodies connected by a spherical joint. Then we study the dynamic behaviour of a hexacopter-solar tracker system. Three case studies were considered in the simulation study of this system. In case 1, we investigated the system behaviour during its hover without forces applied on the actuators. In case 2, we applied forces on the solar tacker actuators of case 1. In case 3, in addition to the forces applied on the solar tacker actuators, we applied the upward thrust to lift the system vertically from its initial position. We have observed that after about 0.45 to 0.5 s, the simulation induced large error causing simulation to stop. It happened due to high stiff differential equation of zigzag motion of the tracker.

NOMENCLATURE

DOF	Degree of Freedom
γ	Vector of right-hand side of acceleration equations
$\xi_i \eta_i \zeta_i$	Local (body-fixed) Cartesian coordinate system
ω_i	Angular velocity of each rotors
ω'	Angular velocity vector of the system that defined in Body-fixed frame
Φ	Vector of constraint
Φ_q	Jacobian matrix of constraints
b_1, b_2	Vectors from the center of mass of the hexacopter to the axes of the two linear actuators
a_k	Vector from the center of mass of the hexacopter to the axis of propeller k
d	Vector with its end on two different bodies(Variable magnitude)
e_0, e_1, e_2, e_3	Euler parameter variable
e_i	Vector of three Euler parameters e_1, e_2, e_3 for body i
f	Total thrust force of the system
τ_p	Total torque of the system
g	Vector of forces for a system
u_p	Vector input of angular velocity
m	Mass of a particle
u_7, u_8	Vector force on the linear actuators
u	Vector input of the force of the hold system
p_i	Vector of four Euler parameters e_0, e_1, e_2, e_3 for body i
q_i	Vector of coordinates for body i
q	Vector of coordinates for a system
r_i	Translational position vector with respect to Global frame for body i
s_i	Vector with both ends on body i (constant magnitude) with respected to Global frame
s'_i	Vector with both ends on body i (constant magnitude) with respect to Body-fixed frame
t	Time
n'	Unit vector in the body-fixed frame
n	Unit vector in the global frame
xyz	Global Cartesian coordinate system

A_i	Rotational transformation matrix for body i in Euler parameter
R_I^B	Rotational transformation matrix of body-fixed frame respected to global frame
G_i	3×4 transformation matrix for body i
I	Identity matrix
λ	Vector of Lagrange multiplier
J'_i	Local (constant) inertia tensor for body i
L_i	3×4 transformation matrix for body i
M_i	6×6 mass matrix for body i containing N_i and J'_i
M	Mass matrix for a system
N_i	3×3 diagonal mass matrix for body i
\mathbf{r}	Vector of link OO_3
r	Length of link OO_3
l	Length from the center of mass to the propeller arms
k_f, k_τ	The rotor specific parameter
\mathbf{a}_i	The position vector of point A_i with respect to $O - xyz$
\mathbf{b}_i	The position vector of point B_i with respect to $O - x_3y_3z_3$
q_i	The height of slider
r_i	The length of link B_iC_i
z_i	The position vector of link B_iC_i

TABLE OF CONTENTS

ABSTRACT	i
NOMENCLATURE	ii
TABLE OF CONTENTS	iv
LIST OF FIGURES	v
LIST OF TABLES	vi
1 INTRODUCTION	1
1.1 Background	1
1.2 Problem Statement	1
1.3 Goal and Objective	1
1.4 Scope	2
2 LITERATURE REVIEW	3
2.1 Unmanned Aerial Vehicle	3
2.2 Solar Tracking Mechanism	4
2.3 Principles of Solar tracker	6
2.4 Energy Output Improvement	6
3 KINEMATIC MODELING FOR MULTI RIGID-BODY UAV	7
3.1 Classical Kinematic Equation for Parallel-Mechanism-Mounted UAV	7
3.2 Inverse Kinematic Equation for Parallel-Mechanism-Mounted UAV	11
4 DYNAMIC MODELING FOR MULTI RIGID-BODY UAV	16
4.1 Dynamic Modeling for UAV	16
4.2 Matlab simulink for UAV	21
4.3 Dynamic Modeling for Multi Rigid-Body UAV	21
4.4 Matlab simulink for Multi Rigid-Body UAV	26
4.5 Summery	28
5 SIMULATION RESULT AND DISCUSSION	29
5.1 Simulation result of Hexacopter	29
5.2 Result of simulation parallel-mechanism-mounded UAV	30
6 CONCLUSION AND RECOMMENDATION	36
References	37
APPENDICES	39

LIST OF FIGURES

Figure 2.1:Single-axis of solar tracker	4
Figure 2.2:Types of dual-axis tracking systems (azimuthal-a, polar-b)	5
Figure 2.3:The U-2PUS parallel pointing system	5
Figure 3.1:Parallel-mechanism system	7
Figure 3.2:Parallel-mechanism-mounted UAV	8
Figure 3.3:Variable length and angle of Parallel-mechanism system	9
Figure 4.1:Hexacopter	16
Figure 4.2:A model of hexacopter	18
Figure 4.3:Flow simulation of hexacopter	21
Figure 4.4:Flow simulation for a parallel-mechanism-mounted UAV	27
Figure 4.5:Flow of work	28
Figure 5.1:Parallel-mechanism-mounted UAV	29
Figure 5.2:Position of the center of mass of hexacopter with respect to the global frame	30
Figure 5.3:Case 1: Position of the epicenter of hexacopter (body 1), actuators (body 2 and 3), and platform attached solar panel (body 7)at the hover point with respect to the global frame	33
Figure 5.4:Case 2: Position of the epicenter of hexacopter (body 1), actuators (body 2 and 3), and platform attached solar panel (body 7)at the hover point with respect to the global frame	34
Figure 5.5:Case 3: Position of the epicenter of hexacopter (body 1), actuators (body 2 and 3), and platform attached solar panel (body 7) with respect to the global frame	35
Figure 6.1:Rotation about x axis	39
Figure 6.2:Pitch angle about y axis	40
Figure 6.3:Yaw angle around z axis	40
Figure 6.4:Vector diagram for derivation of rotation formula	42

LIST OF TABLES

Table 4.1: Components in the Expansion of the Most Common Constraints . . .	24
Table 4.2: Components in the Expansion of the Most Common Constraints . . .	24
Table 5.1: Values of parameters for simulation	31
5.2 Values of vector length for simulation	31
5.3 Values of moment inertia for simulation	32

1. INTRODUCTION

1.1. Background

Unmanned Aerial Vehicles (UAVs) have been widely used to carry cameras, sensors or products for applications such as mapping, frame monitoring, goods delivery, entertainment and more. The most common UAVs are powered by battery only, which have limitation of operation duration. However, current batteries of the system depending on vehicle, payload, and wind conditions enable only flights up to 30 min for quadrotors(Mansouri, Karvelis, Georgoulas, & Nikolakopoulos, 2017), which can limit the usage of these UAVs for long time missions and experiments. On the other hand, solar energy systems have emerged as a viable source of renewable energy over the past two or three decades, and are now widely used in a variety of industrial and domestic applications. Such systems are designed to collect the energy from the sunlight and convert it into electrical power (Polk, 2016). The parallel mechanisms is a good one for saving energy in the system. Parallel mechanisms have a large payload to mass ratio and high stiffness. It is possible to reduce the driving torque, scale down the dimension of the mounting and reduce the complexity of the system (Wu, Chen, & Wang, 2016).

1.2. Problem Statement

The battery supply for UAV has limitation for flying. Battery powered electric UAVs suffer from uncertainties in estimating the remaining charge and hence most flight plans are highly conservative in nature. On the other hand, the battery decrease in capacity with time and usage during operating (Saha et al., 2011). The output current plays a big role in determining the losses inside a battery and is an important parameter to consider when analyzing battery performance (Hartmann et al., 2008). For a long-time mission like large farm observation or border monitoring, a UAV must rebound to its recharging station, which limits its operation range. A technology of energy supply which makes a UAV operate longer and be able to recharge anywhere during its mission will be of an advantage for continuous operation.

1.3. Goal and Objective

The purpose of this work is to study the dynamics behaviour of the parallel mechanism mounted UAV. The attitude of hexacopter is simulated at the hover point and during its mobility when the parallel mechanism has motion. First, we derive the inverse kine-

matic equations for parallel-mechanism which are produced the stroke of the linear actuators as a driver to movability of the parallel mechanism. To describe the behaviour of the whole system, dynamic modeling has been derived. Simulation for a parallel-mechanism-mounted UAV is using to validate the dynamic motion.

1.4. Scope

Dynamic modeling and simulation has been modeled. The total thrust and torque are generated at the hover point and during mobility but the whole system does not have a feedback controller. On the other hand, reaction forces and the coordinates describing motion of a system are obtained from solving the differential equations. The reaction force has an advantage for mechanical structure design. However, the analysis of reaction forces is out of scope of this work. We work on simulation but we do not have experiment for parallel-mechanism-mounted hexacopter. The attitude of the whole system has been explained with position of the hexacopter and the body attached with the solar panel.

2. LITERATURE REVIEW

2.1. Unmanned Aerial Vehicle

The Unmanned Aerial Vehicle (UAV) robot has gained demand on the worldwide markets. There are two types of UAV: fixed wing and rotary wings. One of the most popular is rotary wings UAV because it can take off and land in vertical condition. In addition, it has good mobility and ability on load capacity. The main challenges of rotary UAV for flying through corridors are the limited width and the required agility, especially in outdoor conditions where wind and gusts cause the UAV to drift (Mustapa, Saat, Husin, & Abas, 2014). The development of autonomous UAV has been growing fast as it is more reliable in the application. The automatic take-off system required to enable the UAV begin to fly from the ground. The system should ensure the height of hexacopter in a consistent condition. In these cases, all six motor propeller must produce a six forces against the gravitational force and able to lift the hexacopter. Most of multicopter platform utilize fixed-pitch propellers that control the platform by changing of the rotational velocities (Verbeke, Hulens, Ramon, Goedeme, & De Schutter, 2014). The rotor in pitch does not vary as the blades rotate; control of vehicle motion is achieved by varying the relative speed of each rotor change the thrust and torque produce by each rotors (Allaka, Anasuya, Yamini, Vaidehi, & Ramana, 2011).

Effective and efficient energy supply by solar energy to power UAVs has been an active research for more than four decades. The first solar-powered UAV, Sunrise I of Astro Flight Inc., took its first flight in California in 1974 (Boucher, 1984). In 2003, possible use of a solar-powered UAV for agricultural decision support was reported by (Herwitz et al., 2003). In (Noth, 2008), continuous flight of solar-powered airplanes was considered, and a methodology used for the complete design was presented. It showed that the methodology was very useful and could be applied to a wide range of UAV sizes. With a mechanism simulating the motion of aircraft, virtual flight system was designed for evaluation of a solar-powered UAV by (J.-S. Lee, Park, Jung, & Kee-Ho, 2013). The system also involved power measurement circuit which is designed for monitoring the flow of energy. For improving efficiency of solar energy collection, a UAV with onboard solar tracking system was designed and constructed by (Tegeeder, 2007).

2.2. Solar Tracking Mechanism

Solar trackers can be divided into single-axis trackers and dual-axis trackers by taking into account the mechanical characteristics. The single axis sun tracker only tracks the sun in one direction, from east to west, which is azimuth direction which shows in **Fig. 2.1** (K.-Y. Lee et al., 2017). Lubitz presented that a single-axis sun tracker and a dual-axis sun tracker increase annual solar irradiation incident by an average of 29% and 34% relative to the fixed tilt angle, respectively (Lubitz, 2011). The linear actuator is used for drive the system of single-axis movability with the direction of the sunlight. The



Figure 2.1. Single-axis of solar tracker

dual-axis tracker has two rotational motions which are precise with the trajectory of the sun. Depending on the relative position of the revolute axes, there are two basic types of dual-axis tracking system: azimuthal and polar that shows in **Fig. 2.2**. For the azimuthal trackers, the daily motion is made by rotating the panel around the vertical axis. The polar tracking has two independent motions. The motion is made by the rotating the panel around the polar axis.

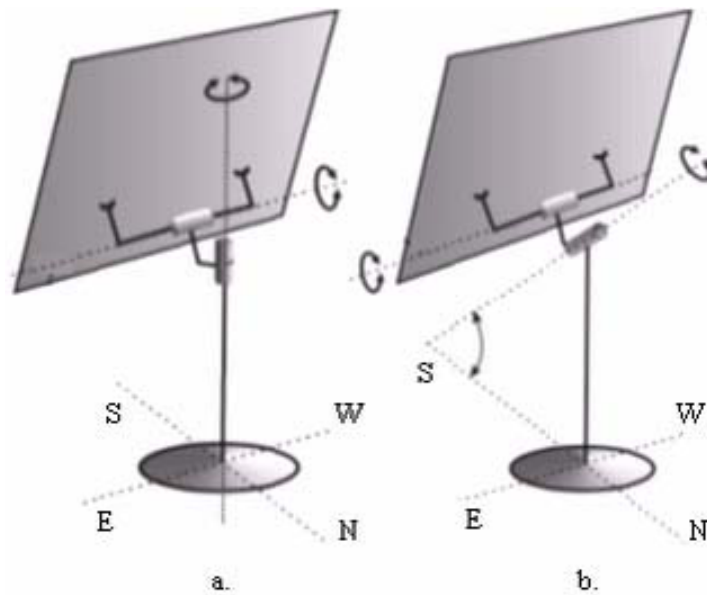


Figure 2.2. Types of dual-axis tracking systems (azimuthal-a, polar-b)

On the other hand, the solar tracker using a U-2PUS parallel robot which has two rigid bodies: one movable platform (MP) and fixed platform (BP) which are linked through two actuators revolute joints. A unique passive universal joint, referred to as gimbal, exhibits the same function of the two revolute joints of the serial mechanism (Cammarata, 2015) in **Fig. 2.3**. The system is connected by a number of kinematic chains (legs). The gimbal can be positioned near the center of hydrodynamic pressure to reduce the torque generated by the thrust of the wind on the surface of the panel. This solution implies smaller actuators as these should only sustain the weight of the structure (Cammarata, 2015)-(Di Gregorio & Sinatra, 2002).

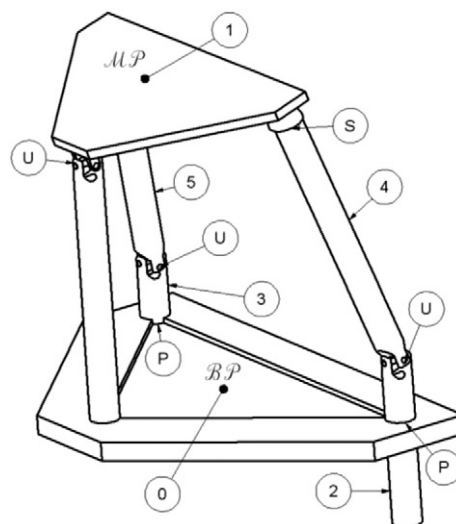


Figure 2.3. The U-2PUS parallel pointing system (Cammarata, 2015)

2.3. Principles of Solar tracker

The position tracking also applies the photosensor balance technique. Two DOF are used for the north/south motion, and another two are used for the east/west motion. At the end of the day, the panel is stationary at the position, moving back the panel to the north direction of the morning by the photosensors receiving light (Hoffmann, Molz, Kothe, Nara, & Tedesco, 2018)-(Al-Mohamad, 2004). Since two-axis systems can achieve an optimal tracking of the sun, they are more popular in all the types of concentrated solar technologies (Al-Mohamad, 2004). Literally, single and dual axis solar trackers are the systems that improve energy efficiency by optimizing collection of sun light irradiating on solar panel. In (Tegeder, 2007), a single-axis solar tracker was designed and tested. The tracking system autonomously rotated an onboard solar panel to find the angle of maximum solar irradiance while the UAV was found to have the maximum and minimum of net energy gain over a conventional solar-powered UAV of 34.5 % and 0.8 % respectively.

2.4. Energy Output Improvement

Dual axis solar tracker has been an interesting research topic for many researchers, because it can outperform single axis solar tracker (Mousazadeh et al., 2009)-(Wu et al., 2016). Many researches on energy gain from solar tracking systems compared to tilted fixed systems have conducted theoretically and experimentally (Mousazadeh et al., 2009). Energy gain from a single axis solar tracker was reported to be 20% (Stern et al., 1998) while energy gain from a dual axis solar tracker was 30-40% (Vorobiev, González-Hernández, & Vorobiev, 2004). J. Wu et al proposed a two-axis decoupled solar tracking system based on parallel mechanism and showed that the tracker requires less driving torque, thus less power dissipation than the conventional serial tracker does (Wu et al., 2016). Furthermore, the tracking system does not need reducer with large reduction ratio. Therefore, complexity and weight of the system are also reduced.

3. KINEMATIC MODELING FOR MULTI RIGID-BODY UAV

3.1. Classical Kinematic Equation for Parallel-Mechanism-Mounted UAV

Kinematics is the study of the motion of the rigid bodies. Classical Kinematic equation of parallel mechanism is analysed in the geometric of the system, which determined the stroke of the linear actuators. Moreover, the motion of the parallel mechanism has been controlled by the stroke of actuators which is moving along z -axis.

Figure 3.1 describes the coordinate system of parallel mechanism which is used as dual axis solar tracker. A moving coordinate system $O - x'_3y'_3z'_3$ is established at point O_3 and the z_3 -axis is along the direction normal to the moving platform. The two rotation axes of the universal joint are parallel to x'_3 and y'_3 axes, respectively. The orientations of rotation of $O_3 - x'_3y'_3z'_3$ with respect to $O_3 - x_3y_3z_3$ can be described by angle (ϕ, θ) in **Fig. 3.3** associated with the rotations about the two axes of the universal joint of the RU joint. **Figure 3.1** also shows the parallel mechanism has 7 rigid bodies connected with joints. Each body has body-fixed coordinate as illustrated in the figure. Body 7 is connected with body 5 and 6 via 2 spherical joints (S) and with body 4 via a universal joint (U). Body 6 is connected to body 2 via a revolute joint (R). Body 5 is connected to body 3 via a universal joint. Body 2 and 3 are connected with body 1 via another translational joints (T). The actuators exert forces on body 2 and 3 along vertical axes.

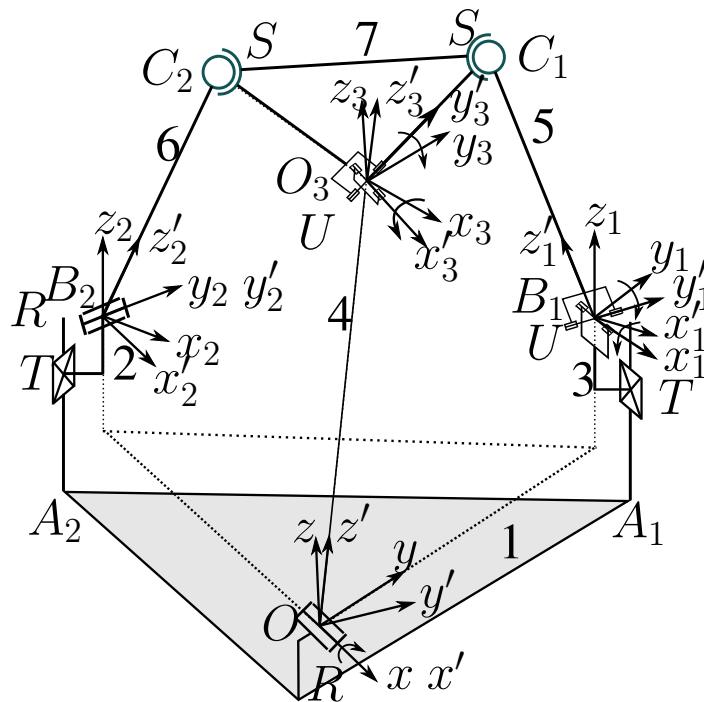


Figure 3.1. Parallel-mechanism system

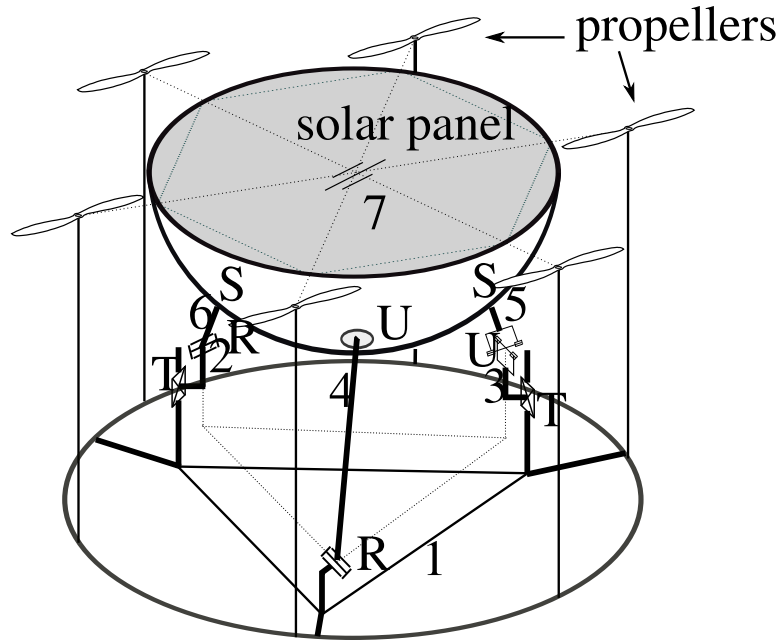


Figure 3.2. Parallel-mechanism-mounted UAV

Figure 3.2 shows the parallel mechanism mounted on hexacopter. Body numbers are labeled as illustrated in the figure. Body fixed frame for the hexacopter (body 1) is attached at the center of mass of the body. Parallel mechanism is a system of solar tracking which is used as dual axis solar trackers, it has been defined the degree of freedom that configuration the motion of the system. DOF for spatial mechanism can be defined by (Nikravesh, 1988):

$$DOF = 6(b - 1) - \sum_{k \in T_J} (n_k c_k) \quad (Eq. 3.1)$$

where b is the number of the body; n_k is the number of each type of joints; c_k is the number of constraints for each type of joints; and T_J is the set of types of joints. For the parallel mechanism shown in **Fig. 3.2**, denote S , U , R and T as spherical joint, universal joint, revolute joint, and translational joint, respectively. Then, we have $b = 7$, $T_J = [S, U, R, T]$, $n_k \in T_J = [2; 2; 2; 2]$, and $c_k \in T_J = [3; 4; 5; 5]$. Therefore DOF can be calculated as:

$$DOF = 6(7 - 1) - 2 \times 3 - 2 \times 4 - 2 \times 5 - 2 \times 5 = 2$$

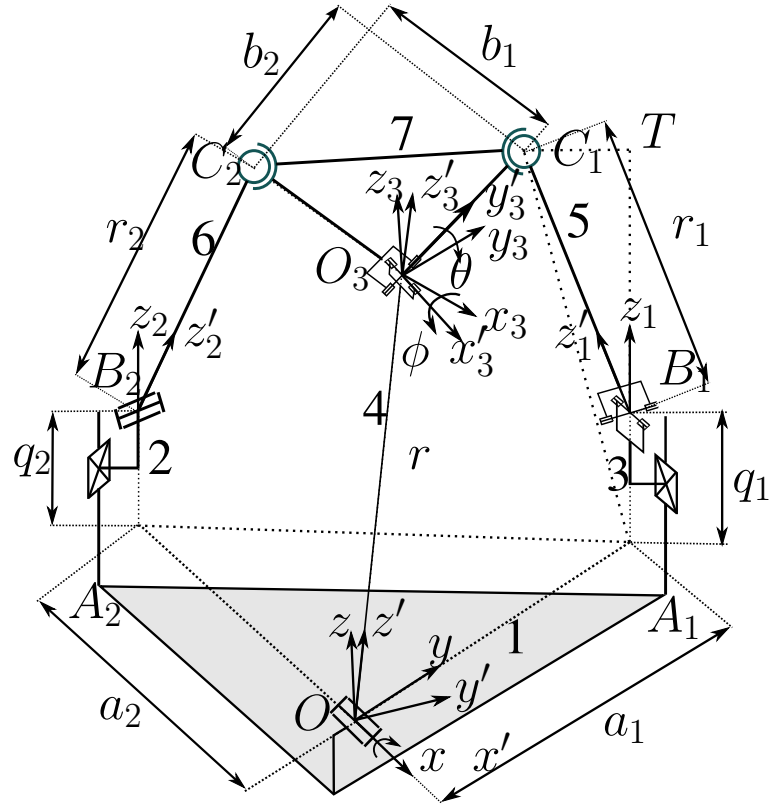


Figure 3.3. Variable length and angle of Parallel-mechanism system

The constraint equation for chain can be written in two ways as:

$$\begin{aligned}\overrightarrow{OO_3} &= \overrightarrow{OA_1} + \overrightarrow{A_1B_1} + \overrightarrow{B_1C_1} + \overrightarrow{C_1O_3} \\ \overrightarrow{OO_3} &= \overrightarrow{OA_2} + \overrightarrow{A_2B_2} + \overrightarrow{B_2C_2} + \overrightarrow{C_2O_3},\end{aligned}$$

where the length of all vectors are described in **Fig. 3.1**. The constraint equation can be expressed as follows

$$\mathbf{r} = r\mathbf{z} \quad (\text{Eq. 3.2})$$

$$\mathbf{r} = \mathbf{a}_i + q_i\mathbf{n}_3 + r_i\mathbf{z}'_i - \mathbf{b}_i \quad i = 1, 2, \quad (\text{Eq. 3.3})$$

where r and \mathbf{z}' are the length and unit vector of link OO_3 on body number 4, q_i is the height of slider on body 2 and 3, r_i and \mathbf{z}'_i are the length and the position unit vector of link B_iC_i on body 5 and 6, \mathbf{a}_i is the position vector of point A_i on body 1 with respect to $O - xyz$, \mathbf{b}_i is the position vector of point C_i on body 7 with respect to $O_3 - x_3y_3z_3$, and $\mathbf{n}_3 = [0 \ 0 \ 1]^T$ is a unit vector

$$\mathbf{r} - \mathbf{a}_i + \mathbf{b}_i = q_i \mathbf{n}_3 + r_i \mathbf{z}'_i$$

Let: $\mathbf{t}_i = \mathbf{r} - \mathbf{a}_i + \mathbf{b}_i$

We have

$$\mathbf{t}_i = q_i \mathbf{n}_3 + r_i \mathbf{z}'_i \quad (\text{Eq. 3.4})$$

$$\mathbf{z}'_i = \frac{\mathbf{t}_i - q_i \mathbf{n}_3}{r_i}$$

Multiplying both side of equation **Eq. 3.4** by $\mathbf{n}_3^T = [0 \ 0 \ 1]$ result:

$$\begin{aligned} \mathbf{n}_3^T \mathbf{t}_i &= q_i \mathbf{n}_3^T \mathbf{n}_3 + r_i \mathbf{n}_3^T \mathbf{z}'_i \\ \mathbf{n}_3^T \mathbf{t}_i &= q_i + r_i \mathbf{n}_3^T \mathbf{z}'_i \\ q_i &= \mathbf{n}_3^T \mathbf{t}_i - r_i \mathbf{n}_3^T \mathbf{z}'_i \end{aligned} \quad (\text{Eq. 3.5})$$

From equation **Eq. 3.5**, we need to find $r_i \mathbf{n}_3^T \mathbf{z}'_i$ on the geometric in **Fig. 3.3**. We have $\Delta A_1 C_1 T$ and $\Delta B_1 C_1 T$ are the triangles which has the right triangles in T .

$$e_1^2 = r_1^2 - (r_1 \mathbf{n}_3^T \mathbf{z}'_1)^2 \quad (\text{Eq. 3.6})$$

And

$$e_1^2 = t_1^2 - (\mathbf{n}_3^T \mathbf{t}_1)^2 \quad (\text{Eq. 3.7})$$

From equation **Eq. 3.6** and **Eq. 3.7**, we get:

$$\begin{aligned} r_1^2 - (r_1 \mathbf{n}_3^T \mathbf{z}'_1)^2 &= t_1^2 - (\mathbf{n}_3^T \mathbf{t}_1)^2 \\ (r_1 \mathbf{n}_3^T \mathbf{z}'_1)^2 &= r_1^2 + (\mathbf{n}_3^T \mathbf{t}_1)^2 - t_1^2 \\ (r_1 \mathbf{n}_3^T \mathbf{z}'_1) &= \sqrt{r_1^2 + (\mathbf{n}_3^T \mathbf{t}_1)^2 - t_1^2} \end{aligned} \quad (\text{Eq. 3.8})$$

Substituting equation **Eq. 3.8** into equation **Eq. 3.5**, yields:

$$\mathbf{q}_i = \mathbf{n}_3^T \mathbf{t}_i - \sqrt{r_i^2 + (\mathbf{n}_3^T \mathbf{t}_i)^2 - t_i^2}, \quad (\text{Eq. 3.9})$$

where $i = 1, 2$ is a number of position in chain. This **Eq. 3.9** describes the stroke of

the linear actuators when we know the rotation matrix to transform vector into the same reference. The degree of freedom of the system produces the two angle of rotation which is defined the matrix rotation of universal joint between body number 4 and body number 7 as shows in **Fig. 3.3**.

3.2. Inverse Kinematic Equation for Parallel-Mechanism-Mounted UAV

Parallel mechanism has two degree of freedom which is rotated in two different axis. Inverse kinematic is used to determine the angles rotated of the system which produces the rotation matrix. Moreover, rotation matrix has transformed the motion of the system from body-fixed frame to the global frame by multiply on the right hand side of the equation.

Rotational matrix of the system has been rotated about two axis: x -axis (angle ϕ) and y -axis (angle θ) that are parallel to axis of the universal joint. Basic rotation matrix around axis is described in *Appendices*. The rotation matrix R_7^{UAV} transforms from body-fixed frame (7) to the global frame (UAV) defined by

$$\begin{aligned}
 R_7^{UAV} &= R(\phi, \theta) = R_x(\phi) R_y(\theta) \\
 &= \begin{bmatrix} 1 & 0 & 0 \\ 0 & \cos \phi & -\sin \phi \\ 0 & \sin \phi & \cos \phi \end{bmatrix} \begin{bmatrix} \cos \theta & 0 & \sin \theta \\ 0 & 1 & 0 \\ -\sin \theta & 0 & \cos \theta \end{bmatrix} \\
 R_7^{UAV} &= \begin{bmatrix} \cos \theta & 0 & \sin \theta \\ \sin \phi \sin \theta & \cos \phi & -\sin \phi \cos \theta \\ -\cos \phi \sin \theta & \sin \phi & \cos \phi \cos \theta \end{bmatrix} \quad (Eq. 3.10)
 \end{aligned}$$

Scenario 1: Sunlight direction sensor is mounted on the UAV

The transformational vector related from body-fixed frame to the global frame as shows in following (Nikravesh, 1988):

$$n = R_7^{UAV} n', \quad (Eq. 3.11)$$

where n is the unit vector of sunlight measured by a sensor attached on the UAV with the coordinate $n = [n_x \ n_y \ n_z]^T$. n' is the unit vector perpendicular to Solar panel with the coordinate $n' = [0 \ 0 \ 1]^T$, and R_7^{UAV} is a matrix rotation from body-fixed frame to the global frame. The relation in **Eq. 3.11** can be expressed in the expanded form as following

in **Eq. 3.12**

$$\begin{bmatrix} n_x \\ n_y \\ n_z \end{bmatrix} = \begin{bmatrix} \cos \theta & 0 & \sin \theta \\ \sin \phi \sin \theta & \cos \phi & -\sin \phi \cos \theta \\ -\cos \phi \sin \theta & \sin \phi & \cos \phi \cos \theta \end{bmatrix} \begin{bmatrix} 0 \\ 0 \\ 1 \end{bmatrix} \quad (\text{Eq. 3.12})$$

From calculation in equation **Eq. 3.12**, the resulting as describe in the equation below:

$$\begin{aligned} n_x &= \sin \theta \\ n_y &= -\sin \phi \cos \theta \\ n_z &= \cos \phi \cos \theta \end{aligned} \quad (\text{Eq. 3.13})$$

From equation **Eq. 3.13**, the result of finding pitch angle is:

$$\theta = \arcsin(n_x)$$

From equation **Eq. 3.13**, the result of finding roll angle is:

$$\begin{aligned} \sin \phi &= \frac{-n_y}{\cos \theta} \\ \phi &= \arcsin\left(\frac{-n_y}{\cos \theta}\right) \\ &= \arcsin\left(\frac{-n_y}{\cos \arcsin(n_x)}\right) \end{aligned}$$

Note: The value of n_x , n_y and n_z are known from sensor attached on UAV. After getting the value of ϕ and θ , the rotation matrix is fully defined. Thus, we would be able to determine the other components containing in the actuator displacement vector q .

$$\mathbf{b}_i = R_7^{UAV} \mathbf{b}'_i \quad (\text{Eq. 3.14})$$

$$\mathbf{r} = r\mathbf{z} \quad (\text{Eq. 3.15})$$

$$\mathbf{z} = R_4^{UAV} \mathbf{z}' \quad (\text{Eq. 3.16})$$

The Rotation Matrix R_4^{UAV} of revolute joint about x -axis transforms the body-fixed frame of body 4 into the global frame (UAV) of body 1, and is described as:

$$R_4^{UAV} = R_x(\gamma) = \begin{bmatrix} 1 & 0 & 0 \\ 0 & \cos(\gamma) & -\sin(\gamma) \\ 0 & \sin(\gamma) & \cos(\gamma) \end{bmatrix}$$

Substitution **Eq. 3.16** with $\mathbf{z}' = [0 \ 0 \ 1]^T$ is expressed in following

$$\mathbf{z} = \begin{bmatrix} 1 & 0 & 0 \\ 0 & \cos(\gamma) & -\sin(\gamma) \\ 0 & \sin(\gamma) & \cos(\gamma) \end{bmatrix} \begin{bmatrix} 0 \\ 0 \\ 1 \end{bmatrix} = \begin{bmatrix} 0 \\ -\sin(\gamma) \\ \cos(\gamma) \end{bmatrix} \quad (\text{Eq. 3.17})$$

Where γ is an angle rotation along x -axis of revolute joint between body number 4 and body number 1 (UAV) as **Fig. 3.3**, and measured from y -axis of body 1 to z' -axis of body 4. To find the value of γ , we used the geometric of parallel mechanism that we have two plan $OA_1B_1C_1$, $OA_2B_2C_2$ perpendicular at point O .

$OA_2B_2C_2$ forms a plan where $t_2 = A_2C_2$ and we have

$$\begin{aligned} \mathbf{t}_2 &\in OA_2B_2C_2 \\ OA_2B_2C_2 &\perp \mathbf{a}_1, \end{aligned}$$

so, the relation of plan perpendicular, we obtained relationship yields

$$\begin{aligned} \mathbf{t}_2 &\perp \mathbf{a}_1 \\ \mathbf{a}_1^T \mathbf{t}_2 &= 0, \end{aligned}$$

we have: $\mathbf{t}_i = \mathbf{r} - \mathbf{a}_i + \mathbf{b}_i$, $i = 1, 2$, for the left hand side loop of **Fig. 3.3** with $i = 2$

$$\begin{aligned} \mathbf{t}_2 &= \mathbf{r} - \mathbf{a}_2 + \mathbf{b}_2 \\ \mathbf{t}_2 - \mathbf{r} + \mathbf{a}_2 - \mathbf{b}_2 &= 0 \\ \mathbf{t}_2 - r\mathbf{z} + \mathbf{a}_2 - \mathbf{b}_2 &= 0, \end{aligned} \quad (\text{Eq. 3.18})$$

multiplying the vector \mathbf{a}_1^T in Eq: 3.18, we obtained the equation in following

$$\begin{aligned}\mathbf{a}_1^T \mathbf{t}_2 - \mathbf{a}_1^T r \mathbf{z} + \mathbf{a}_1^T \mathbf{a}_2 - \mathbf{a}_1^T \mathbf{b}_2 &= 0 \\ r \mathbf{a}_1^T \mathbf{z} + \mathbf{a}_1^T \mathbf{b}_2 &= 0\end{aligned}$$

$$\begin{aligned}r \begin{bmatrix} a_{1x} & a_{1y} & a_{1z} \end{bmatrix} \begin{bmatrix} 0 \\ -\sin(\gamma) \\ \cos(\gamma) \end{bmatrix} + \begin{bmatrix} a_{1x} & a_{1y} & a_{1z} \end{bmatrix} \begin{bmatrix} b_{2x} \\ b_{2y} \\ b_{2z} \end{bmatrix} &= 0 \\ r \begin{bmatrix} a_{1x} & a_{1y} & a_{1z} \end{bmatrix} \begin{bmatrix} 0 \\ -\sin(\gamma) \\ \cos(\gamma) \end{bmatrix} + \begin{bmatrix} a_{1x} & a_{1y} & a_{1z} \end{bmatrix} R_7^{UAV} \begin{bmatrix} b'_{2x} \\ b'_{2y} \\ b'_{2z} \end{bmatrix} &= 0,\end{aligned}\tag{Eq. 3.19}$$

where $\mathbf{b}_2 = R_7^{UAV} \mathbf{b}'_2$ and $\mathbf{a}_1 = [0 \ a_{1y} \ 0]^T$ is a vector along y - axis.

$$\begin{aligned}-ra_{1y}\sin(\gamma) + \mathbf{a}_1^T R_7^T b'_{2y} &= 0 \\ \sin(\gamma) &= \left(\frac{1}{ra_{1y}} \right) \mathbf{a}_1^T R_7^{UAV} b'_2 \\ \gamma &= \arcsin \left(\frac{1}{ra_{1y}} \mathbf{a}_1^T R_7^{UAV} b'_2 \right)\end{aligned}\tag{Eq. 3.20}$$

Therefore the vector is defined.

$$\begin{aligned}\mathbf{t}_i &= \mathbf{r} - \mathbf{a}_i + \mathbf{b}_i \\ \mathbf{t}_i &= r R_4^{UAV} \mathbf{z}' - \mathbf{a}_i + R_7^{UAV} \mathbf{b}'_i,\end{aligned}$$

And finally $\mathbf{q}_i = \mathbf{n}_3^T \mathbf{t}_i - \sqrt{r_i^2 + (\mathbf{n}_3^T \mathbf{t}_i)^2 - t_i^2}$ is fully stated.

Scenario 2: The direction of sunlight is obtained from trajectory of the sun with respect to the location of the UAV

The second scenario is proposed such that vector \vec{n} (*sunlight direction*) attained in different method from the first scenario. In this case, GPS is used as sensor and mounted on the UAV. The UAV position is received; therefore, the orientation of sunlight can be calculated by using the trajectory equation of the sun. The following equations are taken into account (Nikraves, 1988):

$$(R_{UAV}^I)^T n = R_7^{UAV} n',\tag{Eq. 3.21}$$

where: R_{UAV}^I is a matrix rotation of body frame (UAV) respected to global frame (Earth). From equation **Eq. 3.21**, we can solved the value of n as:

$$n = R_{UAV}^I (R_7^{UAV} n')$$

To find the value n , it has been assumed that matrix rotation R_{UAV}^I is known. Vector n is observed in the global frame. Moreover, this vector shows the location of the UAV to calculate the orientation of the sunlight from the trajectory equation of the sun.

4. DYNAMIC MODELING FOR MULTI RIGID-BODY UAV

4.1. Dynamic Modeling for UAV

Dynamic modeling for the system is the best solution for solving problems. To deal with it, kinematic constraints of all joints are determined. Undetermined close form reaction forces at joints are obtained from the kinematic constraints. Using Newton's method, dynamic equation for each body exerted by external forces and reaction forces is formulated. A fully determined equation, which is a system of algebraic-differential equations, is obtained by appending kinematic and dynamic equations.

To describe the dynamics of the multicopter, we used an inertial frame I and a body-fixed frame B as in **Figure 4.1**, such that origin is at the center of gravity. We consider hexacopter with n'_p rotor which lie all in the same plane and total thrust force always points in the same as the direction of the body-fixed z -axis(z_B).

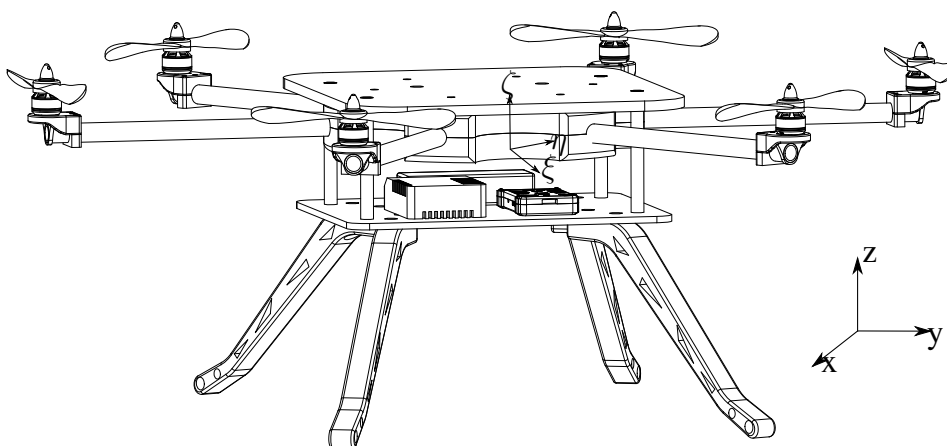


Figure 4.1. Hexacopter

To derive the dynamic model of the hexacopter (position and attitude), we used the Newton-Euler formulation method. There are two equations of the motion, rotational in **Eq. 4.2** and translational in **Eq. 4.1**. Parameter N is a diagonal matrix of mass (m) and moment inertia J' with respect to its center of mass in body-fixed frame exerted by external force f defined in global frame, and torque τ' denoted on the body-fixed frame which has dynamic equation of motion form:

$$N\ddot{r} = f \quad (\text{Eq. 4.1})$$

$$J'\dot{\omega}' + \tilde{\omega}'J'\omega' = \tau', \quad (\text{Eq. 4.2})$$

Note that, translational equation of motion is written on the global frame. This equation can

used to determine the acceleration and the position of the system on the earth by solving differential equations. On the other hand, the rotational equation of motion is written in the body-fixed frame. The angular velocity of the system is defined on the body-fixed frame. The motion of the three angular of roll, pitch and yaw of the system is also defined in the body-fixed frame. The dynamic equation of motion from **Eq. 4.1** and **Eq. 4.2** can be expressed in matrix form as

$$\begin{bmatrix} N & 0 \\ 0 & J' \end{bmatrix} \begin{bmatrix} \ddot{r} \\ \dot{\omega}' \end{bmatrix} + \begin{bmatrix} 0 \\ \tilde{\omega}' J' \omega' \end{bmatrix} = \begin{bmatrix} f \\ \tau' \end{bmatrix}, \quad (\text{Eq. 4.3})$$

where $N = \text{diag}[m, m, m]$, matrix of mass hexacopter. ω' is the angular velocity of the UAV that is defined in body-fixed frame.

The thrust force of each rotors has equation as below

$$F_p = R_I^B [0 \ 0 \ \sum_{i=1}^6 F_i]^T = R_I^B [0 \ 0 \ \sum_{i=1}^6 k_f \omega_i^2]^T, \quad (\text{Eq. 4.4})$$

where $F_i \geq 0$ is the thrust magnitude, ω_i is the angular velocity of each rotors, R_I^B is the rotation matrix from the body-fixed frame to the inertial frame, and k_f is the thrust constant which related with density of air.

Gravity force F_g resulting from from the weigh of hexacopter (m) and gravity g can be written as:

$$F_g = [0 \ 0 \ -mg]^T \quad (\text{Eq. 4.5})$$

The propulsion moment τ' , we consider the configuration as in **Fig. 4.2** and the direction rotation axis of each propeller is parallel to z-axis of the body-fixed frame (z_B), that the propulsion moments and forces within the rotor plane as shows (Moussid, Sayouti, & Medromi, 2015)

$$\begin{aligned} F_{i,z} &= k_f \omega_i^2 \\ M_{i,z} &= -\text{sign}(\omega_i) k_\tau \omega_i^2 \end{aligned} \quad (\text{Eq. 4.6})$$

The thrust force and moment produced by i -th rotor and rotation axis can be modeled such that it is proportional to the square of the angular velocity ω_i . Here, k_f and k_τ are rotor specific parameters. From equation **Eq. 4.6**, substitute in the propulsion moment are

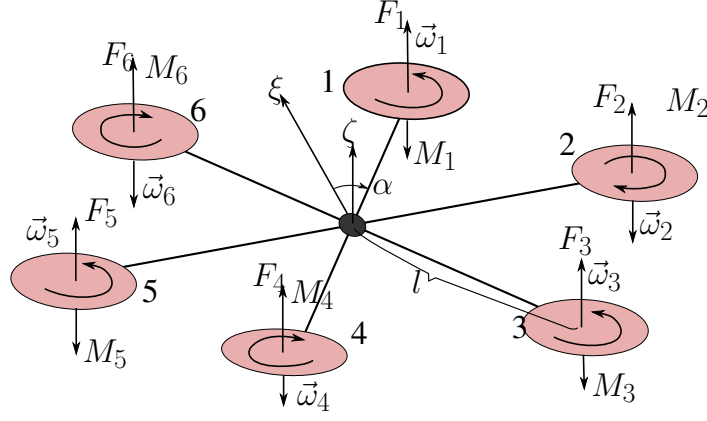


Figure 4.2. A model of hexacopter

$$\tau' = \sum_{i=1}^6 (r^{GP_i} \times F_i + M_i) = \sum_{i=1}^6 \left(\begin{pmatrix} l \cos(\alpha_i) \\ l \sin(\alpha_i) \\ 0 \end{pmatrix} \times \begin{pmatrix} 0 \\ 0 \\ F_{i,z} \end{pmatrix} + \begin{pmatrix} 0 \\ 0 \\ M_{i,z} \end{pmatrix} \right), \quad (\text{Eq. 4.7})$$

where $r^{GP_i} \in R^3$ is the position vector of the i -th propellers with respect to the center of gravity of hexacopter, $l \in R$ is the length of the propeller arms, and α_i is the angle between x_B and the rotor arm. In compact form of the propulsion moment

$$\tau' = B_M u_p$$

Where

$$B_M = \begin{bmatrix} \frac{k_f l}{2} & -k_f l & \frac{k_f l}{2} & \frac{k_f l}{2} & k_f l & \frac{k_f l}{2} \\ \frac{\sqrt{3}}{2} k_f l & 0 & \frac{\sqrt{3}}{2} k_f l & \frac{\sqrt{3}}{2} k_f l & 0 & -\frac{\sqrt{3}}{2} k_f l \\ -k_\tau & k_\tau & -k_\tau & k_\tau & -k_\tau & k_\tau \end{bmatrix}$$

$$u_p = [u_1, u_2, u_3, u_4, u_5, u_6]^T$$

$$= [\omega_1^2, \omega_2^2, \omega_3^2, \omega_4^2, \omega_5^2, \omega_6^2]^T$$

Note that for matrix $B_M \in R^{3 \times 6}$ has a full row rank. If we know the propulsion moment, vector u_p can be found by using Moore-Penrose pseudoinverse of matrix B_M as shows

$$u_p = B_M^t \tau', \quad (\text{Eq. 4.8})$$

where $B_M^t = B_M^T(B_M B_M^T)^{-1}$ is the form of Moore-Penrose pseudo inverse (Šolc & Baránek, 2012).

For a specific multicopter, direct relationship between thrusts of propellers and torque vector can be computed in a simple way. The relationship of total thrust and torque vector are produced from the variables of six rotors. In **Fig. 4.2**, the geometric of the hexacopter can be computed total thrusts and total torques by individual propeller which is easily derived in basic relation from mechanics.

$$\begin{bmatrix} f \\ \tau'_x \\ \tau'_y \\ \tau'_z \end{bmatrix} = \begin{bmatrix} k_f & k_f & k_f & k_f & k_f & k_f \\ \frac{k_f l}{2} & -k_f l & \frac{k_f l}{2} & \frac{k_f l}{2} & k_f l & \frac{k_f l}{2} \\ \frac{k_f l \sqrt{3}}{2} & 0 & \frac{k_f l \sqrt{3}}{2} & \frac{k_f l \sqrt{3}}{2} & 0 & -\frac{k_f l \sqrt{3}}{2} \\ -k_\tau & k_\tau & -k_\tau & k_\tau & -k_\tau & k_\tau \end{bmatrix} \begin{bmatrix} \omega_1^2 \\ \omega_2^2 \\ \omega_3^2 \\ \omega_4^2 \\ \omega_5^2 \\ \omega_6^2 \end{bmatrix}, \quad (\text{Eq. 4.9})$$

where l is a length from the center of hexacopter to the arms, f is the total thrust. τ'_x is the roll torque along x -axis, τ'_y is the pitch torque along y -axis, τ'_z is the yaw torque along z -axis. If we want to find the angular velocity of each rotors, we needed an inverse formulation of **Eq. 4.9** by using Moore-Penrose pseudo inverse. The matrix for computation with Moore-Penrose pseudo inverse is given in (?, ?) as follows

$$\begin{bmatrix} \omega_1^2 \\ \omega_2^2 \\ \omega_3^2 \\ \omega_4^2 \\ \omega_5^2 \\ \omega_6^2 \end{bmatrix} = \frac{1}{6k_f l} \begin{bmatrix} l & 2 & 0 & -\frac{k_f l}{k_\tau} \\ l & 1 & -\sqrt{3} & \frac{k_f l}{k_\tau} \\ l & -1 & -\sqrt{3} & -\frac{k_f l}{k_\tau} \\ l & -2 & 0 & \frac{k_f l}{k_\tau} \\ l & -1 & \sqrt{3} & -\frac{k_f l}{k_\tau} \\ l & 1 & \sqrt{3} & \frac{k_f l}{k_\tau} \end{bmatrix} \begin{bmatrix} f \\ \tau'_x \\ \tau'_y \\ \tau'_z \end{bmatrix} \quad (\text{Eq. 4.10})$$

On the other hand, dynamic equation of motion will be transformed to Euler parameter to satisfy with all mathematical relationship of equation Euler parameter by (Nikraves,

1988) is

$$\begin{aligned}
\omega' &= 2L\dot{p} \\
\ddot{\omega}' &= 2L\ddot{p} \\
A &= GL^T \\
\dot{A} &= 2\dot{G}L^T = 2G\dot{L}^T \\
\tilde{\omega}' &= A^T A = 2L\dot{L}^T
\end{aligned} \tag{Eq. 4.11}$$

Substituting the relationship of Euler parameter in Equation **Eq. 4.2** is rewritten in form

$$\begin{aligned}
2J'L\ddot{p} + 4\tilde{L}\dot{p}J'L\dot{p} &= \tau' \\
2J'L\ddot{p} + 4L\dot{L}^T J'L\dot{p} &= \tau' \\
2J'L\ddot{p} + LH\dot{p} &= \tau'
\end{aligned} \tag{Eq. 4.12}$$

Relationship of constraint equation in Euler parameter of rotation motion is given

$$p^T p - 1 = 0 \tag{Eq. 4.13}$$

And the second time derivative of the equation is

$$p^T \ddot{p} + \dot{p}^T \dot{p} = 0 \tag{Eq. 4.14}$$

Eq. 4.12 and **Eq. 4.14** can be expressed in matrix form of rotational motion:

$$\begin{bmatrix} 2J'L \\ p^T \end{bmatrix} \ddot{p} + \begin{bmatrix} LH \\ \dot{p}^T \end{bmatrix} \dot{p} = \begin{bmatrix} \tau' \\ 0 \end{bmatrix}, \tag{Eq. 4.15}$$

where $H = 4\dot{L}^T J'L$, $\tilde{L}\dot{p} = L\dot{L}^T$, $p = [e_0, e^T]^T = [e_0, e_1, e_2, e_3]^T$, stands for the Euler parameter formulation

From **Eq. 4.1** to **Eq. 4.15**, dynamic equation of motion for unconstraint body of hexacopter can be rewritten in compact form as follows:

$$\begin{bmatrix} N & 0 \\ 0 & 2J'L \\ 0 & p^T \end{bmatrix} \begin{bmatrix} \ddot{r} \\ \ddot{p} \end{bmatrix} + \begin{bmatrix} 0 \\ LH \\ \dot{p}^T \end{bmatrix} \dot{p} = \begin{bmatrix} f \\ \tau' \\ 0 \end{bmatrix} \tag{Eq. 4.16}$$

4.2. Matlab simulink for UAV

Simulink is used a numerical method for solving the non linear differential equation, Runge-Kutta. Figure 4.3 is the flow simulation of the system hexacopter. The first function name MATLAB Function is a head function which is derived the whole dynamic unconstraint body equation of the system hexacopter. The method of calculation in simulink is converted to state space form and using Runge-Kutta for solving non linear differential equation. Next function is the coordinate variable of the hexacopter as a position.

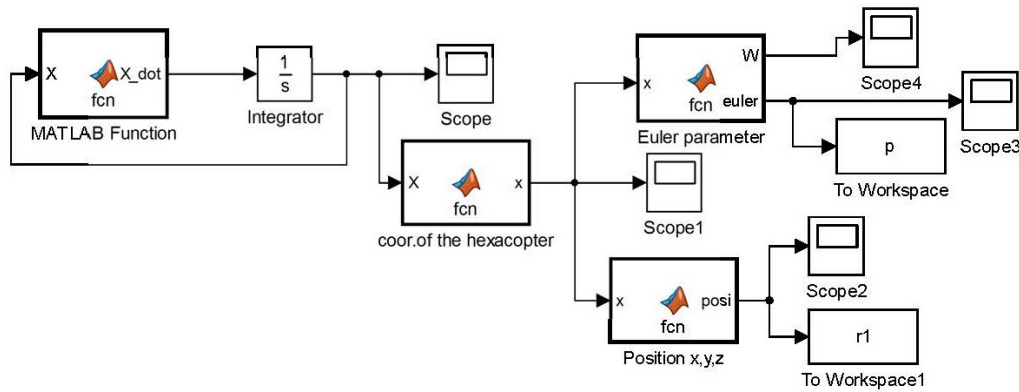


Figure 4.3. Flow simulation of hexacopter

4.3. Dynamic Modeling for Multi Rigid-Body UAV

A system of bodies connected by kinematic joint and/or force elements which created the constraint of motion in the system. The constraint for two or more of the bodies are interconnected by kinematic joints. In the system, coordinate vector for b bodies is denoted by q . Then the kinematic joints in the system can be represented as m independent constraints, normally nonlinear equations in terms of q as:

$$\Phi \equiv \Phi(q) = 0 \quad (\text{Eq. 4.17})$$

A constrained body i is additionally exerted by reaction forces and moments $[f^{(c)}, \tau^{(c)}]_i^T$ from joints. These forces and moments can be transformed to coordinate system consistent with q denoted by $[f^{*(c)}, \tau^{*(c)}]_i^T$ and defined by

$$\begin{bmatrix} f^{*(c)} \\ \tau^{*(c)} \end{bmatrix}_i = \begin{bmatrix} \Phi_r^T \\ \Phi_p^T \end{bmatrix}_i \lambda, \quad (\text{Eq. 4.18})$$

where $\lambda = [\lambda_1, \dots, \lambda_{34}]$ is called Lagrange multiplier, and $[\Phi_r, \Phi_p]_i = \Phi_{q_i}$ is Jacobian matrix of the kinematic constraint, $\Phi \equiv \Phi(q)$ with respected to $q_i = [r^T, p^T]_i^T$. To be used with the formulation **Eq. 4.16**, the moment in **Eq. 4.18** is transformed to be

$$\begin{aligned} f^{(c)} &= f^{*(c)} \\ &= \Phi_r \lambda \\ \tau'^{(c)} &= \frac{1}{2} L_i \tau'^{*(c)} \\ &= \frac{1}{2} L_i \Phi_{p_i}^T \lambda, \end{aligned}$$

then, the equation of translational and rotational of motion in **Eq. 4.1** , **Eq. 4.12** are rewritten as:

$$\begin{aligned} N_i \ddot{r}_i - \Phi_{r_i}^T \lambda &= f_i \\ 2J'_i L_i \ddot{p}_i + L_i H_i \dot{p}_i - \frac{1}{2} L_i \Phi_{p_i}^T \lambda &= \tau'_i \end{aligned} \quad (\text{Eq. 4.19})$$

In matrix form of the equation **Eq. 4.14** and **Eq. 4.19** can be written as

$$\begin{bmatrix} N_i & 0 & \Phi_{r_i}^T \\ 0 & 2J'_i L_i & \frac{1}{2} L_i \Phi_{p_i}^T \\ 0 & p_i^T & 0 \end{bmatrix} \begin{bmatrix} \ddot{r}_i \\ \ddot{p}_i \\ -\lambda \end{bmatrix} + \begin{bmatrix} 0 \\ L_i H_i \dot{p}_i \\ \dot{p}_i^T \dot{p}_i \end{bmatrix} = \begin{bmatrix} f_i \\ \tau'_i \\ 0 \end{bmatrix} \quad (\text{Eq. 4.20})$$

For the system with 7 bodies, Eq. 4.20 of dynamic equation can be obtained as

$$\begin{bmatrix} M & B^T \\ P & 0 \end{bmatrix} \begin{bmatrix} \ddot{q} \\ -\lambda \end{bmatrix} + \begin{bmatrix} c_1 \\ c_2 \end{bmatrix} = \begin{bmatrix} g \\ 0 \end{bmatrix}, \quad (\text{Eq. 4.21})$$

To solve this equation for q and λ , the constraint equation is needed. The second time derivative of the constraint equation **Eq. 4.17** is given by

$$\Phi_q \ddot{q} = \gamma \quad (\text{Eq. 4.22})$$

where $\gamma = -(\Phi_q \dot{q})_q \dot{q}$ is called the right-hand-side of acceleration equation. This equation is appended with **Eq. 4.21** to yield a system of algebraic-differential equation as

$$\begin{bmatrix} M & B^T \\ P & 0 \\ \Phi_q & 0 \end{bmatrix} \begin{bmatrix} \ddot{q} \\ -\lambda \end{bmatrix} + \begin{bmatrix} c_1 \\ c_2 \\ 0 \end{bmatrix} = \begin{bmatrix} g \\ 0 \\ \gamma \end{bmatrix}, \quad (\text{Eq. 4.23})$$

where

$$M = \begin{bmatrix} N_1 & 0 & \dots & 0 & 0 \\ 0 & 2J'_1 L_1 & \dots & 0 & 0 \\ \vdots & \vdots & \ddots & \vdots & \vdots \\ 0 & 0 & \dots & N_7 & 0 \\ 0 & 0 & \dots & 0 & 2J'_7 L_7 \end{bmatrix},$$

$$B = [\Phi_{r_1}, \frac{1}{2}\Phi_{p_1} L_1^T, \dots, \Phi_{r_7}, \frac{1}{2}\Phi_{p_7} L_7^T],$$

$$\Phi_q = [\Phi_{r_1}, \Phi_{p_1}, \dots, \Phi_{r_7}, \Phi_{p_7}],$$

$$P = \begin{bmatrix} 0^T & p_1^T & \dots & 0^T & 0^T \\ \vdots & \vdots & \ddots & \vdots & \vdots \\ 0^T & 0^T & \dots & 0^T & p_7^T \end{bmatrix}, \quad c_1 = \begin{bmatrix} 0 \\ L_1 H_1 \dot{p}_1 \\ \vdots \\ 0 \\ L_7 H_7 \dot{p}_7 \end{bmatrix}, \quad c_2 = \begin{bmatrix} \dot{p}_1^T \dot{p}_1 \\ \vdots \\ \dot{p}_7^T \dot{p}_7 \end{bmatrix},$$

$$g = \begin{bmatrix} f_1 \\ \tau'_1 \\ \vdots \\ f_7 \\ \tau'_7 \end{bmatrix}, \quad h_k = -2\dot{G}_k \dot{L}_i^T s'_k, \quad h_k^B = -2\dot{G}_k \dot{L}_i^T s'^B_k, \quad \text{and} \quad h_k^P = -2\dot{G}_k \dot{L}_i^T s^P_k, \quad k = i, j,$$

where the variable of Φ_q and γ , Jacobian matrix of each joint are summarized in **Table 4.1** and **Table 4.2**.

Table 4.1. Components in the Expansion of the Most Common Constraints
, (Nikravesh, 1988)

Φ	$\Phi_{r_i}^{(m)}$	$\Phi_{P_i}^{(m)}$	$\Phi_{r_j}^{(m)}$	$\Phi_{P_j}^{(m)}$	$\gamma^{(m)}$
$\Phi^{n1,1}$	0^T	$2s_j^T G_i \bar{s}'_i$	0^T	$2s_i^T G_j \bar{s}'_j$	$s_i^T h_j + s_j^T h_i - 2\dot{s}_i^T \dot{s}_j$
$\Phi^{n2,1}$	$-s_i^T$	$-2s_j^T G_i \bar{s}'_i{}^B + 2d^T G_i \bar{s}'_i$	s_i^T	$2s_i^T G_j s_j{}^B$	$-s_i^T (h_i^B - h_j^B) + d^T h_i - 2\dot{s}_i^T \dot{d}$
$\Phi^{(p1,2)}$	0	$-2\tilde{s}_j G_i \bar{s}'_i$	0	$2\tilde{s}_i G_j \bar{s}'_j$	$\tilde{s}_i h_j - \tilde{s}_j h_i - 2\tilde{s}_i \dot{s}_j$
$\Phi^{(p2,2)}$	$-\tilde{s}_i$	$-2\tilde{s}_i G_i \bar{s}'_i{}^B - 2\tilde{d}^T G_i s'_i$	\tilde{s}_i	$2\tilde{s}_i G_j s_j{}^B$	$\tilde{s}_i (h_j^B - h_i^B) - \tilde{d}^T h_i - 2\tilde{s}_i \dot{d}$
$\Phi^{(s,3)}$	I	$2G_i \bar{s}_i^p$	$-I$	$-2G_j \bar{s}_j^p$	$h_i^p - h_j^p$
$\Phi^{(s-s,1)}$	$-2d^T$	$-4d^T G_i \bar{s}_i^p$	$2d^T$	$4d^T G_j \bar{s}_j^p$	$2d^T (h_i^p - h_j^p) - 2\dot{d}^T \dot{d}$

Table 4.2. Components in the Expansion of the Most Common Constraints
, (Nikravesh, 1988)

Φ	$\Phi_{r_i}^{(m)}$	$\frac{1}{2}\Phi_{P_i}^{(m)} L_i^T$	$\Phi_{r_j}^{(m)}$	$\frac{1}{2}\Phi_{P_j}^{(m)} L_j^T$	$\gamma^\#$
$\Phi^{n1,1}$	0^T	$-s_j^T \tilde{s}_i A_i$	0^T	$-s_i^T \tilde{s}_j A_j$	$-2\dot{s}_i^T \dot{s}_j + \dot{s}_i^T \tilde{\omega}_i s_j + \dot{s}_j^T \tilde{\omega}_j s_i$
$\Phi^{n2,1}$	$-s_i^T$	$-(d + s_i^B)^T \tilde{s}_i A_i$	s_i^T	$-s_i^T \tilde{s}_j^B A_j$	$-2\dot{d}^T \dot{s}_i - d^T \tilde{\omega}_i \dot{s}_i + s_i^T (\tilde{\omega}_i \dot{s}_i^B - \tilde{\omega}_j \dot{s}_j^B)$
$\Phi^{(p1,2)}$	0	$\tilde{s}_j \tilde{s}_i A_i$	0	$-\tilde{s}_i \tilde{s}_j A_j$	$-2\tilde{s}_i \dot{s}_j + \tilde{s}_j \tilde{\omega}_i \dot{s}_i - \tilde{s}_i \tilde{\omega}_j \dot{s}_j$
$\Phi^{(p2,2)}$	$-\tilde{s}_i$	$(\tilde{s}_i \tilde{s}_i^B + \tilde{d} \tilde{s}_i) A_i$	\tilde{s}_i	$-\tilde{s}_i \tilde{s}_j^B A_j$	$-2\tilde{s}_i \dot{d} + \tilde{s}_i (\tilde{\omega}_i \dot{s}_i^B - \tilde{\omega}_j \dot{s}_j^B) + \tilde{d} \tilde{\omega}_i \dot{s}_i$
$\Phi^{(s,3)}$	I	$-\tilde{s}_i^p A_i$	$-I$	$\tilde{s}_j^p A_j$	$-\tilde{\omega}_i \dot{s}_i^p + \tilde{\omega}_j \dot{s}_j^p$
$\Phi^{(s-s,1)}$	$-2d^T$	$2d^T \tilde{s}_i^p A_i$	$2d^T$	$-2d^T \tilde{s}_j^p A_j$	$-2\dot{d}^T \dot{d} + 2d^T (\tilde{\omega}_i \dot{s}_i^p - \tilde{\omega}_j \dot{s}_j^p)$

Fig. 3.2 and **Fig. 5.1** show the whole system of an hexacopter and the parallel mechanism. Body numbers are labeled as illustrated in the figure. Body-fixed frame of the parallel mechanism (body 1) is attached at the center of mass of the hexacopter body. On the condition of the combining system, the effect of actuator force have been included in the system during tracking. Then the total force f_p and moment τ_p generated by all propellers are

$$f_p = \sum_k f_k = A_{pf} u_p + F_g \quad (Eq. 4.24)$$

$$\tau_p = \sum_k (\tilde{a}_k f_k + \tau_k) = A_{p\tau} u_p,$$

where $A_{pf} = 1_z[k_f, \dots, k_f]$

$$A_{p\tau} = [k_f \tilde{a}_1 1_z - k_\tau \text{sign}(\omega_1) 1_z, \dots, k_f \tilde{a}_6 1_z - k_\tau \text{sign}(\omega_6) 1_z]$$

Which $1_z = [0, 0, 1]^T$, and a_k is vector from the epicenter of mass of the hexacopter to axis of propeller k . The value of vector a_k illustrated in **Table 5.2**

Two linear actuators are mounted on the hexacopter and exert forces on the body 2 and 3 through the translational joints. The forces are also control input for the system **Eq. 4.23** and denoted by

$$\begin{bmatrix} f_{1-2,\zeta} \\ f_{1-3,\zeta} \end{bmatrix} = \begin{bmatrix} u_7 \\ u_8 \end{bmatrix} \text{ and } \begin{bmatrix} f_{2-1,\zeta} \\ f_{3-1,\zeta} \end{bmatrix} = - \begin{bmatrix} u_7 \\ u_8 \end{bmatrix}, \quad (\text{Eq. 4.25})$$

where u_7 and u_8 are scalars values of force from the actuators in the bodies 2 and 3. Let $u = [u_p, u_7, u_8]^T$, as a control input vector for the whole system. Then, the non-zero external forces and moments which exert on respective body 1, 2 and 3 with gravity force are given by

$$\begin{aligned} g_1 &= \begin{bmatrix} R_1(f_p - 1_z u_7 - 1_z u_8) - 1_z m_1 g \\ \tau_p - \tilde{b}_1 1_z u_7 - \tilde{b}_2 1_z u_8 \end{bmatrix} = \begin{bmatrix} A_{1f} \\ A_{1\tau} \end{bmatrix} u + \begin{bmatrix} g_1 \\ 0 \end{bmatrix} \\ g_2 &= \begin{bmatrix} R_2 1_z u_7 - 1_z m_2 g \\ 0 \end{bmatrix} = \begin{bmatrix} A_{2f} \\ 0 \end{bmatrix} u + \begin{bmatrix} g_2 \\ 0 \end{bmatrix} \\ g_3 &= \begin{bmatrix} R_3 1_z u_8 - 1_z m_3 g \\ 0 \end{bmatrix} = \begin{bmatrix} A_{3f} \\ 0 \end{bmatrix} u + \begin{bmatrix} g_3 \\ 0 \end{bmatrix} \end{aligned} \quad (\text{Eq. 4.26})$$

where

$$A_{1f} = R_1 1_z[k_f, \dots, k_f, -1, -1],$$

$$A_{1\tau} = [A_{p\tau}, -\tilde{b}_1 1_z, -\tilde{b}_2 1_z],$$

$$A_{2f} = R_2 1_z[0, \dots, 0, 1, 0],$$

$$A_{3f} = R_3 1_z[0, \dots, 0, 0, 1],$$

$$g_1 = -1_z m_1 g, \dots, g_7 = -1_z m_7 g$$

and b_1 and b_2 are vectors from the center of mass of the hexacopter to the axes of the two linear actuators which shows in **Table 5.2**. R_i is a rotational matrix for each bodies in the

system. Therefore the dynamic equation of motion **Eq. 4.23** can be rewritten as

$$\begin{bmatrix} M & B^T \\ P & 0 \\ \Phi_q & 0 \end{bmatrix} \begin{bmatrix} \ddot{q} \\ -\lambda \end{bmatrix} + \begin{bmatrix} c_1 \\ c_2 \\ 0 \end{bmatrix} = \begin{bmatrix} g_a \\ 0 \\ \gamma \end{bmatrix} + \begin{bmatrix} A \\ 0 \\ 0 \end{bmatrix} u, \quad (\text{Eq. 4.27})$$

where

$$A = [A_{1f}^T, A_{1\tau}^T, A_{2f}^T, 0^T, A_{3f}^T, 0^T, \dots, 0^T]^T$$

$$g_a = [g_1^T, 0^T, g_2^T, 0^T, \dots, g_7^T, 0^T]^T$$

To support a simulation of parallel-mechanism-mounted UAV using formulation in **Eq. 4.23**, the simple system with two bodies connected by spherical joint in Section **5.3**. in **REPORT PART I** has been verified.

4.4. Matlab simulink for Multi Rigid-Body UAV

The flow simulation in **Fig. 4.4** are described the step calculation of dynamic equation of the whole system. The block name MATLAB Function is a head of function that included all dynamic equation and solving the differential equation. For calculation in Matlab simulink, we are converted to state space form. Addition, the block name Body number 1, 2, 3, and 7 are function of the variable position of bodies 1 (hexacopter), 2 and 3 (linear actuators) and 7 (platform attached solar panel).

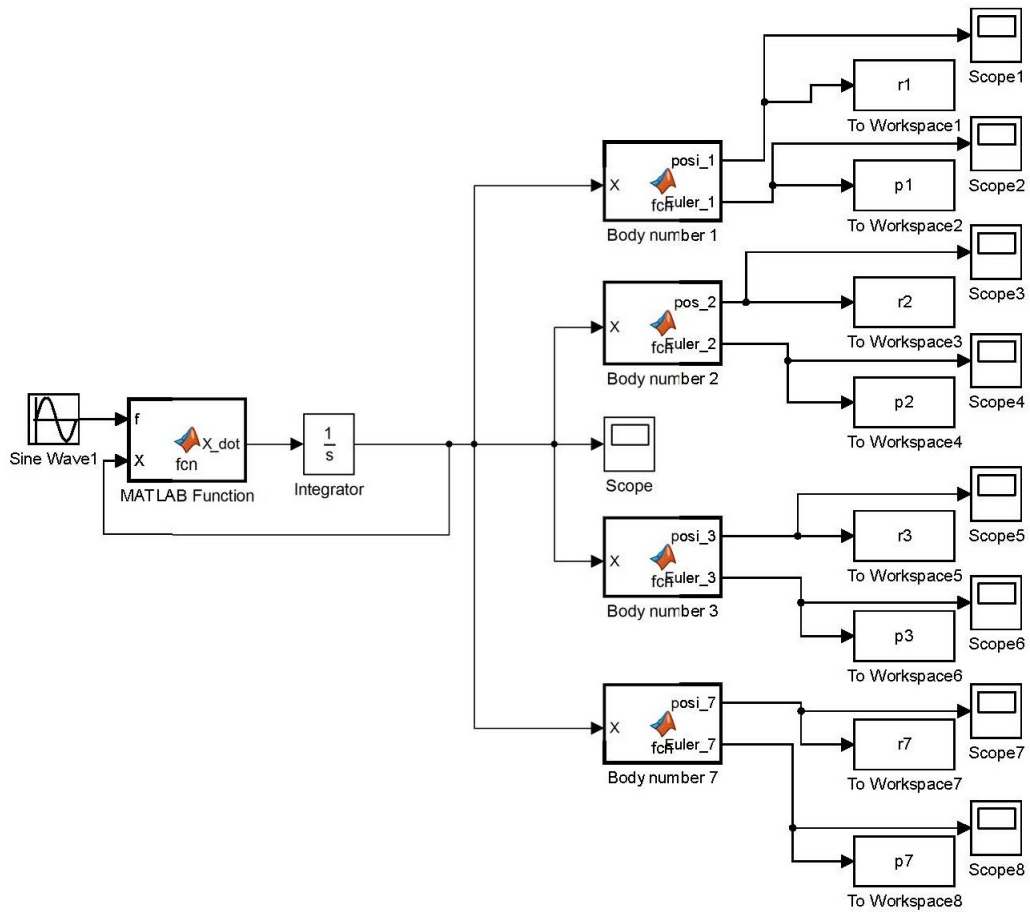


Figure 4.4. Flow simulation for a parallel-mechanism-mounted UAV

4.5. Summery

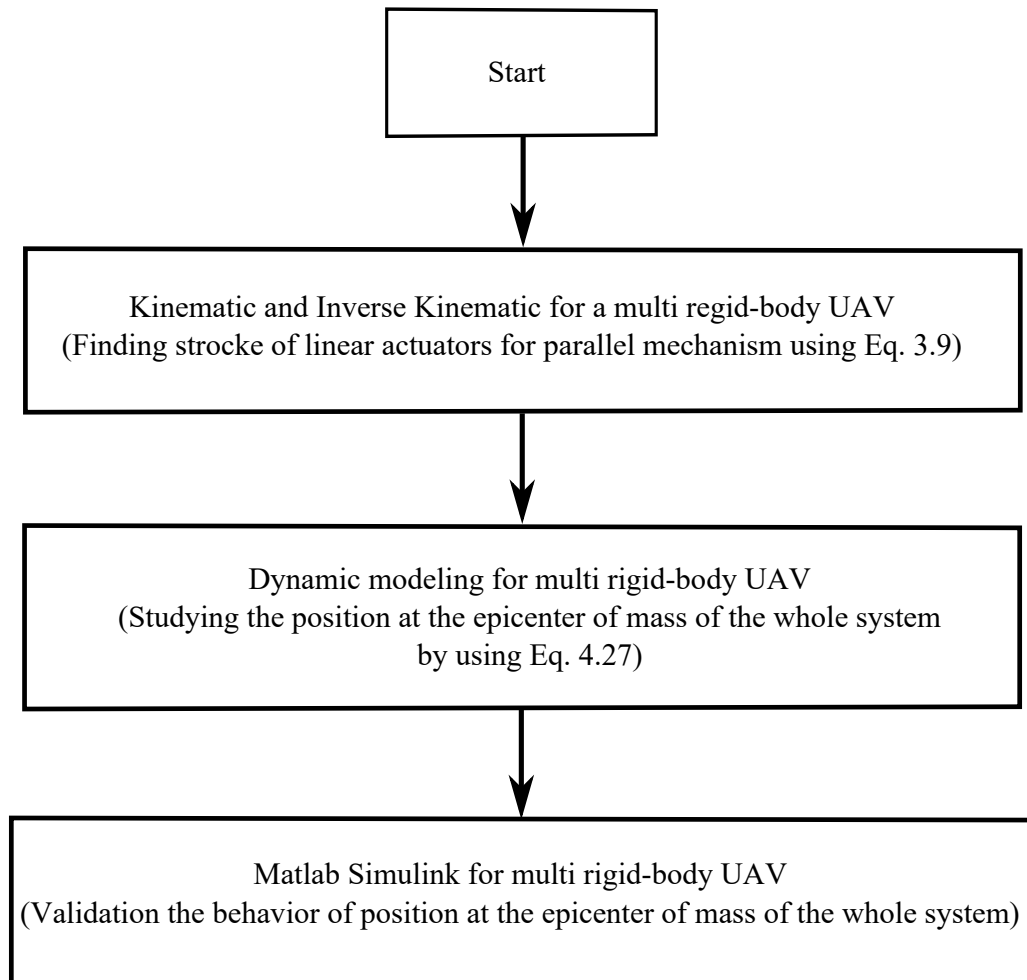


Figure 4.5. Flow of work

Figure 4.5 shows the step of work that we started from kinematic and inverse kinematic equation to obtain the stock of linear actuators for a parallel mechanism. And then, we developed the dynamic modeling for a multi rigid-body UAV and investigated the attitude of the whole system. Matlab simulink is needed to validate the dynamic attitude of the whole system.

5. SIMULATION RESULT AND DISCUSSION

The simulation result of the system needs the initial input value that we are measured from SolidWorks program. **Table 5.1**, **Table 5.2** and **Table 5.3** are shown the value of all variable related with the system. The material using is Carbon fiber (Hexcel AS4C 3000 Filaments), density 1780 kg/m^3 on the system that selected in SolidWorks.

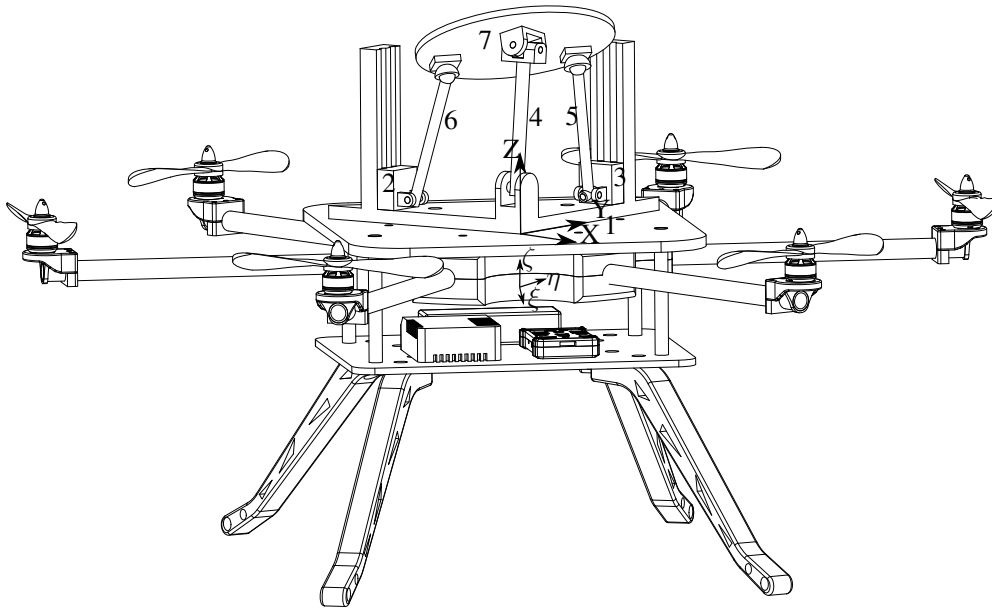


Figure 5.1. Parallel-mechanism-mounted UAV

Simulation result from Matlab Simulink is an approximation value because it uses a Numerical method solve non linear differential equation. Thus, the solution is approximate. Moreover, some error in the system is make from input parameter and the scaled of parallel-mechanism-mounted UAV is not proportional.

5.1. Simulation result of Hexacopter

The simulation of the hexacopter shows the attitude of tracking which obtained position on the step time. The total mass of hexacopter is $m = 5.407 \text{ kg}$ and moment of inertia on the body hexacopter is

$$J' = \begin{bmatrix} 57.2 & 0.492 & -0.201 \\ 0.492 & 58.8 & 0.0056 \\ -0.201 & 0.0056 & 866 \end{bmatrix} \times 10^{-3}, \text{ kg m}^2,$$

as a matrix 3×3 . The result of the hexacopter is generated from dynamic equation **Eq. 4.16** of motion with unconstrained body. On the translation motion (Newton's second Law) is solving differential equation with numerical method in Matlab Simulink. The graphic shows in **Fig. 5.2**, which is a position of the hexacopter with constant thrust force and torque. There are three curves that show the position on x -axis, y -axis and z -axis in parabolic. Because of, the thrust force input is larger than the gravity force of the system. The hexacopter is move up on the another direction. Moreover, the torque input in the system has effected on the system by tracking in the three angle (roll, pitch, and yaw) of rotation matrix that we observed in the global coordinated system.

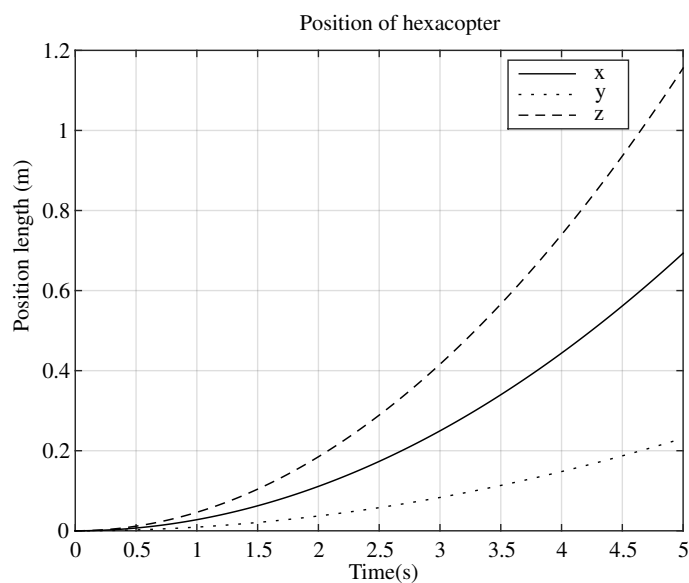


Figure 5.2. Position of the center of mass of hexacopter with respect to the global frame

5.2. Result of simulation parallel-mechanism-mounded UAV

The motion of the whole system has been derived in **Eq. 4.27**, for the position orientation of the system. For determine the equation of differential in 7 bodies for dynamic motion, we used Matlab Simulink by converted this equation to state space forme. In simulation, it has simulated in dynamic only, which does not have controller. The result was discussed in three cases.

Case 1. we investigated the system behaviour during its hover without forces applied on the actuators.

Case 2. we applied forces on the solar tacker actuators of case 1.

$$u_7 = 3\sin(4\pi t)$$

$$u_8 = 3\sin(4\pi t),$$

where u_7 and u_8 are the external force in body-fixed frame on the bodies 2 and 3, respectively.

Case 3. in addition to the forces applied on the solar tracker actuators, we applied the upward thrust to lift the system vertically from its initial position.

The **Table 5.1** shows the value of mass (m_i) each bodies in the whole system. l is a length from the center of hexacopter to the arms and k_f, k_τ are rotor specific parameters.

Table 5.1. Values of parameters for simulation

Parameter	Description	Value	Units
m_1	Mass of body 1	5882.95×10^{-3}	kg
m_2	Mass of body 2	189.7×10^{-3}	kg
m_3	Mass of body 3	189.7×10^{-3}	kg
m_4	Mass of body 4	104.45×10^{-3}	kg
m_5	Mass of body 5	53.25×10^{-3}	kg
m_6	Mass of body 6	54.4×10^{-3}	kg
m_7	Mass of body 7	890.85×10^{-3}	kg
l	Length	400×10^{-3}	m
k_f	Specific parameter	6.546×10^{-6}	Ns^2/rad^2
k_t	Specific parameter	1.2864×10^{-7}	Ns^2/rad^2

The **Table 5.2** shows the value of vectors b_i and a_k which is vector from the epicenter of mass of the hexacopter to axis of propeller k and vector from the center of mass of the hexacopter to the axes of the two linear actuators, respectively.

Table 5.2. Values of vector length for simulation

Parameter	Description	Value	Units
b_1	Vector length	$[-77.58, -37.11, 60.60]^T \times 10^{-3}$	m
b_2	Vector length	$[39.18, 79.38, 65.70]^T \times 10^{-3}$	m
a_1	Vector length	$[339.19, -90.66, 54.06]^T \times 10^{-3}$	m

a_2	Vector length	$[91.71, -338.14, 53.87]^T \times 10^{-3}$	m
a_3	Vector length	$[-246.37, -247.56, 53.62]^T \times 10^{-3}$	m
a_4	Vector length	$[-336.95, 90.52, 53.35]^T \times 10^{-3}$	m
a_5	Vector length	$[-89.47, 338.01, 53.74]^T \times 10^{-3}$	m
a_6	Vector length	$[248.61, 247.42, 53.99]^T \times 10^{-3}$	m

The **Table 5.3** shows the value of the moment inertia J'_i of each bodies that measured in the body-fixed frame.

Table 5.3. Values of moment inertia for simulation

Parameter	Description	Value	Units
J'_1	Moment inertia body 1	$10^{-9} \begin{bmatrix} 62459754.68 & 418.01 & 520754.55 \\ 418.01 & 62804459.83 & 215030.33 \\ 520754.55 & 215030.33 & 89298102.47 \end{bmatrix}$	$\text{kg } m^2$
J'_2	Moment inertia body 2	$10^{-9} \begin{bmatrix} 27742.82 & 0 & -1015.42 \\ 0 & 20147.82 & 0 \\ -1015.42 & 0 & 19872.58 \end{bmatrix}$	$\text{kg } m^2$
J'_3	Moment inertia body 3	$10^{-9} \begin{bmatrix} 27742.83 & 0 & 0 \\ 0 & 27743.24 & 1015.42 \\ 0 & 1015.42 & 19872.58 \end{bmatrix}$	$\text{kg } m^2$
J'_4	Moment inertia body 4	$10^{-9} \begin{bmatrix} 121732 & 0.1 & 0 \\ 0.1 & 124762.7 & 0 \\ 0 & 0 & 5357.6 \end{bmatrix}$	$\text{kg } m^2$
J'_5	Moment inertia body 5	$10^{-9} \begin{bmatrix} 59447.35 & 0 & 0 \\ 0 & 59396.7 & 0 \\ 0 & 0 & 546.95 \end{bmatrix}$	$\text{kg } m^2$
J'_6	Moment inertia body 6	$10^{-9} \begin{bmatrix} 62418.2 & 0 & 0 \\ 0 & 62311.7 & -0.05 \\ 0 & -0.05 & 580.75 \end{bmatrix}$	$\text{kg } m^2$
J'_7	Moment inertia body 7	$10^{-9} \begin{bmatrix} 1233055.05 & 40906.55 & -2729 \\ 40906.55 & 1219762.8 & -435.5 \\ -2729 & -435.5 & 2432416.35 \end{bmatrix}$	$\text{kg } m^2$

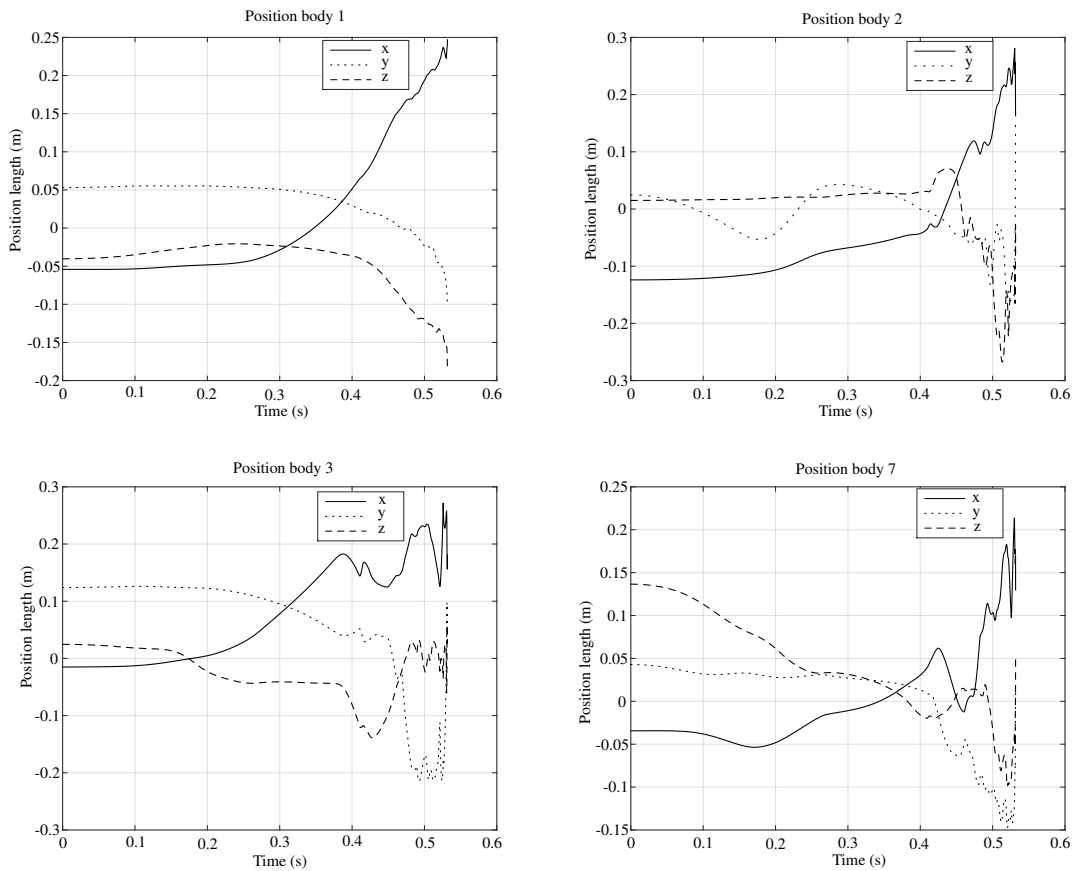


Figure 5.3. Case 1: Position of the epicenter of hexacopter (body 1), actuators (body 2 and 3), and platform attached solar panel (body 7) at the hover point with respect to the global frame

The result as shown in **Figure 5.3**, in **case 1**, there are focus on the position of the bodies 1, 2, 3, and 7. For the position of body 1, which is remain on the hover point at a bit time when we stated operating. After that, the hexacopter has changed the position, because the reaction of gravity force for parallel mechanism is not equivalent to the thrust force of the system. The parallel mechanism has two degree of freedom that it can be effected on the movement of system. When UAV is not equivalent to the initial condition, its means that the rotation matrix has changed, so the sum of vector forces on the UAV are not equal zeros. The sum of vector force can make a new vector force on the another direction.

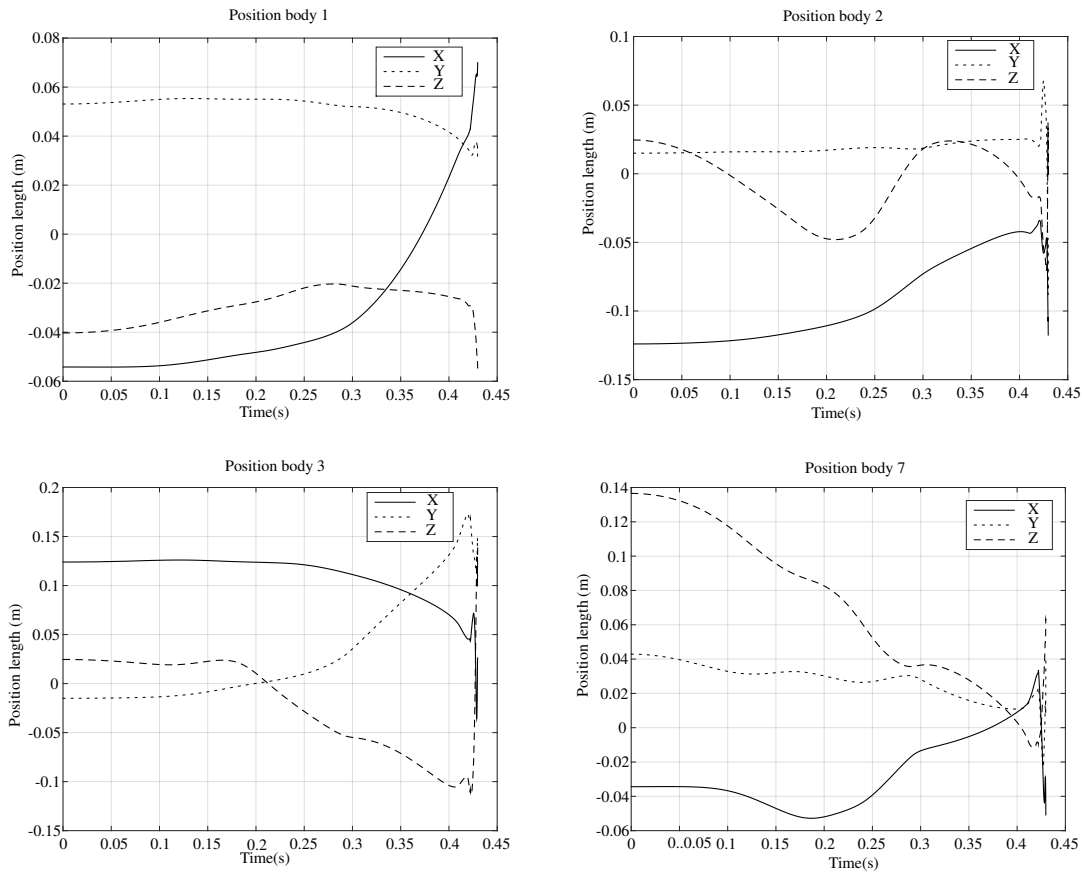


Figure 5.4. Case 2: Position of the epicenter of hexacopter (body 1), actuators (body 2 and 3), and platform attached solar panel (body 7) at the hover point with respect to the global frame

Case 2., we applies forces on the both actuators that makes the system stable at a few second when we observed body 1 (UAV) at the hover point. After that, the system has destabilization which has been rotated along z -axis. It is unbalance that drop out of the whole system. At the time, hexacopter is drop out that is effected from the body number 7 (attached solar panel).

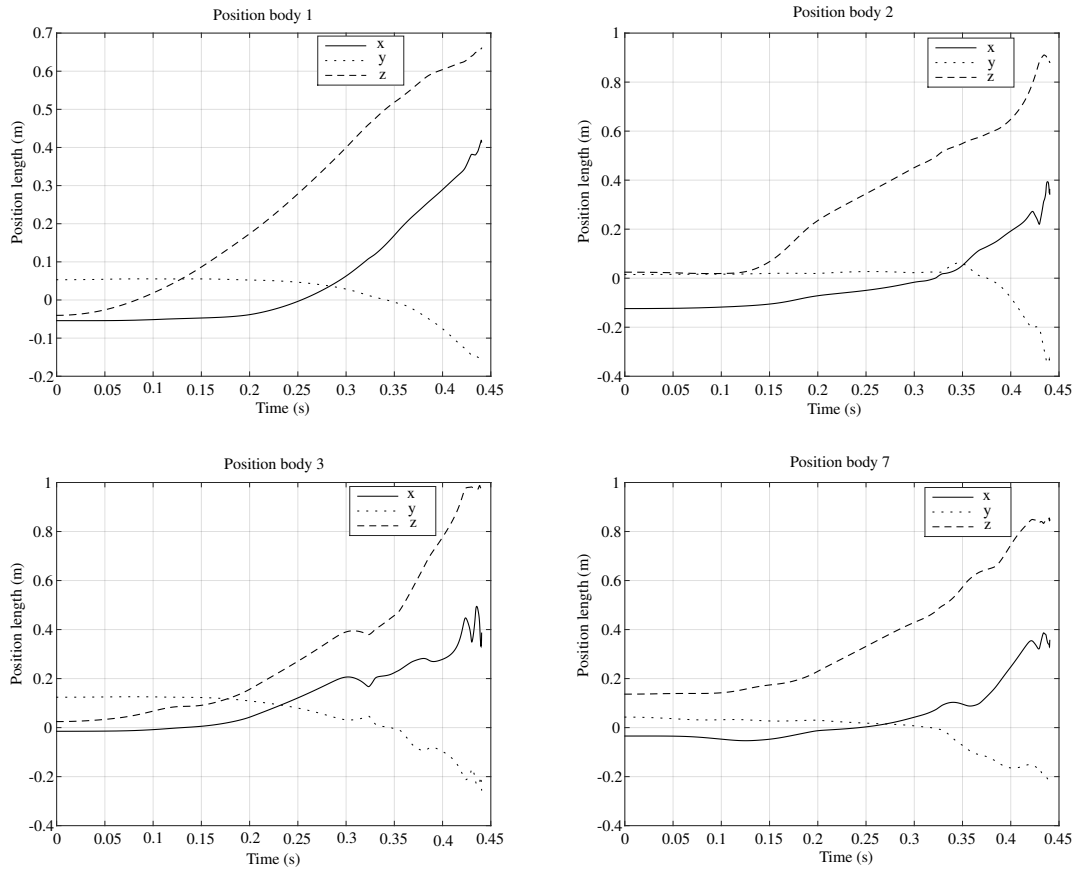


Figure 5.5. Case 3: Position of the epicenter of hexacopter (body 1), actuators (body 2 and 3), and platform attached solar panel (body 7) with respect to the global frame

In **Figure 5.5** are shows in **case 3**, we observe the position of body number 1 for z -axis move up and tracked in the a parabolic curve because it is the second derivative of Newton second Law. During the system move up, the system is destabilization which make the system drop out.

In summery, the result of the whole system is unstable in all cases. There are two types of unstable: one from the disturbance from the external force can not be cancel out, so the hovering can not stable. Other one numerical unstable when we computed up to time 0.5 s, the simulation has stopped, because the numerical method just approximation.

6. CONCLUSION AND RECOMMENDATION

In this thesis, we present kinematic, inverse kinematic, dynamic modeling and simulation for the system. Kinematic and inverse kinematic for the tracker is briefly described using classical method. Dynamic modeling for the system is one of the most challenging engineering problems. To deal with it, kinematic constraints of all joints are determined. Undetermined close form reaction forces at joints are obtained from the kinematic constraints. Using Newton's method, dynamic equation for each body exerted by external forces and reaction forces is formulated. A fully determined equation, which is a system of algebraic-differential equations, is obtained by appending kinematic and dynamic equations. Simulation for a parallel-mechanism-mounted UAV can describe the position of all bodies in the whole system. From the result, there are three cases to discuss. We observed a trajectory at the hover points and displacement of hexacopter and body number 7 (solar panel attached). In case 1, we investigated the system behaviour during its hover without forces applied on the actuators. In case 2, we applied forces on the solar tacker actuators of case 1. In case 3, in addition to the forces applied on the solar tacker actuators, we applied the upward thrust to lift the system vertically from its initial position. We have observed that after about 0.45 to 0.5 s, the simulation induced large error causing simulation to stop. It happened due to high stiff differential equation of zigzag motion of the tracker.

On the dynamic equation using Newton-Euler parameter, it solved in simulation that using Numerical method for approximation result. In addition, we should find a correction factors to minimize error. This suggests that dynamic modelling alone is insufficient to have a stable flight. Therefore, it is absolutely necessary to consider adding a controller to the future work in order achieve flight stability and allow the tracker to optimally collect the solar energy.

References

- Allaka, G., Anasuya, B., Yamini, C., Vaidehi, N., & Ramana, Y. V. (2011). Modelling and analysis of multicopter frame and propeller. *Dept of Mechanical Engg, Swarnandhra College of Engineering & Technology, AP*.
- Al-Mohamad, A. (2004). Efficiency improvements of photo-voltaic panels using a sun-tracking system. *Applied Energy*, 79(3), 345–354.
- Boucher, R. (1984). History of solar flight. In *20th joint propulsion conference* (p. 1429).
- Cammarata, A. (2015). Optimized design of a large-workspace 2-dof parallel robot for solar tracking systems. *Mechanism and machine theory*, 83, 175–186.
- Di Gregorio, R., & Sinatra, R. (2002). Singularity curves of a parallel pointing system. *Meccanica*, 37(3), 255–268.
- Hartmann, R. L., et al. (2008). *An aging model for lithium-ion cells* (Unpublished doctoral dissertation). University of Akron.
- Herwitz, S. R., Dunagan, S., Sullivan, D., Higgins, R., Johnson, L., Zheng, J., . . . others (2003). Solar-powered uav mission for agricultural decision support. In *Geoscience and remote sensing symposium, 2003. igarss'03. proceedings. 2003 ieee international* (Vol. 3, pp. 1692–1694).
- Hoffmann, F. M., Molz, R. F., Kothe, J. V., Nara, E. O. B., & Tedesco, L. P. C. (2018). Monthly profile analysis based on a two-axis solar tracker proposal for photovoltaic panels. *Renewable Energy*, 115, 750–759.
- Lee, J.-S., Park, H.-B., Jung, G.-Y., & Kee-Ho, Y. (2013). Design of virtual flight system for evaluation of solar powered uav. In *Industrial electronics society, iecon 2013-39th annual conference of the ieee* (pp. 3463–3467).
- Lee, K.-Y., Chung, C.-Y., Huang, B.-J., Kuo, T.-J., Yang, H.-W., Cheng, H.-Y., . . . Li, K. (2017). A novel algorithm for single-axis maximum power generation sun trackers. *Energy Conversion and Management*, 149, 543–552.
- Lubitz, W. D. (2011). Effect of manual tilt adjustments on incident irradiance on fixed and tracking solar panels. *Applied energy*, 88(5), 1710–1719.
- Mansouri, S. S., Karvelis, P., Georgoulas, G., & Nikolakopoulos, G. (2017). Remaining useful battery life prediction for uavs based on machine learning. *IFAC-PapersOnLine*, 50(1), 4727–4732.
- Mousazadeh, H., Keyhani, A., Javadi, A., Mobli, H., Abrinia, K., & Sharifi, A. (2009). A review of principle and sun-tracking methods for maximizing solar systems output.

- Renewable and sustainable energy reviews*, 13(8), 1800–1818.
- Moussid, M., Sayouti, A., & Medromi, H. (2015). Dynamic modeling and control of a hexarotor using linear and nonlinear methods. *International Journal of Applied Information Systems*, 9(5).
- Mustapa, Z., Saat, S., Husin, S., & Abas, N. (2014). Altitude controller design for multi-copter uav. In *Computer, communications, and control technology (i4ct), 2014 international conference on* (pp. 382–387).
- Nikravesh, P. E. (1988). *Computer-aided analysis of mechanical systems* (Vol. 186). Prentice-hall Englewood Cliffs, NJ.
- Noth, A. (2008). *Design of solar powered airplanes for continuous flight* (Unpublished doctoral dissertation). ETH Zurich.
- Polk, S. (2016, September 13). *Solar energy collector*. Google Patents. (US Patent 9,443,999)
- Saha, B., Koshimoto, E., Quach, C. C., Hogge, E. F., Strom, T. H., Hill, B. L., . . . Goebel, K. (2011). Battery health management system for electric uavs.
- Šolc, F., & Baránek, R. (2012). Attitude control of multicopter.
- Stern, M., Duran, G., Fourer, G., Mackamul, K., Whalen, W., Loo, M. v., & West, R. (1998). *Development of a low-cost integrated 20-kw-ac solar tracking subarray for grid-connected pv power system applications. final technical report* (Tech. Rep.). National Renewable Energy Lab., Golden, CO (US); Utility Power Group, Chatsworth, CA (US).
- Tegeder, T. D. (2007). Development of an efficient solar powered unmanned aerial vehicle with an onboard solar tracker.
- Verbeke, J., Hulens, D., Ramon, H., Goedeme, T., & De Schutter, J. (2014). The design and construction of a high endurance hexacopter suited for narrow corridors. In *Unmanned aircraft systems (icuas), 2014 international conference on* (pp. 543–551).
- Vorobiev, P. Y., González-Hernández, J., & Vorobiev, Y. V. (2004). Optimization of the solar energy collection in tracking and non-tracking photovoltaic solar system. In *Electrical and electronics engineering, 2004.(iceee). 1st international conference on* (pp. 310–314).
- Wu, J., Chen, X., & Wang, L. (2016). Design and dynamics of a novel solar tracker with parallel mechanism. *IEEE/ASME Transactions on Mechatronics*, 21(1), 88–97.

APPENDICES

Background of rotation matrix using Euler Angle

A basic rotation (also called elemental rotation) is a rotation about one of the axes of a coordinate system. The following three basic rotation matrices rotate vectors by an angle, roll ϕ about the x axis, pitch θ about the y axis, and yaw ψ about the z axis, in three dimensional coordinate. As shown in **Figure 6.1.** the roll angle is defined as the rotation about the x axis by ϕ angle.

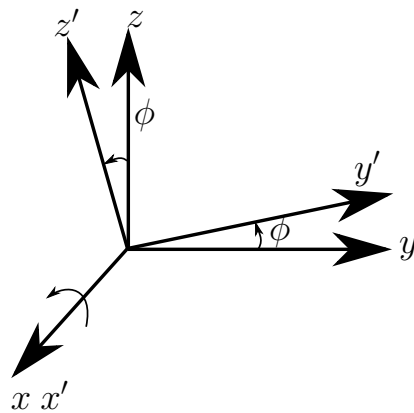


Figure 6.1. Rotation about x axis

The rotation matrix about x axis is written as:

$$R(\phi) = \begin{bmatrix} 1 & 0 & 0 \\ 0 & \cos \phi & -\sin \phi \\ 0 & \sin \phi & \cos \phi \end{bmatrix}$$

The pitch angle is defined as the rotation θ about the y axis as shown in **Figure 6.2.** Therefore,

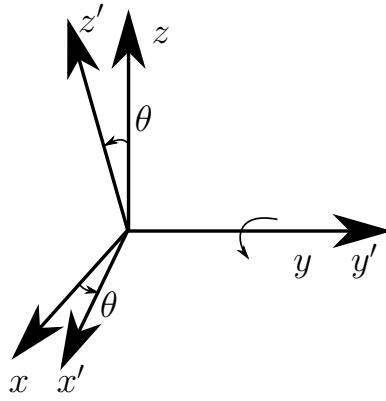


Figure 6.2. Pitch angle about y axis

$$R(\theta) = \begin{bmatrix} \cos \theta & 0 & -\sin \theta \\ 0 & 1 & 0 \\ \sin \theta & 0 & \cos \theta \end{bmatrix}$$

The yaw angle is defined as the rotation ψ about the z axis. The resulting coordinate system can be seen in **Figure 6.3.**

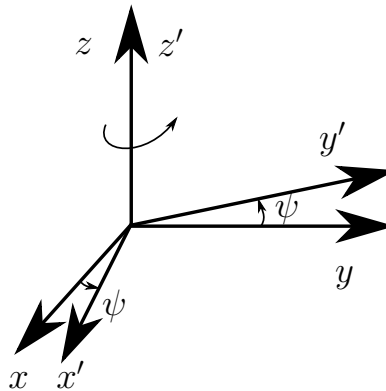


Figure 6.3. Yaw angle around z axis

The matrix rotation is shown:

$$R(\psi) = \begin{bmatrix} \cos \psi & \sin \psi & 0 \\ -\sin \psi & \cos \psi & 0 \\ 0 & 0 & 1 \end{bmatrix}$$

Background of rotation matrix using Euler Parameter

In the following section, rotation matrix which associate with Euler parameter will be used instead of Euler Angle. Euler's theorem states in that a coordinate transformation can be accomplished by a single rotation about a suitable axis. Accordingly, it is an essential way to establish one representation of the coordinate transformation that can rotate the vector from body-fixed frame to global frame. It can be derived by **Figure 6.4.** shown below, the initial position \vec{s} of the vector \overrightarrow{OP} and the final position \vec{s}' is denoted by \overrightarrow{OP}' . The unit vector along the orientation axis of rotation is denoted by \vec{u} . Vector \vec{s} can be expressed as the sum of three vectors:

$$\vec{s} = \overrightarrow{ON} + \overrightarrow{NQ} + \overrightarrow{QP} \quad (\text{Eq. 6.1})$$

The direct distance between points O and N is $\vec{u} \cdot \vec{s}$, so vector \overrightarrow{ON} can be written as following:

$$\overrightarrow{ON} = \vec{u}(\vec{u} \cdot \vec{s}) \quad (\text{Eq. 6.2})$$

Vector \overrightarrow{NP}' can also be described as follows:

$$\overrightarrow{NP}' = \vec{s}' - \overrightarrow{ON} = \vec{s}' - \vec{u}(\vec{u} \cdot \vec{s})$$

Hence,

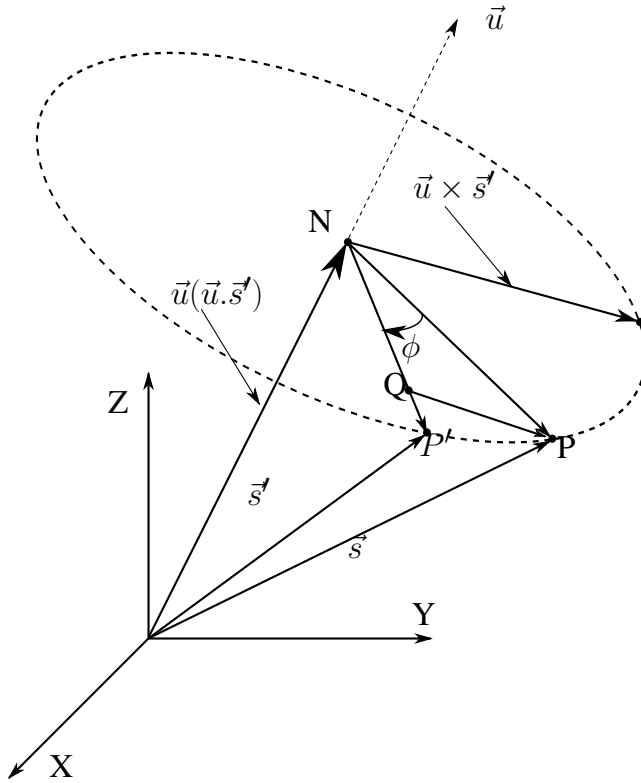


Figure 6.4. Vector diagram for derivation of rotation formula

$$\overrightarrow{NQ} = [\vec{s}' - \vec{u}(\vec{u} \cdot \vec{s}')] \cos \phi \quad (\text{Eq. 6.3})$$

The magnitude of vector $\overrightarrow{NP'}$ is the same as that of vectors \overrightarrow{NP} and $\vec{u} \times \vec{s}'$. Therefore, vector \overrightarrow{QP} may be expressed as

$$\overrightarrow{QP} = (\vec{u} \times \vec{s}') \sin \phi \quad (\text{Eq. 6.4})$$

Substitution of **Eq. 6.2.**, **Eq. 6.3.** and **Eq. 6.4.** into **Eq. 6.1.**, together with a slight rearrangement of terms, leads to the *rotation formula*:

$$\vec{s} = \vec{s}' \cos \phi + \vec{u}(\vec{u} \cdot \vec{s}')(1 - \cos \phi) + \vec{u} \times \vec{s}' \sin \phi \quad (\text{Eq. 6.5})$$

By means of the standard trigonometric relationships

$$\begin{aligned} \cos\phi &= 2\cos^2\frac{\phi}{2} - 1 \\ \sin\phi &= 2\sin\frac{\phi}{2}\cos\frac{\phi}{2} \\ 1 - \cos\phi &= 2\sin^2\frac{\phi}{2} \end{aligned}$$

and the new quantities

$$\begin{aligned} e_0 &= \cos\frac{\phi}{2} \\ \vec{e} &= \vec{u} \sin\frac{\phi}{2} \end{aligned} \tag{Eq. 6.6}$$

the rotation formula of **Eq. 6.5.** can be put in a more useful form:

$$\vec{s} = (2e_0^2 - 1)\vec{s}' + 2e(e^T\vec{s}') + 2e_0\vec{e} \times \vec{s}' \tag{Eq. 6.7}$$

Algebraic representation of **Eq. 6.7.**, using the component form $e = [e_1, e_2, e_3]^T$, yields

$$s = (2e_0^2)s' + 2e(e^T s') + 2e_0(\tilde{e}s')$$

or

$$s = [(2e_0^2 - 1)I + 2ee^T + 2e_0\tilde{e}]s' \tag{Eq. 6.8}$$

where I is the 3×3 identity matrix and, by the definition in reference (Nikravesh, 1988),

$$\tilde{e} = \begin{bmatrix} 0 & -e_3 & e_2 \\ e_3 & 0 & -e_1 \\ -e_2 & e_1 & 0 \end{bmatrix}$$

From relationship $s = As'$ and **Eq. 6.8.** where, A is Rotation Matrix from Body-fixed frame to Initial frame, we get

$$A = 2[(e_0^2 - 1)I + ee^T + e_0\tilde{e}] \tag{Eq. 6.9}$$

More explicitly,

$$A = 2 \begin{bmatrix} e_2^2 + e_1^2 - \frac{1}{2} & e_1e_2 - e_0e_3 & e_1e_3 + e_0e_2 \\ e_1e_2 + e_0e_3 & e_0^2 + e_2^2 - \frac{1}{2} & e_2e_3 - e_0e_1 \\ e_1e_3 - e_0e_2 & e_2e_3 + e_0e_1 & e_0^2 + e_3^2 - \frac{1}{2} \end{bmatrix} \quad (\text{Eq. 6.10})$$

Taking the transpose of both sides of **Eq. 6.9.** yields

$$A^T = (2e_0^2 - 1)I + 2(ee^T - e_0\tilde{e}) \quad (\text{Eq. 6.11})$$

The four quantities $e_0, e_1, e_2,$ and e_3 are called *Euler parameters*. **Eq. 6.6.** indicates that the Euler parameters are not independent. Since $\cos^2(\frac{\phi}{2}) + u^T u \sin^2(\frac{\phi}{2}) = 1$, or $\cos^2(\frac{\phi}{2}) + (u \sin\frac{\phi}{2})^T (u \sin\frac{\phi}{2}) = 1$ then

$$e_0^2 + e^T e = 1 \quad (\text{Eq. 6.12})$$

For example

$$e_0^2 + e_1^2 + e_2^2 + e_3^2 = 1$$

If the four **Euler parameters** are put in a 4-vector as follows:

$$P = [e_0, e^T]^T = [e_0, e_1, e_2, e_3]^T \quad (\text{Eq. 6.13})$$

then **Eq. 6.12.** is written as

$$\begin{aligned} P^T P &= 1 \\ P^T P - 1 &= 0 \end{aligned} \quad (\text{Eq. 6.14})$$

If the matrix rotation A (rotate from body frame to initial frame) is defined, Euler parameter elements also can find as the following

$$A = \begin{bmatrix} a_{11} & a_{12} & a_{13} \\ a_{21} & a_{22} & a_{23} \\ a_{31} & a_{32} & a_{33} \end{bmatrix}$$

To set the initial condition for the euler parameters, the relationship between euler parameters and rotation matrix is needed. The rotation matrix A can be obtained from the configuration of each corresponding body. The detailed of how the rotation matrix is de-

terminated is shown in (? , p. 164). Then, the euler parameters are calculated as follow:

$$\begin{aligned}e_1 &= \frac{a_{32} - a_{23}}{4e_0} \\e_2 &= \frac{a_{13} - a_{31}}{4e_0} \\e_3 &= \frac{a_{21} - a_{12}}{4e_0} \\e_0^2 &= \frac{\text{tr}(A) + 1}{4}\end{aligned}$$

REPORT PART III

ESTIMATION OF THE CENTER OF MASS FOR A QUADROTOR BY USING UNSCENTED KALMAN FILTER

ABSTRACT

Quadrotor commonly has the symmetric shape which consists of four individual rotors attached to a rigid cross airframe. Its center of mass is not really fixed in the epicenter of its shape if it lifts any load that is not located in the epicenter of the quadrotor. Moreover, if the load's location is changed, the center of mass of the quadrotor system is also changed. In order to estimate the changing or unknown center of mass of the quadrotor while it is flying, this thesis has used Unscented Kalman Filter. The dynamic modeling is presented to form a general model of dynamic rotational motion equation of the quadrotor that the center of mass is assumed to be able to change at each time, while the Euler angle is used to model the kinematic attitude equation of the quadrotor. Furthermore, the Unscented Kalman Filter is applied to estimate the center of mass of the quadrotor. To prove that the method can satisfy the objective, this thesis has simulated the data of modeling equations in MATLAB in eight different cases. Hence, the results show that the filters perform very accurately in the estimation of the center of mass. Since the results are very accurately, Unscented Kalman filter is appealing for practical purposes, such as designing a controller.

ABBREVIATIONS AND SYMBOLS

Symbols	Descriptions
KF	Kalman Filter
EKF	Extended Kalman Filter
UKF	Unscented Kalman Filter
x_k	State vector x at time k
$x_{k+1 k}$	State vector x at time $k + 1$ given k
$\hat{x}_{k+1 k}$	Estimation of state vector x at time $k + 1$ given k
P	Error covariance matrix
Q	Process noise covariance matrix
R	Measurement noise covariance matrix
K	Kalman gain or blending factor
$X_{k k}$	Set of sigma points at time k given k
$X_{k+1 k}$	Set of transformed sigma points at time k given $k + 1$
$X_{k+1 k}^{(r)}$	Set of resampled sigma points at time $k + 1$ given k
$\{A\}$	Global coordinate with axes $\{X, Y, Z\}$
$\{B\}$	Body fixed coordinate with axes $\{x, y, z\}$
R	Rotation matrix
$c\phi$	Denotes cosine of ϕ angle
$s\phi$	Denotes sine of ϕ angle
F_i	Thrust generated from i th rotor of the quadrotor
M_i	Reaction torque generated from i th rotor of the quadrotor
c	drag factor
Ω	Angular velocity of $\{B\}$ respect to $\{A\}$ expressed in $\{B\}$
Ω_\times or $\tilde{\Omega}$	Skew-symmetric matrix of Ω
ϕ	Roll angle
θ	Pitch angle
ψ	Yaw angle
J	Constant inertia matrix of the quadrotor expressed in $\{B\}$
I	Identity matrix
τ_{ext}	External combination torques applied to the quadrotor airframe expressed in $\{B\}$
d_i	Distance from epicenter of the quadrotor to i th rotor axes

C Cofactor matrix

δr_x x -axis coordinate of the center of mass of the quadrotor of $\{B\}$

δr_y y -axis coordinate of the center of mass of the quadrotor of $\{B\}$

TABLE OF CONTENTS

ABSTRACT	i
ABBREVIATIONS AND SYMBOLS.....	ii
TABLE OF CONTENTS	iv
LIST OF FIGURES.....	v
LIST OF TABLES	vi
1 INTRODUCTION	1
1.1 Background.....	1
1.2 Statement of Problem	1
1.3 Objective	1
1.4 Scope.....	1
2 METHODOLOGY	3
2.1 Basis of Dynamic Modeling of Quadrotor	3
2.2 Dynamic Modeling of the Quadrotor	6
2.3 State Space Transformation of Dynamic Equation.....	12
2.4 Implementation of Unscented Kalman Filter	15
3 RESULTS AND DISCUSSION.....	18
3.1 Results	18
3.2 Discussion.....	29
4 CONCLUSIONS AND RECOMMENDATION.....	30
4.1 Conclusions.....	30
4.2 Recommendation for Future works	30
REFERENCES.....	31

LIST OF FIGURES

Figure 2.1.1: Notation for quadrotor equations of motion, [1]	3
Figure 2.2.1: Free-body diagrams of the quadrotor which its the center of mass is not in the epicenter	6
Figure 3.1.1: The value of thrusts F_1 , F_2 , F_3 and F_4 for case studies 3 and 7	20
Figure 3.1.2: The value of thrusts F_1 , F_2 , F_3 and F_4 for case studies 4 and 8	20
Figure 3.1.3: Estimation of x axis of the center of mass of the quadrotor for case 1	21
Figure 3.1.4: Estimation of y axis of the center of mass of the quadrotor for case 1	21
Figure 3.1.5: Estimation of x axis of the center of mass of the quadrotor for case 2	22
Figure 3.1.6: Estimation of y axis of the center of mass of the quadrotor for case 2	22
Figure 3.1.7: Estimation of x axis of the center of mass of the quadrotor for case 3	23
Figure 3.1.8: Estimation of y axis of the center of mass of the quadrotor for case 3	23
Figure 3.1.9: Estimation of x axis of the center of mass of the quadrotor for case 4	24
Figure 3.1.10: Estimation of y axis of the center of mass of the quadrotor for case 4	24
Figure 3.1.11: Estimation of x axis of the center of mass of the quadrotor for case 5	25
Figure 3.1.12: Estimation of y axis of the center of mass of the quadrotor for case 5	25
Figure 3.1.13: Estimation of x axis of the center of mass of the quadrotor for case 6	26
Figure 3.1.14: Estimation of y axis of the center of mass of the quadrotor for case 6	26
Figure 3.1.15: Estimation of x axis of the center of mass of the quadrotor for case 7	27
Figure 3.1.16: Estimation of y axis of the center of mass of the quadrotor for case 7	27
Figure 3.1.17: Estimation of x axis of the center of mass of the quadrotor for case 8	28
Figure 3.1.18: Estimation of y axis of the center of mass of the quadrotor for case 8	28

LIST OF TABLES

Table 2.4.1: Initial Parameters for True Process	17
Table 2.4.2: Initial Parameters for Estimation Process	17
Table 3.1.1: Test matrix assuming the center of mass of the quadrotor, $\delta r_x = 0.05m$ and $\delta r_y = 0.1m$, are fixed	18
Table 3.1.2: Test studies with assuming the center of mass of the quadrotor changes over time	19

1. INTRODUCTION

1.1. Background

Aerial robotics is a rapidly-growing field of robotics and multirotor aircraft. Likewise, a quadrotor is one of common multirotor aerial platform which consists of four individual rotors attached to a rigid cross airframe. Small quadrotors have been demonstrated to explore and map the 3-D environments; transport, manipulate, and assembly objects; and to acrobatic tricks such as juggling, balancing, and flipping, [1]. Generally, control of quadrotor is accomplished by differential control of the thrust generated by each rotor. Furthermore, the control strategies are relied on simplified models which have both a minimum number of states and minimum number of inputs. Additionally, the controls of quadrotor, which already existed, have been modeled by fixing the center of mass, [1] and [2]. In actual application, the center of mass of quadrotor is not really fixed. It can be changed at each time depending on the actual situation and its application during performing. However, knowing exact center of mass provides more advantages in modeling and control as well.

1.2. Statement of Problem

The quadrotor generally has the symmetric shape and its center of mass seems to be in the epicenter of its shape. However, when it lifts any load which is not placed on the epicenter of its shape, the center of mass of the whole system is not in the epicenter anymore. Since during its flight, the center of mass can change each time, it is difficult to model and control the quadrotor as well. Consequently, the center of mass of the system can not be determined easily. By using the existed control methods, which have fixed center of mass, may not result in good performance because the center of mass of the quadrotor system can vary anytime.

1.3. Objective

The objective of this thesis is to estimate the center of mass of the quadrotor by using the Unscented Kalman Filter. This estimation focuses on both fixed center of mass and changing center of mass over time of the quadrotor.

1.4. Scope

Generally, the moment of inertia about center of mass of the quadrotor depends on where the center of mass locates. If the center of mass changes, the moment of inertia is also changed. However, in this thesis, we assume the inertia matrix to be constant during the flight. Furthermore, when the quadrotor is translated and rotated, it induces the aerodynamic friction

forces and the aerodynamic friction torques respectively. These two parameters are neglected in the thesis research. Additionally, in this thesis, we do not have a prototype to do experiment. However, we do it by simulation instead.

2. METHODOLOGY

We have many steps to achieve the estimating center of mass of a quadrotor by using the Unscented Kalman Filter. Firstly, we derive the dynamic modeling equations of the rotating motion of a quadrotor by assuming the center of mass not to be in the epicenter of the quadrotor's shape, as shown in, **Figure 2.2.1**. Secondly, we transform them to the continuous nonlinear state space forms because the equations that we derived are in the continuous nonlinear difference equation forms. Then, these forms are transformed to the discrete-time nonlinear state space forms which has two different types (deterministic or pure model which is not included noises to the model and stochastic or true model which is added noises to the model) by using the Euler Approximation. Thirdly, we model these derived equation by the Unscented Kalman Filter (UKF). Finally, we will simulate the true model and estimate its parameters (The Center of Mass coordinates) by UKF.

2.1. Basis of Dynamic Modeling of Quadrotor

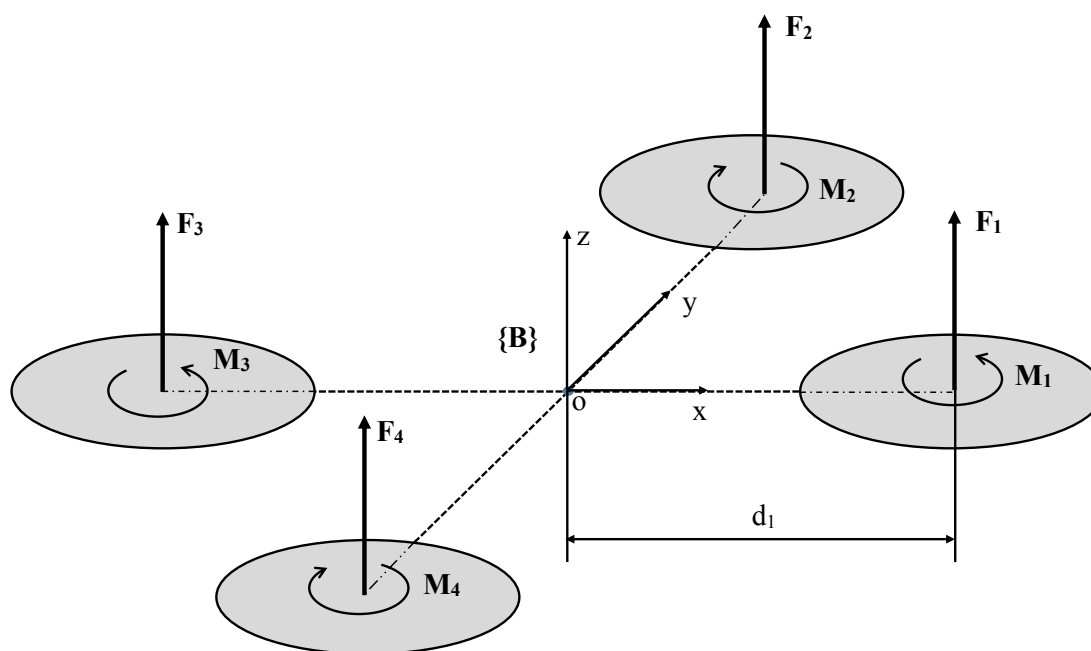


Figure 2.1.1. Notation for quadrotor equations of motion, [1]

The quadrotor is a common aerial vehicle which consists of four individual rotors attached to a rigid cross airframe. Each rotor plays important role in generating thrust for controlling the quadrotor. In the magazine [1], they assume the rotor i rotates positively about the z axis (counterclockwise) if i is even, and rotates clockwise if i is odd, shown in **Figure 2.1.1**.

To model the rigid body equation of motion of the airframe, let $\{A\} = \{X, Y, Z\}$ be an inertial frame or global coordinate with unit vectors along the axes denoted by $\{a_1, a_2, a_3\}$ expressed in $\{A\}$. Let $\{B\} = \{x, y, z\}$ be a body fixed frame for the airframe with unit vectors $\{b_1, b_2, b_3\}$ with respect to $\{A\}$. Then, the models of the rigid body equation of motion of the airframe from [1] are shown below

$$\dot{\xi} = v, \quad (2.1.1)$$

$$m\dot{v} = mg\vec{z} + \mathbf{R}F_{ext} \quad (2.1.2)$$

$$\dot{\mathbf{R}} = \mathbf{R}\Omega_{\times}, \quad (2.1.3)$$

$$J\dot{\Omega} = -\Omega \times J\Omega + \tau_{ext} \quad (2.1.4)$$

where vector $\xi = [\xi_1, \xi_2, \xi_3]^T \in \{A\}$ denotes the position of the center of mass of the quadrotor. The vector $v = [\dot{\xi}_1, \dot{\xi}_2, \dot{\xi}_3]^T \in \{A\}$ is the linear velocity of $\{B\}$ with respect to $\{A\}$ expressed in $\{A\}$. m and g are the mass of the rigid body and the gravitational acceleration respectively. The vector $F_{ext}, \tau_{ext} \in \{B\}$ are the combination external forces and torques applied to the quadrotor airframe by the aerodynamics of the rotors expressed in $\{B\}$. In [4], F_{ext} and $\tau_{ext} \in \{B\}$ are determined by

$$F_{ext} = F - F_{aero} \quad (2.1.5)$$

$$T_{ext} = T - T_{aero}$$

where $F_{aero} = K_t v$ and $T_{aero} = K_r \Omega$ are the aerodynamic friction forces and the aerodynamic friction torques respectively. K_t and K_r are two diagonal aerodynamic friction matrices. The forces F and torque T are produced by the rotors of the quadrotor and they are obtained by

$$F = \begin{bmatrix} 0 \\ 0 \\ \sum_{i=1}^4 F_i \end{bmatrix} \quad (2.1.6)$$

$$T = \begin{bmatrix} d(F_2 - F_4) \\ d(F_3 - F_1) \\ c \sum_{i=1}^4 (-1)^{i+1} F_i \end{bmatrix} \quad (2.1.7)$$

where d is the distance from the epicenter of a quadrotor to the rotor axes and $c > 0$ is the drag factor.

Vector $\Omega = [\Omega_x, \Omega_y, \Omega_z]^T \in \{B\}$ is the angular velocity of $\{B\}$ with respect to $\{A\}$ expressed in $\{B\}$. $J \in \mathbb{R}^{3 \times 3}$ is the constant inertia matrix expressed in $\{B\}$. The Ω_\times is denoted as the skew-symmetric matrix that is shown in (Eq. 2.1.8) or it is denoted as the cross product of Ω with any vector in \mathbb{R}^3 as shown in equation (Eq. 2.1.9) below

$$\Omega_\times = \Omega \times = \tilde{\Omega} = \begin{bmatrix} 0 & -\Omega_z & \Omega_y \\ \Omega_z & 0 & -\Omega_x \\ -\Omega_y & \Omega_x & 0 \end{bmatrix} \quad (2.1.8)$$

$$\Rightarrow \tilde{\Omega}v = \begin{bmatrix} \Omega_y \dot{\xi}_3 - \Omega_z \dot{\xi}_2 \\ \Omega_z \dot{\xi}_1 - \Omega_x \dot{\xi}_3 \\ \Omega_x \dot{\xi}_2 - \Omega_y \dot{\xi}_1 \end{bmatrix}$$

$$\begin{aligned} \Omega_\times v = \Omega \times v &= \begin{bmatrix} \Omega_x \\ \Omega_y \\ \Omega_z \end{bmatrix} \times \begin{bmatrix} \dot{\xi}_1 \\ \dot{\xi}_2 \\ \dot{\xi}_3 \end{bmatrix} \\ &= \begin{bmatrix} \Omega_y \dot{\xi}_3 - \Omega_z \dot{\xi}_2 \\ \Omega_z \dot{\xi}_1 - \Omega_x \dot{\xi}_3 \\ \Omega_x \dot{\xi}_2 - \Omega_y \dot{\xi}_1 \end{bmatrix} \end{aligned} \quad (2.1.9)$$

The matrix $\mathbf{R} = [b_1, b_2, b_3] \in SO_3$ in the special orthogonal group, while $a_1 = \mathbf{R}b_1$, $a_2 = \mathbf{R}b_2$ and $a_3 = \mathbf{R}b_3$. In the magazine [1], we have the rotation matrix below

$$\begin{aligned} \mathbf{R} = R_Z R_X R_Y &= \begin{bmatrix} c\psi & -s\psi & 0 \\ s\psi & c\psi & 0 \\ 0 & 0 & 1 \end{bmatrix} \begin{bmatrix} 1 & 0 & 0 \\ 0 & c\phi & -s\phi \\ 0 & s\phi & c\phi \end{bmatrix} \begin{bmatrix} c\theta & 0 & s\theta \\ 0 & 1 & 0 \\ -s\theta & 0 & c\theta \end{bmatrix} \\ \mathbf{R} &= \begin{bmatrix} c\psi c\theta - s\phi s\psi s\theta & -c\phi s\psi & c\psi s\theta + c\theta s\phi s\psi \\ c\theta s\psi + c\psi s\phi s\theta & c\phi c\psi & s\psi s\theta - c\psi c\theta s\phi \\ -c\phi s\theta & s\phi & c\phi c\theta \end{bmatrix} \end{aligned} \quad (2.1.10)$$

where c and s are shorthand forms for cosine and sine, respectively. R_X , R_Y and R_Z are the rotation matrix about axis X , Y and Z axes, respectively.

2.2. Dynamic Modeling of the Quadrotor

In order to model the dynamic of the quadrotor, we firstly assume its center of mass not to be in the epicenter of the quadrotor's shape as shown in, **Figure 2.2.1**. By assuming the inertia matrix $J \in \mathbb{R}^{3 \times 3}$ to be constant and invertible, we obtained the equation of rotational motion of quadrotor as the following

$$\dot{\mathbf{R}} = \mathbf{R}\tilde{\Omega}, \quad (2.2.1)$$

$$J\dot{\tilde{\Omega}} = -\tilde{\Omega} \times J\tilde{\Omega} + \tau_{ext} \quad (2.2.2)$$

where, rotation matrix \mathbf{R} is obtained from the equation (**Eq. 2.1.10**),

$$\mathbf{R} = \begin{bmatrix} c\psi c\theta - s\phi s\psi s\theta & -c\phi s\psi & c\psi s\theta + c\theta s\phi s\psi \\ c\theta s\psi + c\psi s\phi s\theta & c\phi c\psi & s\psi s\theta - c\psi c\theta s\phi \\ -c\phi s\theta & s\phi & c\phi c\theta \end{bmatrix} \quad (2.2.3)$$

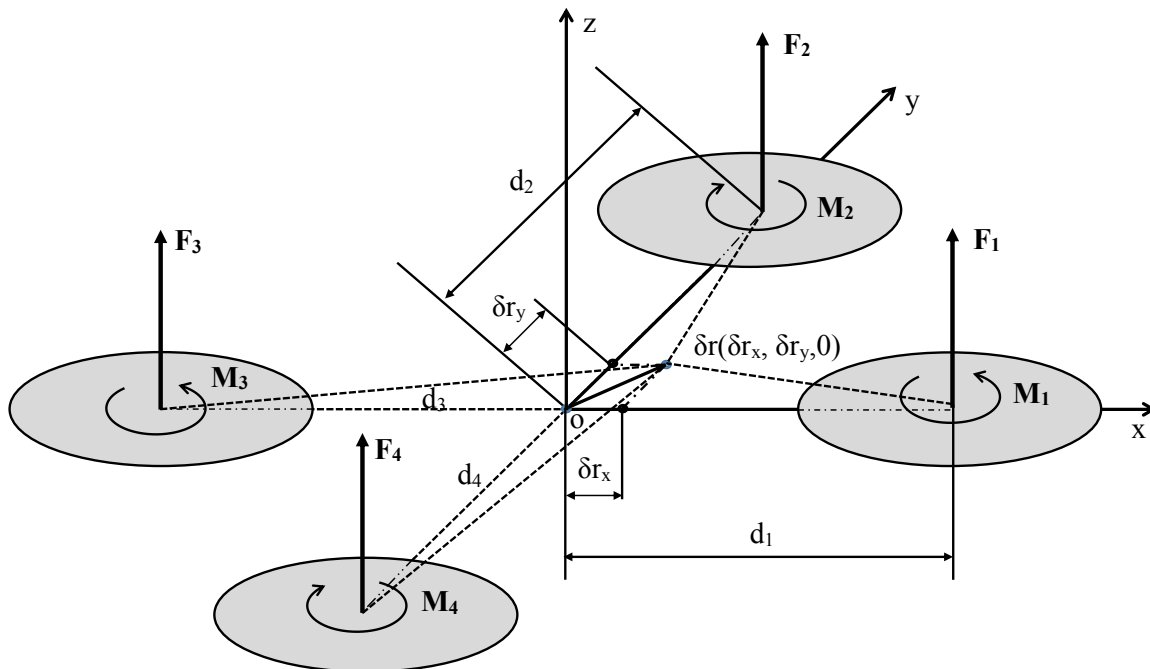


Figure 2.2.1. Free-body diagrams of the quadrotor which its the center of mass is not in the epicenter

Then from the equation (Eq. 2.2.1), we obtained as the following

$$\mathbf{R} = R_Z R_X R_Y$$

$$\Rightarrow \dot{\mathbf{R}} = \dot{R}_Z R_X R_Y + R_Z \dot{R}_X R_Y + R_Z R_X \dot{R}_Y$$

substituted by (2.2.1),

$$\begin{aligned} \Rightarrow \mathbf{R}\tilde{\Omega} &= (R_Z \tilde{\omega}_z) R_X R_Y + R_Z (R_X \tilde{\omega}_x) R_Y + R_Z R_X (R_Y \tilde{\omega}_y) \\ \Leftrightarrow (\mathbf{R}\tilde{\Omega})^T &= [(R_Z \tilde{\omega}_z) R_X R_Y + R_Z (R_X \tilde{\omega}_x) R_Y + R_Z R_X (R_Y \tilde{\omega}_y)]^T \end{aligned}$$

where,

$$\omega_x = \begin{bmatrix} \dot{\phi} \\ 0 \\ 0 \end{bmatrix}, \omega_y = \begin{bmatrix} 0 \\ \dot{\theta} \\ 0 \end{bmatrix}, \omega_z = \begin{bmatrix} 0 \\ 0 \\ \dot{\psi} \end{bmatrix},$$

Since,

$$\begin{aligned} \tilde{\Omega}^T &= -\tilde{\Omega} = -\Omega \times, \\ \mathbf{R}^T &= R_Y^T R_X^T R_Z^T \end{aligned}$$

Then,

$$\begin{aligned} \Rightarrow -\Omega \times \mathbf{R}^T &= -R_Y^T R_X^T (\omega_z \times R_Z^T) - R_Y^T (\omega_x \times R_X^T) R_Z^T - (\omega_y \times R_Y^T) R_X^T R_Z^T \\ \Leftrightarrow \Omega \times \mathbf{R}^T &= R_Y^T R_X^T \omega_z \times R_Y^T R_X^T R_Z^T + R_Y^T \omega_x \times R_Y^T R_X^T R_Z^T + \omega_y \times R_Y^T R_X^T R_Z^T \\ \Leftrightarrow \Omega \times \mathbf{R}^T &= R_Y^T R_X^T \omega_z \times R^T + R_Y^T \omega_x \times R^T + \omega_y \times R^T \\ \Leftrightarrow \Omega \times \mathbf{R}^T &= (R_Y^T R_X^T \omega_z + R_Y^T \omega_x + \omega_y) \times R^T \\ \Rightarrow \Omega &= R_Y^T R_X^T \omega_z + R_Y^T \omega_x + \omega_y \end{aligned} \tag{2.2.4}$$

Since,

$$R_Z = \begin{bmatrix} c\psi & -s\psi & 0 \\ s\psi & c\psi & 0 \\ 0 & 0 & 1 \end{bmatrix}, R_X = \begin{bmatrix} 1 & 0 & 0 \\ 0 & c\phi & -s\phi \\ 0 & s\phi & c\phi \end{bmatrix}, R_Y = \begin{bmatrix} c\theta & 0 & s\theta \\ 0 & 1 & 0 \\ -s\theta & 0 & c\theta \end{bmatrix}$$

$$\begin{aligned} \Rightarrow R_Y^T R_X^T &= \begin{bmatrix} c\theta & 0 & s\theta \\ 0 & 1 & 0 \\ -s\theta & 0 & c\theta \end{bmatrix}^T \begin{bmatrix} 1 & 0 & 0 \\ 0 & c\phi & -s\phi \\ 0 & s\phi & c\phi \end{bmatrix}^T = \begin{bmatrix} c\theta & 0 & -s\theta \\ 0 & 1 & 0 \\ s\theta & 0 & c\theta \end{bmatrix} \begin{bmatrix} 1 & 0 & 0 \\ 0 & c\phi & s\phi \\ 0 & -s\phi & c\phi \end{bmatrix} \\ &= \begin{bmatrix} c\theta & s\theta s\phi & -s\theta c\phi \\ 0 & c\phi & s\phi \\ s\theta & -c\theta s\phi & c\theta c\phi \end{bmatrix} \end{aligned}$$

then,

$$\Rightarrow R_Y^T R_X^T \omega_z = \begin{bmatrix} c\theta & s\theta s\phi & -s\theta c\phi \\ 0 & c\phi & s\phi \\ s\theta & -c\theta s\phi & c\theta c\phi \end{bmatrix} \begin{bmatrix} 0 \\ 0 \\ \dot{\psi} \end{bmatrix} = \begin{bmatrix} -s\theta c\phi \dot{\psi} \\ s\phi \dot{\psi} \\ c\theta c\phi \dot{\psi} \end{bmatrix}$$

and,

$$\begin{aligned} R_Y^T \omega_x &= \begin{bmatrix} c\theta & 0 & s\theta \\ 0 & 1 & 0 \\ -s\theta & 0 & c\theta \end{bmatrix}^T \begin{bmatrix} \dot{\phi} \\ 0 \\ 0 \end{bmatrix} \\ &= \begin{bmatrix} c\theta & 0 & -s\theta \\ 0 & 1 & 0 \\ s\theta & 0 & c\theta \end{bmatrix} \begin{bmatrix} \dot{\phi} \\ 0 \\ 0 \end{bmatrix} = \begin{bmatrix} c\theta \dot{\phi} \\ 0 \\ s\theta \dot{\phi} \end{bmatrix} \end{aligned}$$

Then, substituting to the equation (Eq. 2.2.4), we get

$$\begin{aligned} \Omega &= \begin{bmatrix} -s\theta c\phi \dot{\psi} \\ s\phi \dot{\psi} \\ c\theta c\phi \dot{\psi} \end{bmatrix} + \begin{bmatrix} c\theta \dot{\phi} \\ 0 \\ s\theta \dot{\phi} \end{bmatrix} + \begin{bmatrix} 0 \\ \dot{\theta} \\ 0 \end{bmatrix} \\ &= \begin{bmatrix} c\theta \dot{\phi} + 0\dot{\theta} - s\theta c\phi \dot{\psi} \\ 0\dot{\phi} + \dot{\theta} + s\phi \dot{\psi} \\ s\theta \dot{\phi} + 0\dot{\theta} + c\theta c\phi \dot{\psi} \end{bmatrix} \\ &= \begin{bmatrix} c\theta & 0 & -s\theta c\phi \\ 0 & 1 & s\phi \\ s\theta & 0 & c\theta c\phi \end{bmatrix} \begin{bmatrix} \dot{\phi} \\ \dot{\theta} \\ \dot{\psi} \end{bmatrix} \end{aligned}$$

$$\Rightarrow \Omega = \begin{bmatrix} c\theta & 0 & -s\theta c\phi \\ 0 & 1 & s\phi \\ s\theta & 0 & c\theta c\phi \end{bmatrix} \begin{bmatrix} \dot{\phi} \\ \dot{\theta} \\ \dot{\psi} \end{bmatrix}$$

or,

$$\Omega = H \begin{bmatrix} \dot{\phi} \\ \dot{\theta} \\ \dot{\psi} \end{bmatrix}$$

$$\Rightarrow \begin{bmatrix} \dot{\phi} \\ \dot{\theta} \\ \dot{\psi} \end{bmatrix} = H^{-1} \begin{bmatrix} \Omega_x \\ \Omega_y \\ \Omega_z \end{bmatrix} \quad (2.2.5)$$

Where,

$$H = \begin{bmatrix} c\theta & 0 & -s\theta c\phi \\ 0 & 1 & s\phi \\ s\theta & 0 & c\theta c\phi \end{bmatrix}$$

$$H^{-1} = \begin{bmatrix} c\theta & 0 & -s\theta c\phi \\ 0 & 1 & s\phi \\ s\theta & 0 & c\theta c\phi \end{bmatrix}^{-1} = \frac{1}{\det(H)} \mathbf{C}^T$$

where,

$$\det(H) = c^2\theta c\phi + s^2\theta c\phi = c\phi(c^2\theta + s^2\theta) = c\phi$$

and cofactor matrix \mathbf{C} ,

$$\mathbf{C} = \begin{bmatrix} c\theta c\phi & s\theta s\phi & -s\theta \\ 0 & c\phi & 0 \\ s\theta c\phi & -c\theta s\phi & c\theta \end{bmatrix}$$

$$\Rightarrow \mathbf{C}^T = \begin{bmatrix} c\theta c\phi & s\theta s\phi & -s\theta \\ s\theta c\phi & c\phi & -c\theta s\phi \\ -s\theta & 0 & c\theta \end{bmatrix}$$

Then,

$$H^{-1} = \frac{1}{c\phi} \begin{bmatrix} c\theta c\phi & 0 & s\theta c\phi \\ s\theta s\phi & c\phi & -c\theta s\phi \\ -s\theta & 0 & c\theta \end{bmatrix} \quad (2.2.6)$$

where, $\phi \neq \frac{\pi}{2} + n\pi$, and n is integer number from $-\infty$ to $+\infty$.

In **(Eq. 2.2.2)**, we ignore the aerodynamic friction torque and the aerodynamic friction force. Thus, the total external torques τ_{ext} applied to the rigid airframe remain only the torques generated from each rotors, F_i , and the reaction torques, M_i , to each rotor of the quadrotor. The total external torques τ_{ext} can be defined according to **Figure 2.2.1** and obtained as the following

$$\tau_{ext} = \sum_{i=1}^4 (d_i - \delta r) \times F_i + \sum_{i=1}^4 (-1)^{i+1} M_i \quad (2.2.7)$$

where,

$$\begin{aligned} \sum_{i=1}^4 (d_i - \delta r) \times F_i &= (d_1 - \delta r) \times F_1 + (d_2 - \delta r) \times F_2 \\ &+ (d_3 - \delta r) \times F_3 + (d_4 - \delta r) \times F_4 \end{aligned} \quad (2.2.8)$$

and,

$$\begin{aligned} \bullet \quad (d_1 - \delta r) \times F_1 &= \begin{bmatrix} d_1 - \delta r_x \\ -\delta r_y \\ 0 \end{bmatrix} \times \begin{bmatrix} 0 \\ 0 \\ F_1 \end{bmatrix} \\ &= \begin{bmatrix} -\delta r_y F_1 \\ -(d_1 - \delta r_x) F_1 \\ 0 \end{bmatrix} \end{aligned}$$

$$\begin{aligned} \bullet \quad (d_2 - \delta r) \times F_2 &= \begin{bmatrix} -\delta r_x \\ d_2 - \delta r_y \\ 0 \end{bmatrix} \times \begin{bmatrix} 0 \\ 0 \\ F_2 \end{bmatrix} \\ &= \begin{bmatrix} (d_2 - \delta r_y)F_2 \\ \delta r_x F_2 \\ 0 \end{bmatrix} \end{aligned}$$

$$\begin{aligned} \bullet \quad (d_3 - \delta r) \times F_3 &= \begin{bmatrix} -d_3 - \delta r_x \\ -\delta r_y \\ 0 \end{bmatrix} \times \begin{bmatrix} 0 \\ 0 \\ F_3 \end{bmatrix} \\ &= \begin{bmatrix} -\delta r_y F_3 \\ (d_3 + \delta r_x)F_3 \\ 0 \end{bmatrix} \end{aligned}$$

$$\begin{aligned} \bullet \quad (d_4 - \delta r) \times F_4 &= \begin{bmatrix} -\delta r_x \\ -d_4 - \delta r_y \\ 0 \end{bmatrix} \times \begin{bmatrix} 0 \\ 0 \\ F_4 \end{bmatrix} \\ &= \begin{bmatrix} -(d_4 + \delta r_y)F_4 \\ \delta r_x F_4 \\ 0 \end{bmatrix} \end{aligned}$$

$$\bullet \quad \sum_{i=1}^4 (-1)^{i+1} M_i = \begin{bmatrix} 0 \\ 0 \\ M_1 - M_2 + M_3 - M_4 \end{bmatrix}$$

Then, the total external torques τ_{ext} can be fully determined by

$$\tau_{ext} = \begin{bmatrix} -\delta r_y(F_1 + F_2 + F_3 + F_4) + l(F_2 - F_4) \\ \delta r_x(F_1 + F_2 + F_3 + F_4) + l(F_3 - F_1) \\ M_1 - M_2 + M_3 - M_4 \end{bmatrix} \quad (2.2.9)$$

Likely, (Eq. 2.2.2) can be derived as

$$\dot{\Omega} = -J^{-1}\Omega \times J\Omega + J^{-1}\tau_{ext}$$

Then, this equation is substituted by **(Eq. 2.2.9)**, we get **(Eq. 2.2.10)**

$$\begin{bmatrix} \dot{\Omega}_x \\ \dot{\Omega}_y \\ \dot{\Omega}_z \end{bmatrix} = -J^{-1} \begin{bmatrix} \Omega_x \\ \Omega_y \\ \Omega_z \end{bmatrix} \times J \begin{bmatrix} \Omega_x \\ \Omega_y \\ \Omega_z \end{bmatrix} + J^{-1} \begin{bmatrix} -\delta r_y(F_1 + F_2 + F_3 + F_4) + l(F_2 - F_4) \\ \delta r_x(F_1 + F_2 + F_3 + F_4) + l(F_3 - F_1) \\ M_1 - M_2 + M_3 - M_4 \end{bmatrix} \quad (2.2.10)$$

where, for the i th rotor, d_i is the distance from the epicenter of the quadrotor to the axes of i th rotor and $d = [d_1, d_2, d_3, d_4]^T$ and $l = d_1 = d_2 = d_3 = d_4$. $\delta r = [\delta r_x, \delta r_y, \delta r_z]^T \in \{B\}$ denotes the actual center of mass of the quadrotor expressed in $\{B\}$. However, δr_z is assumed to be zero. F_1, F_2, F_3 and F_4 are the forces generated from the rotor 1, 2, 3 and 4 respectively, while M_1, M_2, M_3 and M_4 are the reaction torques due to the rotor 1, 2, 3 and 4 drag respectively acting on the airframe. $\Omega = [\Omega_x, \Omega_y, \Omega_z]^T$ is the angular velocity of $\{B\}$ with respect to $\{A\}$ expressed in $\{B\}$.

2.3. State Space Transformation of Dynamic Equation

In the previous sections, we have obtained the continuous difference equations of the rotation motion for the quadrotor shown below in **(Eq. 2.2.5)** and **(Eq. 2.2.10)**. In this section, these equations are transformed to the discrete state space form. The procedures of the transformation are demonstrated as the following

We have **(Eq. 2.2.5)** and **(Eq. 2.2.10)** can be transformed into state space form. Let's us denote

$$\begin{aligned} q_1 &= \phi, & q_2 &= \theta, & q_3 &= \psi \\ q_4 &= \Omega_x, & q_5 &= \Omega_y, & q_6 &= \Omega_z \\ q_7 &= \delta r_x, & q_8 &= \delta r_y \end{aligned}$$

then, we can write

$$\begin{aligned} q &= [q_1 \quad q_2 \quad \dots \quad q_8]^T \in \mathbb{R}^8 \\ \Rightarrow \begin{bmatrix} \dot{q}_1 \\ \dot{q}_2 \\ \dot{q}_3 \end{bmatrix} &= \begin{bmatrix} cq_2 & 0 & -sq_2cq_1 \\ 0 & 1 & sq_1 \\ sq_2 & 0 & cq_2cq_1 \end{bmatrix} \begin{bmatrix} q_4 \\ q_5 \\ q_6 \end{bmatrix}, \end{aligned}$$

$$\begin{bmatrix} \dot{q}_4 \\ \dot{q}_5 \\ \dot{q}_6 \end{bmatrix} = -J^{-1} \begin{bmatrix} q_4 \\ q_5 \\ q_6 \end{bmatrix} \times J \begin{bmatrix} q_4 \\ q_5 \\ q_6 \end{bmatrix} + J^{-1} \begin{bmatrix} -q_8(F_1 + F_2 + F_3 + F_4) + l(F_2 - F_4) \\ q_7(F_1 + F_2 + F_3 + F_4) + l(F_3 - F_1) \\ M_1 - M_2 + M_3 - M_4 \end{bmatrix},$$

and,

$$\begin{bmatrix} \dot{q}_7 \\ \dot{q}_8 \end{bmatrix} = \begin{bmatrix} 0 \\ 0 \end{bmatrix}$$

Hence, we achieved the continuous state space form as below

$$\dot{q} = \begin{bmatrix} \dot{q}_1 \\ \dot{q}_2 \\ \dot{q}_3 \\ \dot{q}_4 \\ \dot{q}_5 \\ \dot{q}_6 \\ \dot{q}_7 \\ \dot{q}_8 \end{bmatrix} = \begin{bmatrix} \begin{bmatrix} cq_2 & 0 & -sq_2cq_1 \\ 0 & 1 & sq_1 \\ sq_2 & 0 & cq_2cq_1 \end{bmatrix} \begin{bmatrix} q_4 \\ q_5 \\ q_6 \end{bmatrix} \\ -J^{-1} \begin{bmatrix} q_4 \\ q_5 \\ q_6 \end{bmatrix} \times J \begin{bmatrix} q_4 \\ q_5 \\ q_6 \end{bmatrix} + J^{-1} \begin{bmatrix} -q_8(F_1 + F_2 + F_3 + F_4) + l(F_2 - F_4) \\ q_7(F_1 + F_2 + F_3 + F_4) + l(F_3 - F_1) \\ M_1 - M_2 + M_3 - M_4 \end{bmatrix} \\ \begin{bmatrix} 0 \\ 0 \end{bmatrix} \end{bmatrix}$$

or,

$$\dot{q} = G(q) \tag{2.3.1}$$

where,

$$G(q) \equiv \begin{bmatrix} \begin{bmatrix} cq_2 & 0 & -sq_2cq_1 \\ 0 & 1 & sq_1 \\ sq_2 & 0 & cq_2cq_1 \end{bmatrix} \begin{bmatrix} q_4 \\ q_5 \\ q_6 \end{bmatrix} \\ -J^{-1} \begin{bmatrix} q_4 \\ q_5 \\ q_6 \end{bmatrix} \times J \begin{bmatrix} q_4 \\ q_5 \\ q_6 \end{bmatrix} + J^{-1} \begin{bmatrix} -q_8(F_1 + F_2 + F_3 + F_4) + l(F_2 - F_4) \\ q_7(F_1 + F_2 + F_3 + F_4) + l(F_3 - F_1) \\ M_1 - M_2 + M_3 - M_4 \end{bmatrix} \\ \begin{bmatrix} 0 \\ 0 \end{bmatrix} \end{bmatrix}$$

From (Eq. 2.3.1), we now transform it to the discrete-time state space form by using

the Euler Approximation

$$\dot{q} \approx \frac{q_{k+1} - q_k}{\Delta t}$$

where, Δt is the step time and its value should be small enough and scalar. Then, the (Eq. 2.3.1) can be substituted as the following

$$\begin{aligned} \frac{q_{k+1} - q_k}{\Delta t} &= G_k(q) \\ \Rightarrow q_{k+1} &= \Delta t G_k(q) + q_k \end{aligned}$$

or, it can be written as the discrete-time nonlinear deterministic difference equation as below

$$q_{k+1} = \left[\begin{array}{c} \begin{matrix} cq_2 & 0 & -sq_2cq_1 \\ 0 & 1 & sq_1 \\ sq_2 & 0 & cq_2cq_1 \end{matrix} \begin{bmatrix} q_4 \\ q_5 \\ q_6 \end{bmatrix} \\ -J^{-1} \begin{bmatrix} q_4 \\ q_5 \\ q_6 \end{bmatrix} \times J \begin{bmatrix} q_4 \\ q_5 \\ q_6 \end{bmatrix} + J^{-1} \begin{bmatrix} -q_8(F_1 + F_2 + F_3 + F_4) + l(F_2 - F_4) \\ q_7(F_1 + F_2 + F_3 + F_4) + l(F_3 - F_1) \\ M_1 - M_2 + M_3 - M_4 \\ 0 \\ 0 \end{bmatrix} \end{array} \right]_k \Delta t + q_k \quad (2.3.2)$$

or, it can be written as the discrete-time nonlinear stochastic difference equation by adding noise $w_k \in \mathbb{R}^8$ shown below

$$q_{k+1} = \left[\begin{array}{c} \begin{matrix} cq_2 & 0 & -sq_2cq_1 \\ 0 & 1 & sq_1 \\ sq_2 & 0 & cq_2cq_1 \end{matrix} \begin{bmatrix} q_4 \\ q_5 \\ q_6 \end{bmatrix} \\ -J^{-1} \begin{bmatrix} q_4 \\ q_5 \\ q_6 \end{bmatrix} \times J \begin{bmatrix} q_4 \\ q_5 \\ q_6 \end{bmatrix} + J^{-1} \begin{bmatrix} -q_8(F_1 + F_2 + F_3 + F_4) + l(F_2 - F_4) \\ q_7(F_1 + F_2 + F_3 + F_4) + l(F_3 - F_1) \\ M_1 - M_2 + M_3 - M_4 \\ 0 \\ 0 \end{bmatrix} \\ \Delta t + q_k + w_k \end{array} \right]_k \quad (2.3.3)$$

$$q_{k+1} = f_d(q_k, 0) + w_k$$

where,

$$f_d(q_k, 0) = \Delta t G_k(q) + q_k$$

2.4. Implementation of Unscented Kalman Filter

The previous section, we have derived the discrete-time nonlinear stochastic difference equation as shown in (**Eq. 2.3.3**). However, to implement the UKF, we have to know some measurements also. Actually, the angular velocity $\Omega = [\Omega_x, \Omega_y, \Omega_z]^T$ can be measured by sensors as well. In this section, however, the measurement state equation can be assumed by extracting the $\Omega = [\Omega_x, \Omega_y, \Omega_z]^T$ from the true equation (**Eq. 2.3.3**). Then, the measurement state equation can be determined by

$$\begin{aligned} z_{k+1} &= Cq_{k+1} + v_{k+1}, \\ \text{or, } z_{k+1} &= h_d(q_{k+1}, 0) + v_{k+1} \end{aligned} \quad (2.4.1)$$

where,

$$C = \begin{bmatrix} 0 & 0 & 0 & 1 & 0 & 0 & 0 & 0 \\ 0 & 0 & 0 & 0 & 1 & 0 & 0 & 0 \\ 0 & 0 & 0 & 0 & 0 & 1 & 0 & 0 \end{bmatrix},$$

and,

$$h_d(q_{k+1}, 0) = Cq_{k+1},$$

and $v_k \in \mathbb{R}^8$ is the measurement noises at time k .

After getting the discrete-time nonlinear stochastic difference equation of the quadrotor and its measurement as in (Eq. 2.3.3) and (Eq. 2.4.1) respectively, we then simulate the true process for collecting the true data of the measurement to implement in UKF. The simulation is performed in the program "MATLAB 2014a" script. Additionally, to simulate the true process, we need to initialize the value of some parameters as shown in **Table 2.4.1**. After obtaining the data, the UKF algorithm can be derived briefly as the following

- Firstly, we initial the state estimate $\hat{q}_{0|0} \in \mathbb{R}^8$ and its positive definite error covariance matrix $P_{0|0} \in \mathbb{R}^{8 \times 8}$. Secondly, we initial the process covariance noise $Q \in \mathbb{R}^{8 \times 8}$ and the measurement covariance noise $R \in \mathbb{R}^{3 \times 3}$. Finally, we initial the parameters α , β , k , and λ .

★ **Note:** All initial parameters can be tuned to get the better result. However, in the tuning parameters, sometimes there is a problem with the positive definiteness of the error covariance matrix P . So when we are tuning these parameters, we start initializing them from the small value. As a result, we have obtained the initial parameters as shown in **Table 2.4.2**.

- After the some above parameters are initialized, the steps time update and measurement update are then implemented by using the UKF algorithm.

Table 2.4.1. Initial Parameters for True Process

Parameters	Initial Value of the Parameters
l	0.5
$M_1 = M_2 = M_3 = M_4$	4
Δt	0.001
$q_{0 0}$	$\begin{bmatrix} 0 & 0 & 0 & 0.1 & 0.2 & 0.3 & 0.05 & 0.1 \end{bmatrix}^T$
C	$\begin{bmatrix} 0 & 0 & 0 & 1 & 0 & 0 & 0 & 0 \\ 0 & 0 & 0 & 0 & 1 & 0 & 0 & 0 \\ 0 & 0 & 0 & 0 & 0 & 1 & 0 & 0 \end{bmatrix}$
J	$10^{-9} \times \begin{bmatrix} 57253259 & 492519.58 & -201867.25 \\ 492519.58 & 58818844.45 & 5649.67 \\ -201867.25 & 5649.67 & 86609602.22 \end{bmatrix}$
Q	$10^{-6} \times \text{diag} \begin{bmatrix} 0.01 & 0.02 & 0.01 & 0.01 & 0.02 & 0.04 & 0.01 & 0.01 \end{bmatrix}$
R	$10^{-3} \times \text{diag} \begin{bmatrix} 0.1 & 0.2 & 0.1 \end{bmatrix}$

Table 2.4.2. Initial Parameters for Estimation Process

Parameters	Initial Value of the Parameters
Δt	0.001
$\hat{q}_{0 0}$	$\begin{bmatrix} 1 & 5 & 0.2 & 4 & 5 & 6 & 0.5 & -0.5 \end{bmatrix}^T$
α	0.1
β	2
k	0.1
$P_{0 0}$	$10^{-5} \times \text{diag} \begin{bmatrix} 0.05 & 0.07 & 0.02 & 0.09 & 0.05 & 0.02 & 0.076 & 0.07 \end{bmatrix}$
Q	$10^{-7} \times \text{diag} \begin{bmatrix} 0.7 & 0.5 & 0.1 & 0.2 & 0.6 & 0.4 & 0.2 & 0.2 \end{bmatrix}$
R	$10^{-2} \times \text{diag} \begin{bmatrix} 0.03 & 0.05 & 0.07 \end{bmatrix}$

3. RESULTS AND DISCUSSION

3.1. Results

In the simulation of the UKF in estimating the center of mass of the quadrotor, we have simulated eight different cases. Four cases correspond to the assumption that the center of mass of the quadrotor is fixed, see in **Table 3.1.1**. The remaining four cases assume that center of mass of the quadrotor changes over time, see in **Table 3.1.2**). The initial estimated x-axis and y-axis of the center of mass were chosen to be $\hat{\delta r}_x = 0.5m$ and $\hat{\delta r}_y = -0.5m$, respectively, in all cases. Then, we have obtained the results as the following

Table 3.1.1. Test matrix assuming the center of mass of the quadrotor, $\delta r_x = 0.05m$ and $\delta r_y = 0.1m$, are fixed

Case Studies	Descriptions
Case 1	The thrusts of each rotor are chosen to be constant and equal to each other, where $F_1 = F_2 = F_3 = F_4 = 10N$. In this case, the results have been shown in Figure 3.1.3 and Figure 3.1.4 .
Case 2	The thrusts of each rotor are assumed to be constant and be different from each other, where $F_1 = 7N$, $F_2 = 9N$, $F_3 = 11N$, $F_4 = 13N$. In this case, the results have been shown in Figure 3.1.5 and Figure 3.1.6 .
Case 3	The thrusts of each rotor are chosen to be trigonometric functions and be equal to each other, where their values are show in Figure 3.1.1 . In this case, the results have been shown in Figure 3.1.7 and Figure 3.1.8 .
Case 4	The thrusts of each rotor are chosen to be trigonometric function and be not equal to each other, where their values have been expressed in Figure 3.1.2 . In this case, the results have been shown in Figure 3.1.9 and Figure 3.1.10 .

Table 3.1.2. Test studies with assuming the center of mass of the quadrotor changes over time

Case Studies	Descriptions
Case 5	The thrusts of each rotor are chosen to be constant and be equal to each other, where $F_1 = F_2 = F_3 = F_4 = 10N$. In this case, the results have been shown in Figure 3.1.11 and Figure 3.1.12 .
Case 6	The thrusts of each rotor are assumed to be constant and be different from each other, where $F_1 = 7N$, $F_2 = 9N$, $F_3 = 11N$, $F_4 = 13N$. In this case, the results have been shown in Figure 3.1.13 and Figure 3.1.14 .
Case 7	The thrusts of each rotor are chosen to be trigonometric functions and be equal to each other, where their values are show in Figure 3.1.1 . In this case, the results have been shown in Figure 3.1.15 and Figure 3.1.16 .
Case 8	The thrusts of each rotor are chosen to be trigonometric function and be not equal to each other, where their values have been expressed in Figure 3.1.2 . In this case, the results have been shown in Figure 3.1.17 and Figure 3.1.18 .

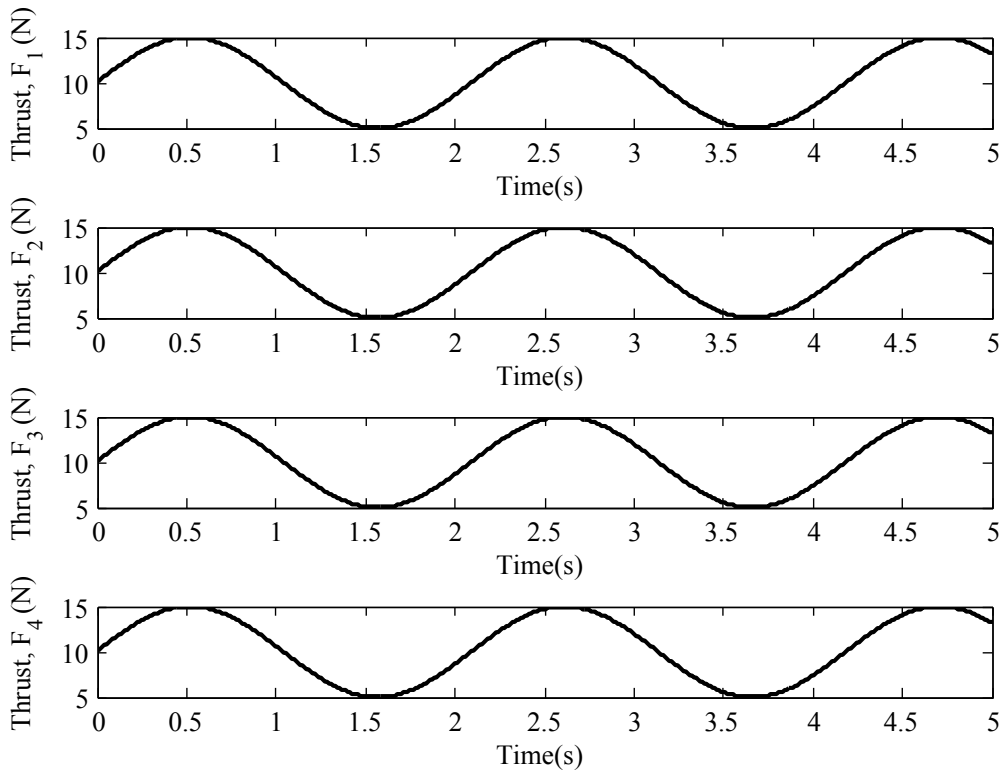


Figure 3.1.1. The value of thrusts F_1 , F_2 , F_3 and F_4 for case studies 3 and 7

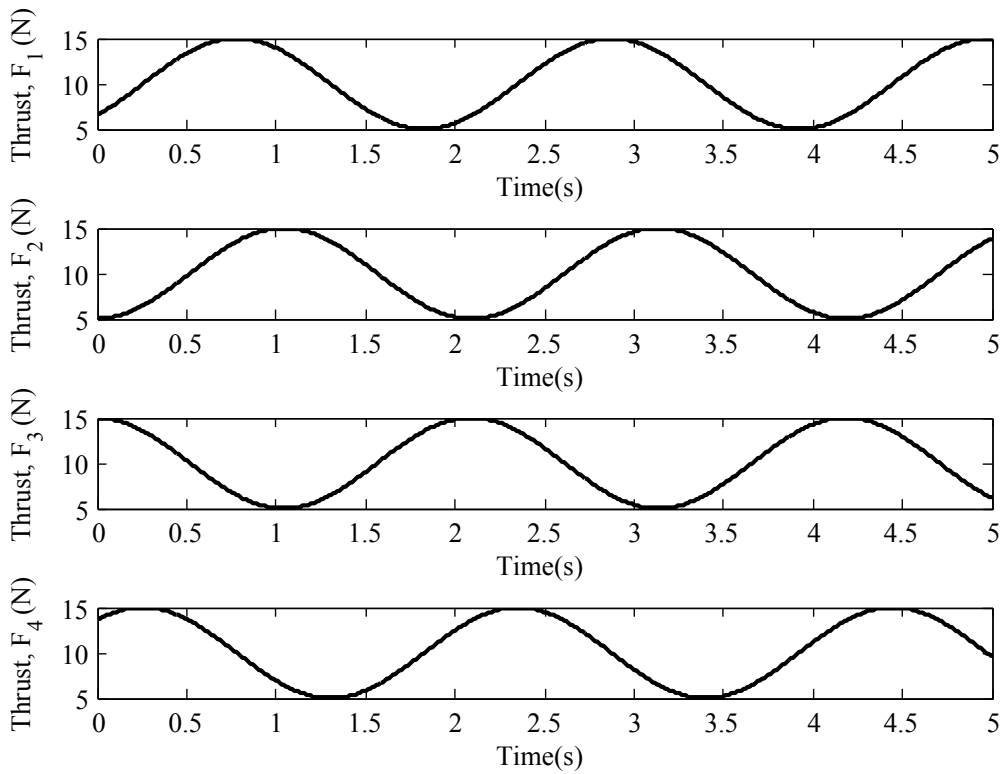


Figure 3.1.2. The value of thrusts F_1 , F_2 , F_3 and F_4 for case studies 4 and 8

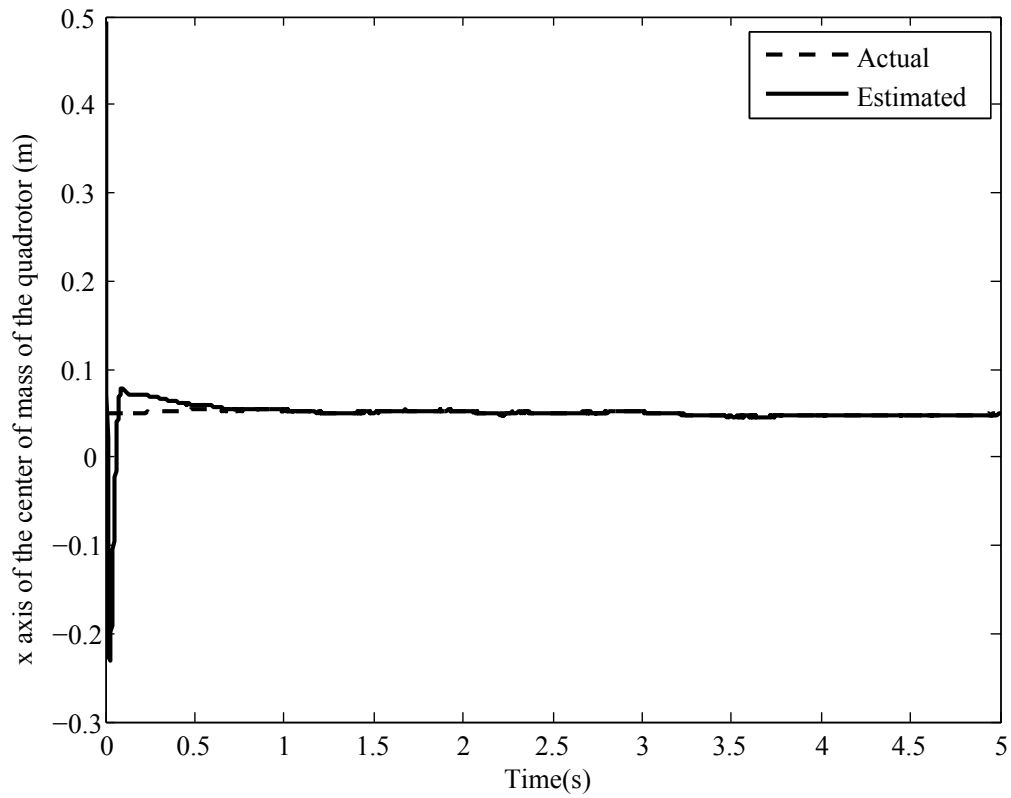


Figure 3.1.3. Estimation of x axis of the center of mass of the quadrotor for case 1

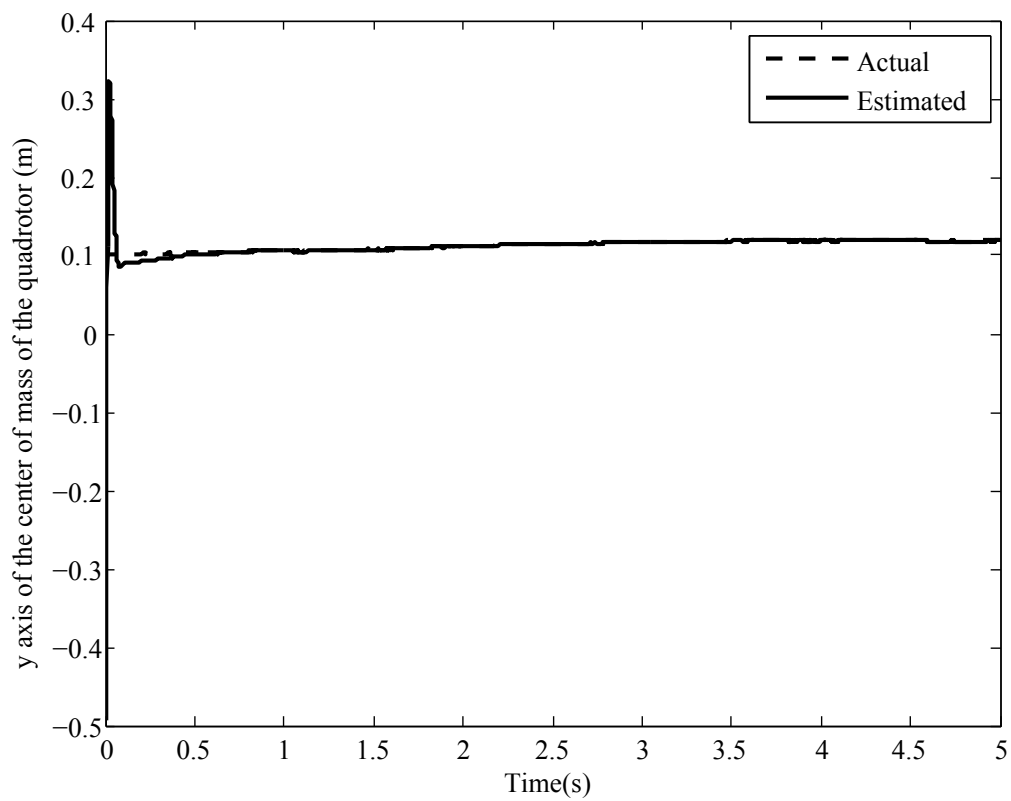


Figure 3.1.4. Estimation of y axis of the center of mass of the quadrotor for case 1

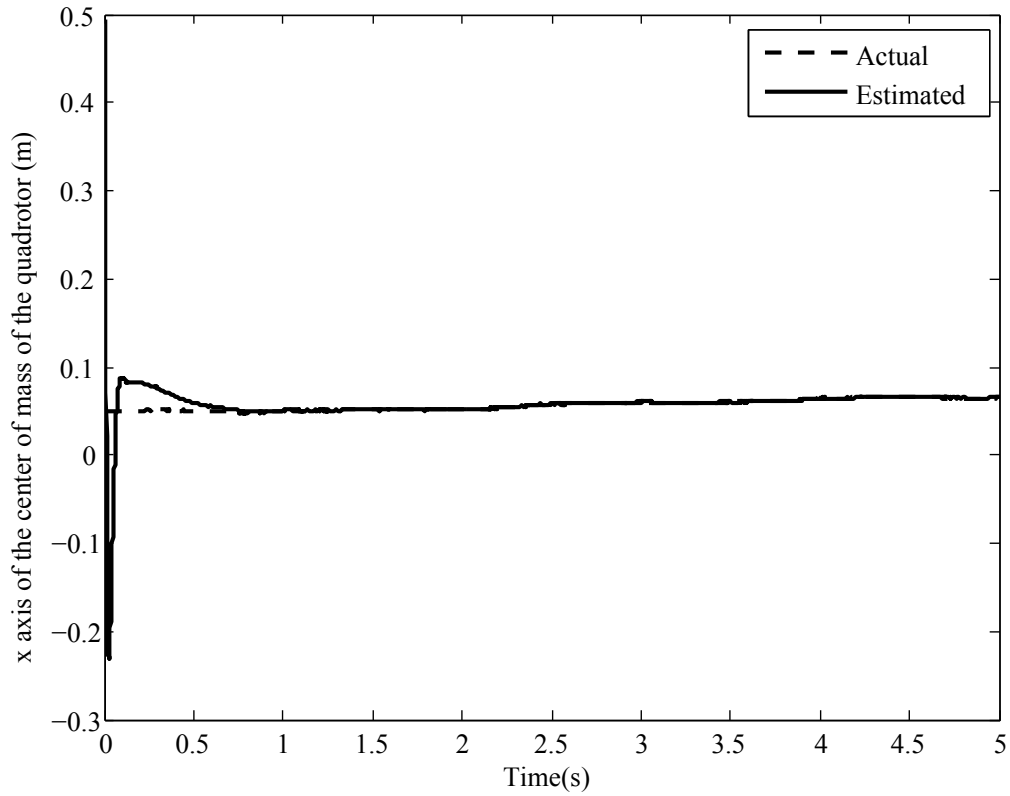


Figure 3.1.5. Estimation of x axis of the center of mass of the quadrotor for case 2

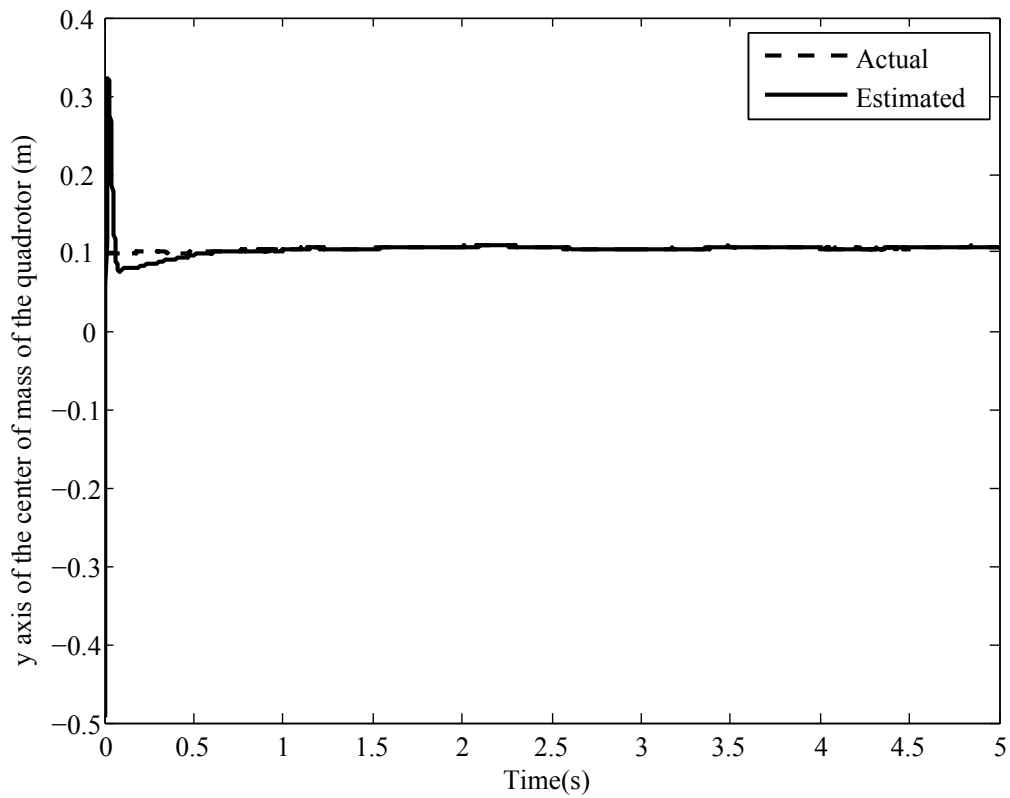


Figure 3.1.6. Estimation of y axis of the center of mass of the quadrotor for case 2

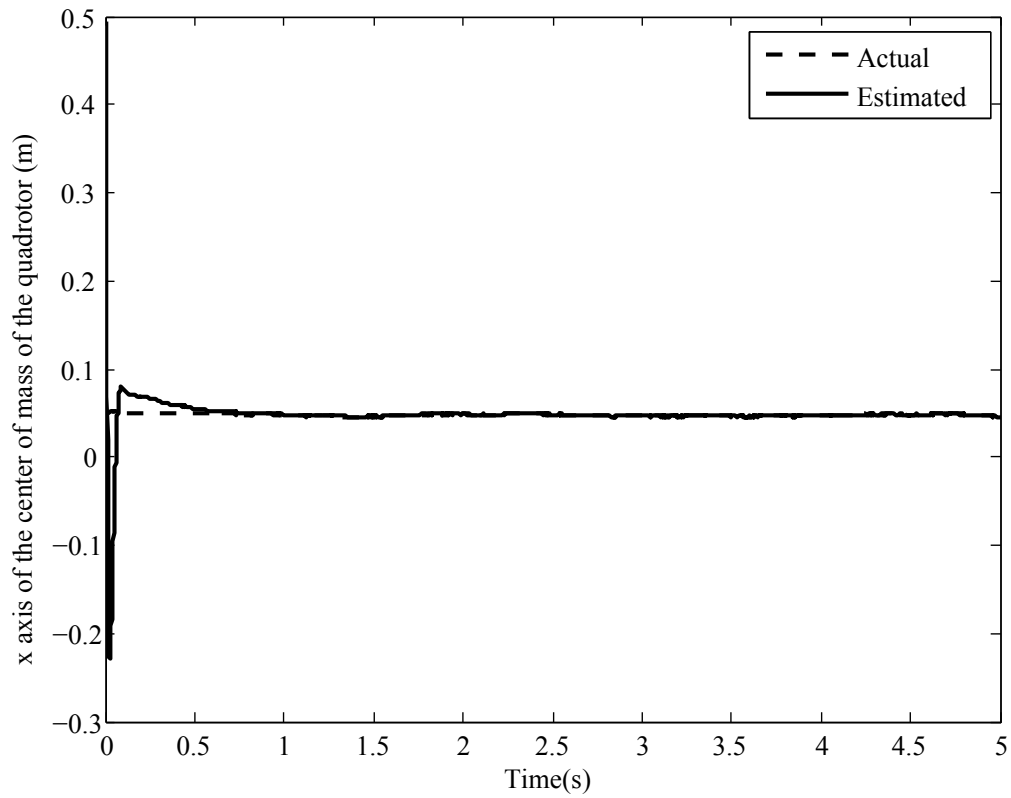


Figure 3.1.7. Estimation of x axis of the center of mass of the quadrotor for case 3

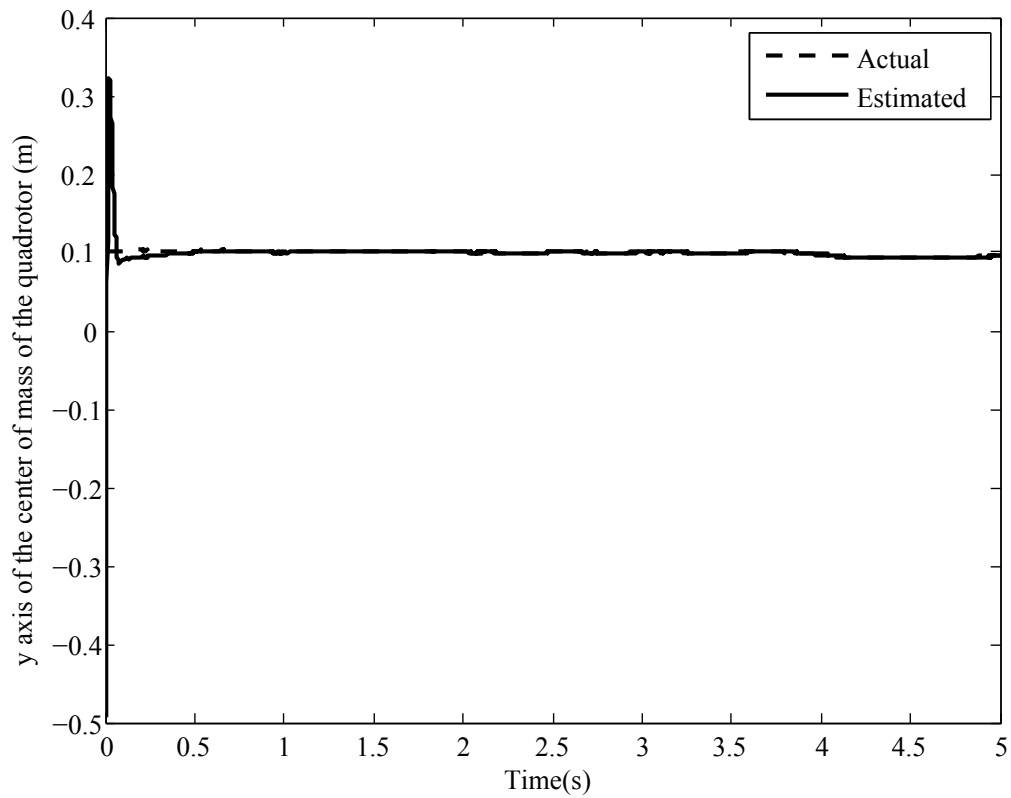


Figure 3.1.8. Estimation of y axis of the center of mass of the quadrotor for case 3

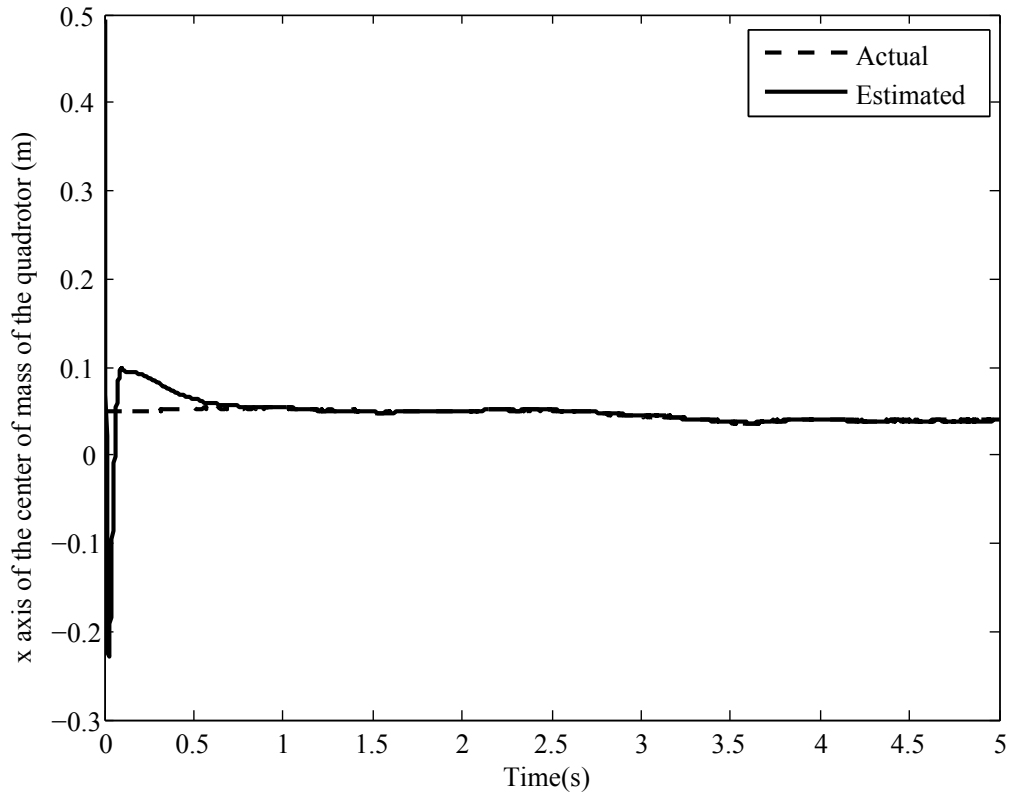


Figure 3.1.9. Estimation of x axis of the center of mass of the quadrotor for case 4

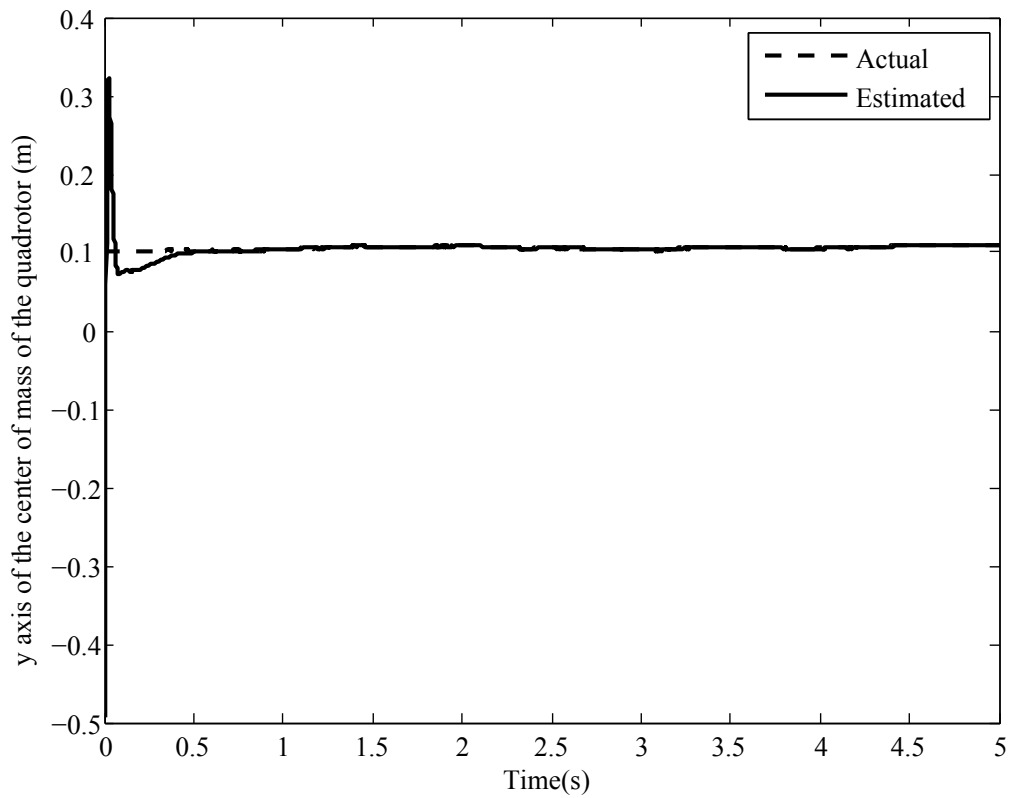


Figure 3.1.10. Estimation of y axis of the center of mass of the quadrotor for case 4

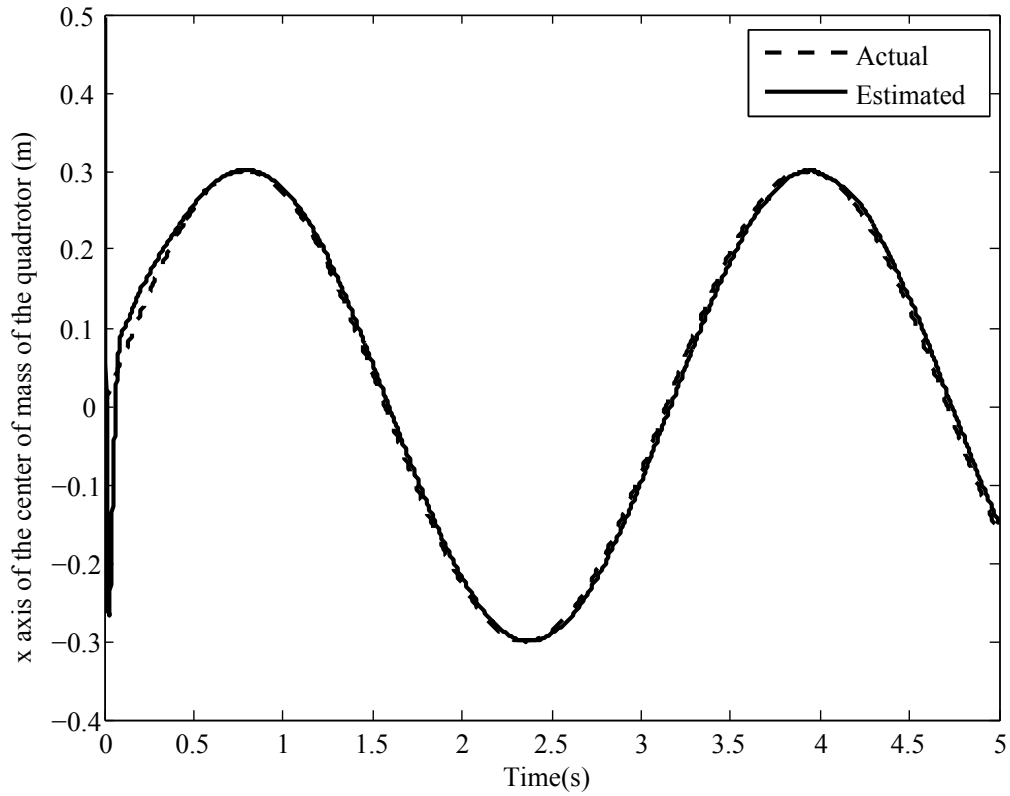


Figure 3.1.11. Estimation of x axis of the center of mass of the quadrotor for case 5

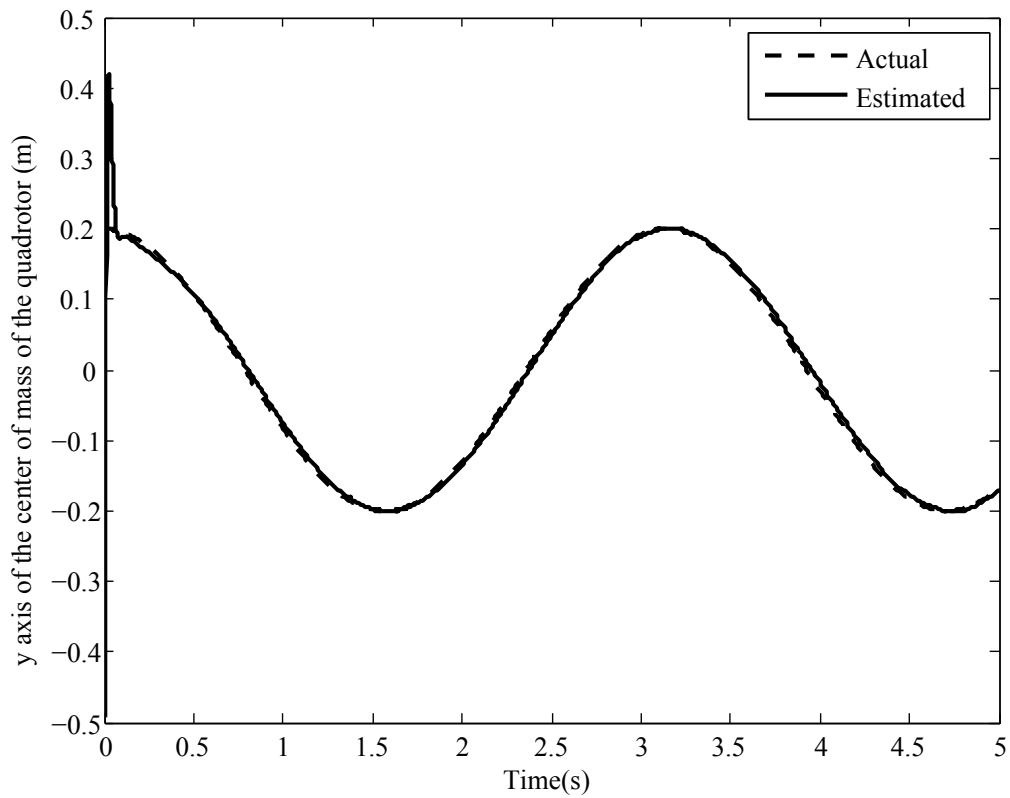


Figure 3.1.12. Estimation of y axis of the center of mass of the quadrotor for case 5

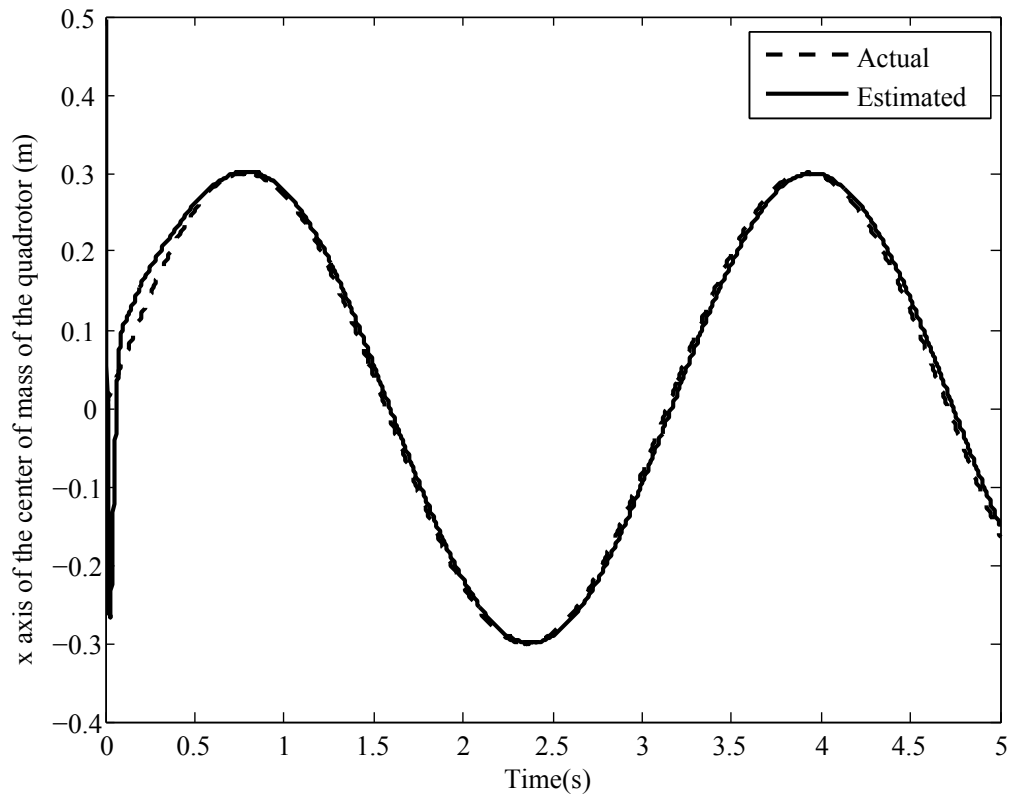


Figure 3.1.13. Estimation of x axis of the center of mass of the quadrotor for case 6

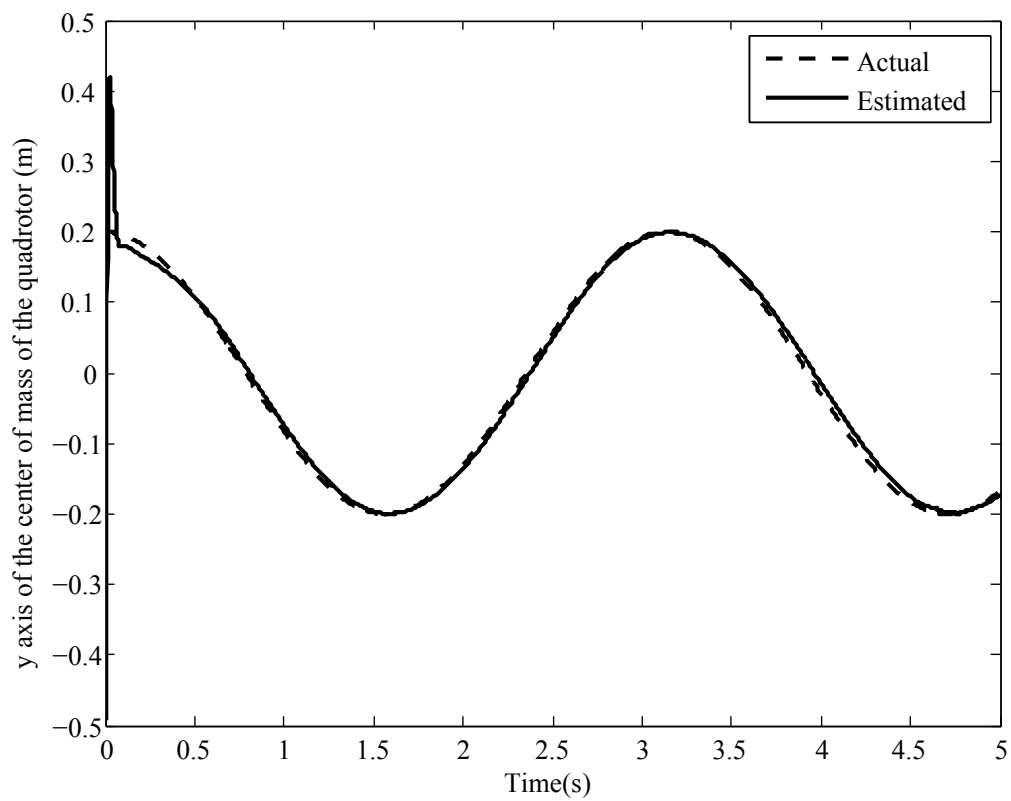


Figure 3.1.14. Estimation of y axis of the center of mass of the quadrotor for case 6

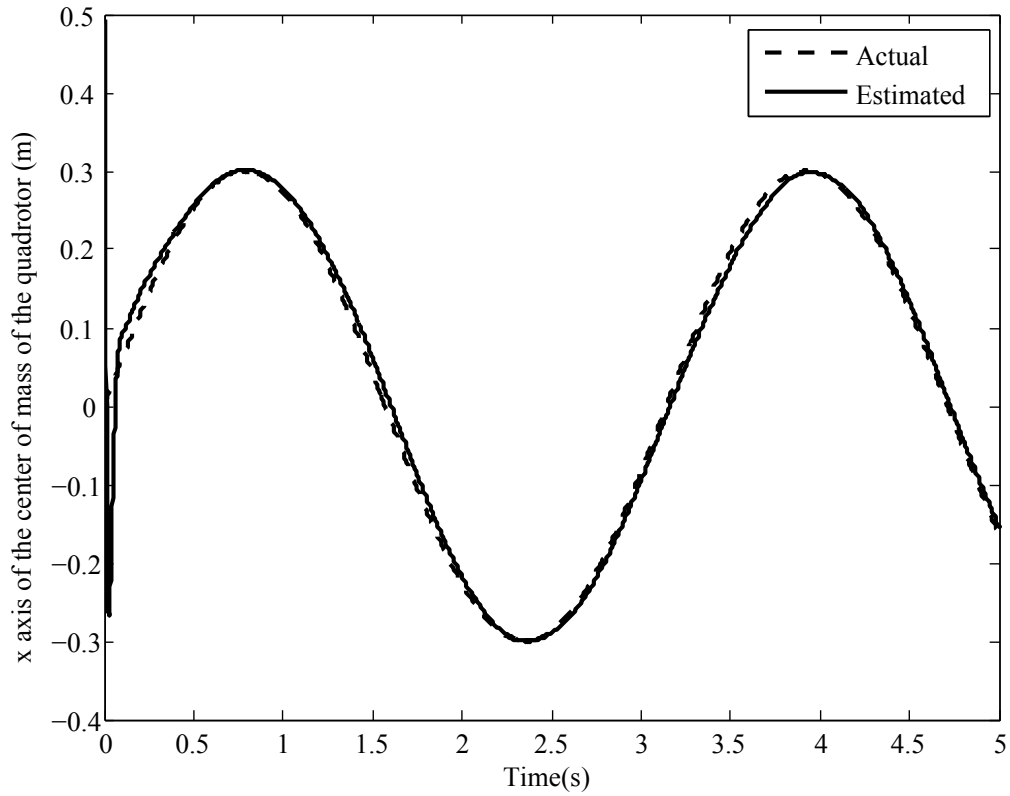


Figure 3.1.15. Estimation of x axis of the center of mass of the quadrotor for case 7

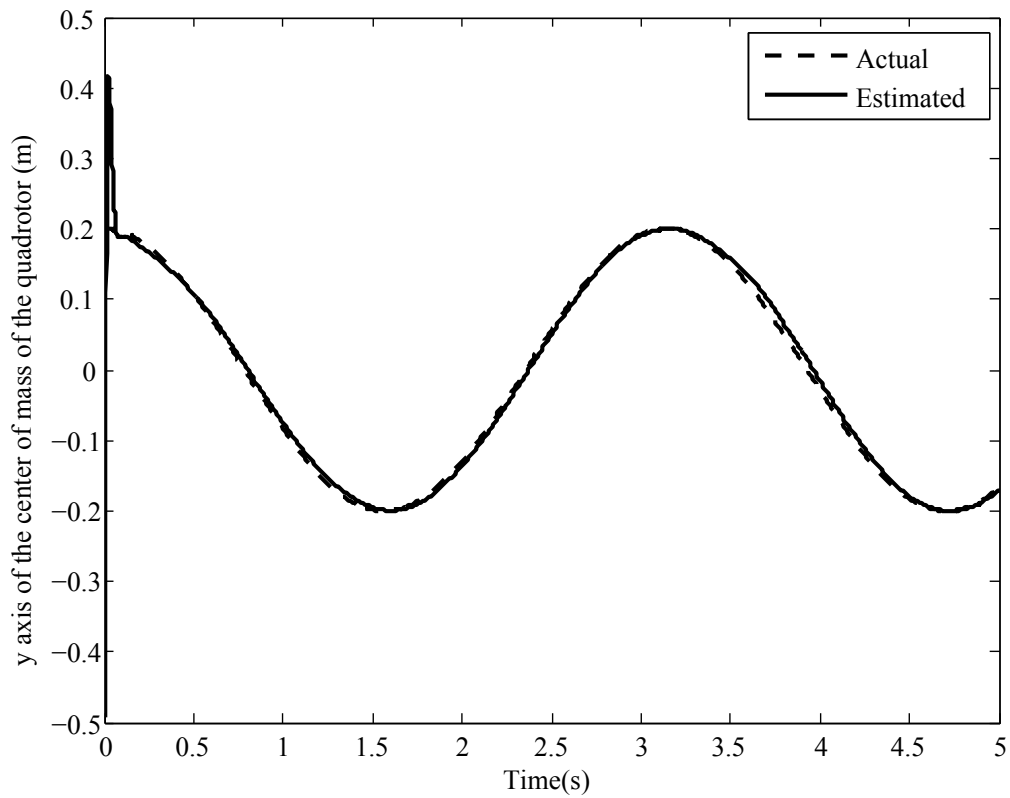


Figure 3.1.16. Estimation of y axis of the center of mass of the quadrotor for case 7

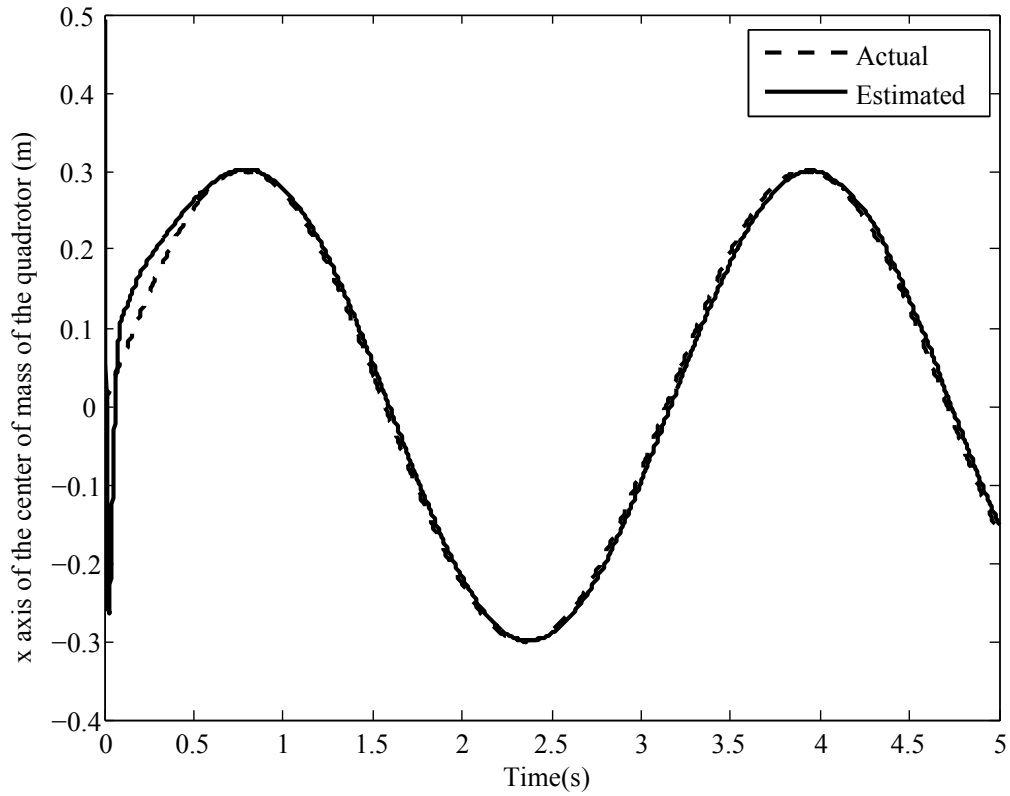


Figure 3.1.17. Estimation of x axis of the center of mass of the quadrotor for case 8

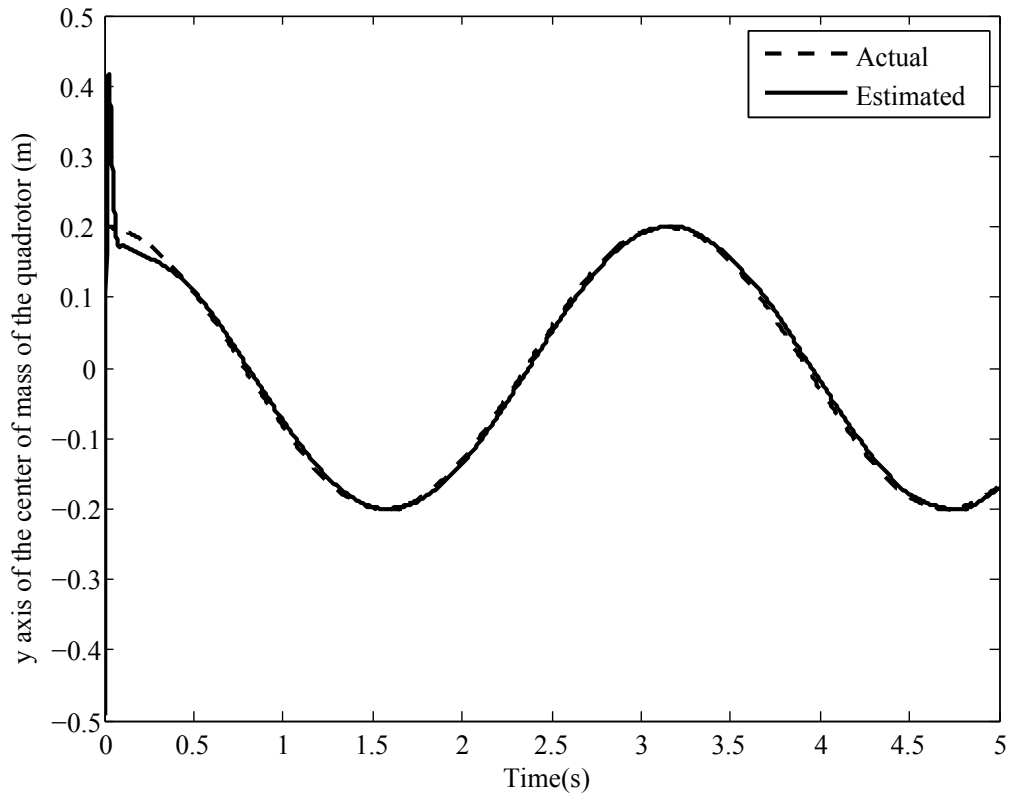


Figure 3.1.18. Estimation of y axis of the center of mass of the quadrotor for case 8

3.2. Discussion

Since the quadrotor's attitude can change during the flight, we have simulated eight various cases to estimate the center of mass of the quadrotor, shown in **Table 3.1.1** and **Table 3.1.2**. These cases are studied to prove that the UKF can estimate not only the center of mass of the quadrotor in simple attitude but also in complex attitude. However, these eight cases are separated into two important parts that are the fixed center of mass of the quadrotor and the changing center of mass of the quadrotor. In the fixed center of mass of the quadrotor part as shown in **Table 3.1.1**, we expect the quadrotor is lifting the loads fixed to the quadrotor while it is flying. In the changing center of mass of the quadrotor part as shown in **Table 3.1.2**, we expect the quadrotor is lifting the loads that can move on the quadrotor during the flight. In these two parts, we expect the quadrotor is flying upward in case 1, tilting in case 2, flying upward and downward back and forth in case 3, and rotating back and forth about x -axis and y -axis in case 4. After we have done the simulation of all eight cases above, we observed that the estimated curves of $\hat{\delta r}_x$ and $\hat{\delta r}_y$ at each case rapidly converge to the actual curve as well even though the initial value of the estimated states are very far from the actual value. It takes about $0.5s$ for UKF to make the estimated curves reaching to the actual. After $0.5s$, the estimated curves almost completely overlap the actual curves even though the actual values are rapidly changed over time. This means that UKF performs very accurately in estimation of the center of mass of the quadrotor. So, the results are acceptable in practice such as designing controller.

4. CONCLUSIONS AND RECOMMENDATION

4.1. Conclusions

This thesis research aims to predict the center of mass of the quadrotor in both fixed center of mass and changing center of mass of the quadrotor. To accomplish the goals, we have used dynamic modeling, Euler angle and Unscented Kalman Filter and have simulated for the results in eight different cases. we have used dynamic modeling to model the rotational equation of motion of the quadrotor which its center of mass is not only fixed in the epicenter of its shape but also changing during the flight. The Euler angles have been used to model the kinematic attitude of the quadrotor. The Unscented Kalman filter algorithm is applied to the modeled equations for estimating the center of mass of the quadrotor. The simulation in eight different cases proved that the UKF can estimate the center of mass of the quadrotor very rapidly, not only in the simple attitude but also in the complex attitude. According to the results of the thesis research, the estimation of the center of mass of the quadrotor by using Unscented Kalman Filter algorithm is very reliable that can be accepted to manipulate in actual application.

4.2. Recommendation for Future works

Although the estimation of center of mass of the quadrotor have been done by this research, there are many works could be researched in the future. The following topics are suggested for future works

- Estimation of the moment of inertia and drag forces of the quadrotor
- Design an adaptive controller for dealing with the changing of center of mass and moment of inertia.

REFERENCES

References

- [1] Robert Mahony, Vijay Kumar, and Peter Corke. “Multirotor aerial vehicles”. *IEEE Robotics and Automation magazine*, 20(32), 2012.
- [2] Tarek Madani and Abdelaziz Benallegue. “Backstepping control for a quadrotor helicopter”. In *Intelligent Robots and Systems, 2006 IEEE/RSJ International Conference on*, pages 3255–3260. IEEE, 2006.

List of manuscripts that resulted from your AOARD supported project: In standard format showing authors, title, journal, for each category list the following:

a) papers submitted in local journals,

[1] (submitted) Sothy Theang, Sopagna Ath and Sarot Srang, "Inverse kinematic analysis of parallel mechanism for maximum power generation on UAV," *Techno-Science Research Journal*, 2019.

[2] Sarot Srang, "Dynamic modeling for a multi rigid body UAV," *Techno-Science Research Journal*, 2019.

b) manuscripts under preparation for submitted to local journals

[1] Sopagna Ath and Sarot Srang, "Dynamic modeling and simulation for 2DOF parallel mechanism," *Techno-Science Research Journal*, 2019.

[2] Sothy Theang and Sarot Srang, "Dynamic modeling and simulation for a parallel mechanism mounted UAV," *Techno-Science Research Journal*, 2019.

[3] Rotanak Chhean and Sarot Srang, "Estimation of the center of mass for a quadrotor by using unscented Kalman filter," *Techno-Science Research Journal*, 2019.